A POTENTIAL NEW STRUCTURAL DESIGN FOR FLEXIBLE PAVEMENT

Quanxin Xu

TU Delft Delft University of Technology

A POTENTIAL NEW STRUCTURAL DESIGN FOR FLEXIBLE PAVEMENT

Master Thesis

By

Quanxin Xu

in partial fulfilment of the requirements for the degree of

Master of Science

in Civil Engineering

at Faculty of Civil Engineering and Geosciences,
Delft University of Technology,
to be defended publicly on Friday August 25th, 2017 at 13:00 hrs.

Under the supervision of Graduation Committee:

Prof. dr. ir. S.M.J.G. Erkens	Pavement Engineering, CEG, TU Delft
Ir. C. Kasbergen	Pavement Engineering, CEG, TU Delft
Ir. L.J.M. Houben	Pavement Engineering, CEG, TU Delft
Ir. A. R. G. van de Wall	KWS Infra bv
Dr.ir. H. Farah	Transport & Planning, CEG, TU Delft

Abstract

Throughout the history of pavement structure, the parallel layer structure has dominated the structural design of pavements. In other words, the entire road pavement share a uniform thickness design regardless how many lanes there are. However, due to traffic regulations and driving habits, the traffic flow most probably does not distribute evenly on a multi-lane road. Modern pavement design methods usually choose the lane that bears the heaviest traffic load as the design lane to determine the thickness design of the entire pavement. Hence there could be a certain over-design in the less trafficked lanes. This study aims to propose and evaluate a new structural design for flexible pavement by reducing the thickness of asphalt layers of the lightly trafficked lanes.

The traffic data of a real motorway in the Netherlands was analysed, based on which a new pavement structural design of a 3-lane road was established. Two finite element models, for both original and new designs, were established in CAPA-3D to calculate the stress and strain responses under different traffic load combinations. Following the Dutch design method the fatigue and deformation performance predictions of the two pavement designs were executed and compared. The results showed that the new design indeed improve the material cost-efficiency without compromising the performance of the pavement structure.

Taking advantage of the finite element models, a real-life simulation was also applied. The strain output of the simulation was used to calculate the rutting depth following the American design method. Both calculated rutting depth and the deformation output of the real-time simulation supported the earlier conclusions. An extra simulation of truck platooning was briefly executed and discussed as well.

Furthermore, the construction and maintenance feasibilities of the new design were explored. It was proved that the new design can be constructed by the existing equipment and machines. The current maintenance methods and procedures can also be applied to the new design.

Acknowledgements

This thesis is a result of my master research study over the past year, in order to achieve the Master of Science degree in Structural Engineering at Delft University of Technology (TU Delft). This research study could not be made possible without the support of both Pavement Engineering Section of TU Delft and KWS Infra. Hereby I would like to express my sincere gratitude to all the people who have assisted and encouraged me with their genuine advice and guidance during my entire master period.

My first thank goes to Mr. Cor Kasbergen for being my daily supervisor over the past year. He diligently guided me throughout my entire master research study. Form the very first day, Cor kept offering me practical and conducive advice on both academic and daily life. His optimism and passion immensely infected me and will definitely continue infecting me in the next stage of my life.

Secondly, I want to thank Prof. Sandra Erkens and Prof. Tom Scarpas for their genuine guidance and instructive discussions at our monthly meetings. Their critical and insightful questions pushed me to elevate my research into a higher level.

I am also thankful for the assistance of Mr. Alex van de Wall and Mr. Gerard Cuppens from InfraLinQ - KWS Infra. The conversations with them not only laid the foundation of this research, but also provided me some insights into the Dutch pavement industry.

Furthermore, Dr.ir. Haneen Farah from Transport & Planning Department and Ir. Lambert Houben kindly and patiently answered my questions related to their expertise, for which I am genuinely grateful.

For the past two years I have been going through some truly hard time, my colleagues from Pavement Engineering Section and friends from TU Delft truly aided me to set my life back on track. Maybe not all of them have helped me directly, but the friendly and warm working environment they created together definitely influenced me positively. I will cherish these memories and friendships for the rest of my life.

Last but foremost, I would like to express my greatest gratitude to my beloved mother and farther for their profound and unconditional love. I dedicate this thesis to them and wish he would be proud of me somewhere up there.

Xu, Quanxin

徐泉心

August, 2017

Delft, the Netherlands

Contents

List of Abbreviations

AASHO/AASHTO	American Association of State Highway (and Transportation) Officials
AC	Asphalt Concrete
ACEA	European Automobile Manufacturers' Association
BB	Breedband (Broadband)
CAPA-3D	Computer Aided Pavement Analysis – 3D
CROW	Centrum voor Regelgeving en Onderzoek in de Wegenbouw
DL	Dubblellucht (Dual Tire)
EL	Enkellucht (Single Tire)
ESAL	Equivalent Single Axle Load
FEM	Finite Element Method
HMA	Hot Mix Asphalt
GWT	Ground Water Table
LLAP	Long Life Asphalt Pavement
MEPDG	Mechanistic-Empirical Pavement Design Method
NCAT	National Center for Asphalt Technology
NCHRP	National Cooperative Highway Research Program
NDW	National Data Warehouse
OIA	Ontwerp Instrumentarium Asfaltverhardingen
PA/PAP	Porous Asphalt (Pavement)
RAW	Rationalisatie en Automatisering Wegenbouw
SB	Super Breedband (Super Broadband)

List of Figures

List of Tables

1. Introduction and literature review

1.1. Introduction

Since the very beginning of the development of pavement, parallel layer structures have traditionally been the foremost, if not the only, choice of road constructions. Whether it is a flexible, rigid or composite pavement, they all share a similar structure, which contains a top layer, base or subbase and subgrade [1] [9]. From this perspective, the structural design of a road is relatively simple and involves less risk to public safety than a building design. The thickness of each layer is therefore one of the most significant elements of the structural design of a pavement. The term “conservative” in the context of pavement design however, usually refers to economic risks of investing too much or too little, especially in materials, which transfer into the thickness and material selection of each layer. Over the past decades, various methods have been developed to determine the thickness of a pavement. They all more or less rely on some empirical functions which tend to lead to an over-design [23]. Even when a design method is not initially on the safe side, it can be calibrated in the field due to other unexpected failures by extra safety or in this case thickness design. Furthermore, a parallel layer structure requires the entire cross-section of the road to share a uniform thickness [9]. No matter how many lanes there are, the one bearing the heaviest traffic load always dominates the thickness design of the entire structure. Since modern traffic regulations are very strict about the use of each lane, especially for highways or motorways, theoretically there could be a huge material waste in those lanes with less traffic. This provides us with an opportunity to rethink the structural design of the pavement structure. By reducing the thickness of the less trafficked part, the asphalt layer specifically, even if only by millimeters, still a huge amount of material can be saved considering the large scale of a road in the longitudinal direction. The construction company can save a lot on material cost, as the asphalt layers usually contain the most expensive material. Besides, the reduction of the asphalt layer thickness is also eco-friendly because firstly, bitumen is a non-renewable resource; secondly, the production of asphalt binder consumes a huge amount of energy; and thirdly, certain countries, the Netherlands for example, are also in lack of aggregates [28]. The new structural design will be beneficial in economic, environmental as well as social perspectives.

This thesis will look into the possibility of a more economical and efficient structural design for flexible pavements. By using finite element analysis software, CAPA-3D more specifically, the performance, in both short-term and long-term, will be compared between the new design and the original design. After that, the feasibility of the construction of the new design using the existing equipment and machines will be discussed. This thesis therefore will offer an outlook of the potential of the new structural design in not only pavement design but also construction perspective.

1.2. Literature review

1.2.1. History of pavement structures

Pavements have been constructed for thousands of years. Different structure types in each period of time were developed to satisfy the current needs [1]. Pavements evolved with the invention and improvement of wheels and wagons. The Romans developed a pavement with layer system, which contains a top layer, base/subbase and subgrade [2]. They cobbled the roads with this layer system that was dependent on the subgrade. The layers underneath were in sequence from bottom to top of rubble stones, smaller stones, gravel with a sand layer and on the very top the large smoothed blocks of stone or lava is placed to provide a durable surface. The thickness of the each layer back then was significantly larger than pavements nowadays, plus the extreme large stiffness and durability of the materials they used such as lava and stone, which gave these roads a very long durable service time. Some of the roads even exist today after more than 2500 years.

Since then this parallel layer system has dominated the design of the road structure. The thickness of the pavement changed (reduced most of the times) as the invention and application of new materials occurred. In the late 18th and 19th centuries, pioneers such as Tresaguet and Macadam [3], strengthened the Roman road structure further. Their basic principle was to lay bigger stones first and then fill the gaps with smaller rocks. During this period the thickness of the pavement decreased dramatically compared to its predecessor.

The invention of automobile and rubber tyres triggered the introduction of tar to the pavement industry. The speed increasing of the vehicles started to draw the attention of driving safety on the pavement. Furthermore the rubber tires also “sucked” the dust from the pavement surface and loosen the stones causing blinding clouds of dusts. Hence by blending tar with sand and stone, a sort of

wearing course of the pavement was applied [4], which contributed a further reduction of the total thickness.

After entering the 20th century, with the development of powered vehicles and growth of traveling speed as well as the raising concern about comfort and safety, asphalt concrete (AC) began to play a major role in the pavement industry. The tremendous boost of traffic volume after World War II required a re-raising in the thickness of the asphalt layer, so did the total thickness of the pavement [5].

To sum up, through the history of pavement development, the pavement structure, particularly the thickness, evolved as the invention of new methods of traffic and construction material and techniques. For Romans and Greeks they used large blocks of stone to obtain durable and drainable pavement surface. To support the stone top layer, thicker and more stable sub-layers were required. Also back that time people built roads purely based on experience. For Romans such important transport networks required reliable, in this case, much thicker design. After 1800 people start to use finer aggregates for the pavement surface to acquire a smoother driving experience, as the speed of vehicles kept increasing. In this period the thickness of the pavement was dramatically decreased. After entering 20th century, especially after the 2nd World War, the weight and amount of traffic continued increasing, leading to a rising trend for the thickness design. Nowadays, the LLAP and PAP contain much thicker asphalt players in order to meet the designed long service lifetime. In conclusion, a U-shape trend of the thickness can be witnessed (figure 1.1). As for the present day the thickness of pavement has become relatively large [1].

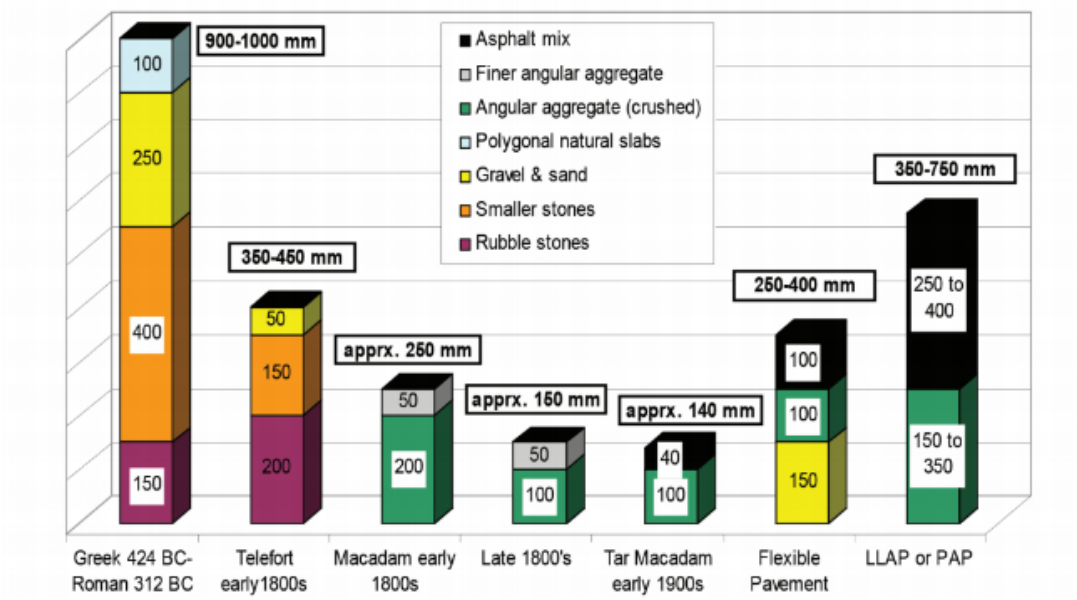

Figure 1.1 Historical evolution of typical cross-section of pavements [1]

1.2.2. Pavement structural design methods and software

Prior to the early 20th century, the thickness of pavement layers was purely based on experience [6]. The invention of automobile increased the travel speed and drawn more attention to the driving safety and comfort, which stimulated the society to treat road design more seriously. Hence the mechanistic design method, which links performance to material properties and failure mechanics, as well as the empirical-mechanistic design method were introduced. At the same time experiments were being developed to investigate binder with tar or natural asphalt [7].

The growing importance and development of car transport during and after the two World Wars required the pavement technology to take a further step beyond empiricism. The growth in traffic volume, tyre pressures as well as travel speeds led to a new requirement of the functional performance definition [8]. This definition became the foundation of the later service class which enables the road designers to link the costs with the desired performance. Besides, the rising demand of a better understanding and prediction of pavement performance, knowledge of its structural behaviour and its failure in time was required, which resulted in the AASHO (American Association of State Highway Officials) road test [9].

Through AASHO (was renamed as AASHTO later) road test, the relationship between pavement performance and loading was investigated for the first time [10]. Two main concepts were established, Present Serviceability Index (PSI) and load equivalency factor, which aimed to predict the serviceability of the road, represented by roughness, patch work, rutting and cracking, under the giving working conditions, particularly time and load [11]. This research helped develop a pavement design procedure to meet the growing demands of traffic. Although the AASHO study is almost 60 years old, many of its procedures and concepts are still used or have a great influence on the pavement design today, not only in USA but also the rest of the world [12].

The AASHTO design method, despite its ground-breaking systematic study on pavement deterioration, was highly dependent on empirical analysis [13]. Compared to its predecessors, the AASHTO design method indeed introduced a series of more accurate and complex regression equations to fit the performance of pavements under specific working conditions, such as traffic loading, climate and material properties, applied in the AASHO road test. This could lead to serious problems when users try to extrapolate the AASHTO method to other working conditions or pavement standards [9]. Furthermore, during the AASHO road test, the relationship between stress/strain and strength of materials was not established. However, this relationship is quite essential to enable users to estimate

pavement performance especially when new materials or structures, which have no data coming from field tests yet, are applied. Given all these drawbacks, a mechanistic based design method was developed to support the existing empirical method [14]. Stress and strain distribution in layered pavement systems were analysed, as well as their relationships with material properties, fatigue and permanent deformation. Up to this point, a mechanistic-empirical method had been established for pavement design [15].

Since then other studies continued to refine the results. Decades later, nowadays, the development of material characterization and modelling enable us to model pavement structures more and more accurately, especially by applying finite element software using non-linear viscoelastic models [16], to simulate and calculate the stress and strain distribution at any position, even under moving loads [17]. Furthermore, damage initiation and progression can also be taken into account as well as effects of joints, cracks and other geometry related issues [18]. Specialized software is also developed for pavement design and calculation, such as 3D-Move [19], CAPA-3D, Viscoroute [20] etc. All these methods can be used to help pavement design, though mainly for research purpose. Due to cost or regulation problem they are rarely used in practice.

1.2.3. Pavement distresses

A pavement, as a wearing structure, continually undergoes various types of loads, i.e. traffic, moisture, temperature etc. The loads induce stresses into the pavement structure and have a chance to lead to minor defects. As the time goes on, these minor defects accumulate gradually and evolve into different types of distresses that eventually lead to the failure of the pavement [21]. A number of categories of pavement distresses have been identified and defined, however, not all pavements will endure all of the distress types. Meanwhile, pavements also exhibit distresses in various severity levels [22].

A proper designed pavement should be able to fulfil its intended function through life time. Since it is not economically or technically feasible to analyse all types of distresses, most of the pavement design methods only choose limited representations as the reliability analysis criteria. For instance, in the Mechanistic-Empirical Pavement Design Guide (MEPDG) [15], rutting, load related cracking and non-load related cracking are chosen as three criteria to proceed incremental damage calculation. The Dutch design method, Ontwerp Instrumentarium Asfaltverhardingen (OIA), also regards the resistance against fatigue and permanent deformation as design criteria [23].

In both cases, the principal criterion for the fatigue or load related cracking of the pavement is the horizontal strain at the bottom of the asphalt layers. Cracking has many forms and causes, however, for the load related cracking, it has been widely accepted that the cracking occurs due to repeated tensile strains, of which the maximum one occurs at the bottom of the asphalt layers, especially when the layer is placed on an unbound base [24]. This is the so-called bottom-up fatigue cracking. Once the crack initiated at the bottom of asphalt layer, it propagates upwards, gradually weakens the pavement and eventually reached the surface and results in failure of the structure.

The principal criterion for permanent deformation is the vertical strain at the top of the subgrade [23]. Permanent deformation, such as rutting, is believed to be mainly caused by the subgrade deformation which is a result of accumulation of permanent strain throughout the entire pavement structure. The Dutch design method determines that if the vertical strain at the top of subgrade, in some cases unbound base as well, is below a certain value, excessive subgrade deformation will not occur, hence the chance of subgrade related deformation at the surface of pavement will be diminished. With the development of the technology and knowledge, it becomes more and more widely accepted that the rutting depth of the pavement is an accumulation of the deformations in all layers, from top to bottom, of the entire pavement structure [52].

1.2.4. Traffic distribution

The primary purpose of a pavement is to support vehicles, whose type and volume have a significant impact on pavement design. Vehicles, or traffic, is expressed by two major parameters: the amount and their axle load classes. In short, pavement design requires a prediction in the amount of loading that a pavement will receive during its life time. The loading can be a mixture of passenger cars and trucks. In most of the design methods, vehicular traffic loads are transferred into axle loads for the sake of easier calculation [25]. Knowing the estimate amount and loads distribution of traffic flow is the cornerstone of the pavement design procedure. Unfortunately, these axle loads can vary significantly depending on the type of vehicles. To simplify this variability, the concept of ESAL is introduced. ESAL, short for Equivalent Single Axle Load, is to equal all the axle weights to one common or equivalent axle, usually 18,000 pounds (80kN) in the US design method [15] while 100kN in the Dutch design method [23]. However, it is noticeable that as the development of modern design software, the applicability of ESAL may differ in different calculation conditions.

A pavement is a parallel layer structure with a uniform thickness along the cross section. For a multi-lane road, a design lane is chosen to undergo the design procedure [26]. Due to traffic regulations and

driving habits, the traffic on a road almost never distributes on each lanes evenly [27]. For a higher standard road, a motorway in particular, the difference between lanes' axle number can be quite big. Obviously, the design lane is the lane where the largest number of ESAL occurs, which is usually the outermost lane of a multi-lane road. In the Dutch design method, a correction factor for multi lanes is introduced. By definition, it determines that when Stroomwegen contains 3 or more lanes, 90% of the total axle loads will be experienced by the design lane [23]. This leads to an unfortunate result that all the other lanes have to share the same structural thickness of the heavy traffic lane, which can be considered as a non-ignorable over-design, since in reality the traffic load level as well as amount of other lanes are both significantly lower than the heavy traffic lane's. Although the thickness of asphalt layers is relatively small compared to other civil engineering structures, there still could be a huge amount of material waste considering the large scale of a road in the longitudinal direction. This provides us with an opportunity to rethink the structural design of the pavement structure.

1.2.5. Conclusions

The following conclusions can be drawn from the literature review:

- Throughout the history of pavement, the thickness of layers changed. Since the first introduction of asphaltic material, the thickness of the asphalt layers have continuously increased till today.
- The parallel-layer system is the foremost, if not the only, choice for pavement structural design.
- Currently most of the pavement design methods are mechanical-empirical methods. The procedures of pavement response calculation and distresses evaluation have been developed based on field tests as well as mechanical theories applied on parallel-layer pavement structures.
- Neither the amount nor the load classes of traffic flow distribute evenly on all the lanes of a road. However the entire pavement structure is designed to share a uniform thickness of the chosen design lane which bears the largest traffic loads.

The literature review clearly indicates that there could be a considerable amount of material waste in the less trafficked part of the pavement. By reducing the thickness of the less trafficked part, especially for the asphalt layer, a considerable amount of material cost can be saved, as the asphalt layer usually contains the most expensive materials. Besides, the reduction of the asphalt layer thickness is also eco-friendly because firstly, bitumen is a non-renewable resource; secondly, the production of asphalt

binder consumes a huge amount of energy; and thirdly, certain countries, the Netherlands for example, are also lack of aggregates [28]. The new structural design will be beneficial in economic, environmental as well as social perspective.

1.3. Approach and research methodology

In this section the aim of this thesis is elaborated as well as the methodology applied to fulfil these targets. Besides, a brief outline of this thesis is presented.

1.3.1. Research objectives

This research aims at investigating the possibility of reducing the thickness of pavement layers, especially the asphalt layers, to save construction materials without compromising the performance, both short-term and long-term, of the entire road. Preferably a specific new designed pavement structure will be proposed. This structure will need to be proved to hold the same serviceability according to the current design standards. Finally the feasibility of construction and maintenance should also be discussed. Ideally the new designed pavement structure can be achieved by using the existing construction equipment and machines.

1.3.2. Research methodology

Currently most of the pavement design methods and software are based on a parallel-layer system. However for the new designed pavement structure there could be a big possibility that an odd shaped design would be proposed. Hence the finite element analysis software is introduced to perform the strain and stress responses calculation. All the needed data for modelling and simulation will be determined in advance. A model of original pavement structure design is also established for comparison.

The same pavement performance prediction procedures of the current Dutch design method will be used here to evaluate the serviceability of both original and new designed pavement structures.

Taking advantage of the FEM software, a real-life long-term simulation will also be executed. The resilient strain data acquired from this test can also be used in the rutting depth calculation following the American design method (MEPDG).

The construction and maintenance feasibility of the new designed pavement structure will be discussed based on an industry research and investigation on existing equipment and machines.

1.3.3. Thesis outline

This thesis will contain six chapters:

Chapter 1 provides a general introduction and background of this research, including the development of pavement structure as well as design methods and software, a brief summary of pavement distress, and uneven traffic distribution. The motivation and objectives of this research are also given in this chapter.

Chapter 2 proposes a newly designed pavement structure based on the traffic data analysis and thickness design by Dutch pavement design software OIA. The parameters preparation, including traffic loading, material and time input, for the finite element model is made here. Two models, both original and new designs, are established by the end of this chapter.

Chapter 3 executes the simulations under all axle load classes and tire types combinations and acquires all the corresponding strain and stress responses. The strain patterns are analysed. The performance predictions, including fatigue and permanent deformation, are also performed and discussed in this chapter.

Chapter 4 establishes two real-life long-term simulations for the two pavement structures. The resilient strains carried out form the simulation are used as input for the rutting depth calculation. Besides, a basic simulation of truck platooning is also executed.

Chapter 5 discusses the feasibility of constructions and maintenance using existing equipment and machines. Advice on future expanding is also given in the last section of this chapter.

Finally, chapter 6 provides the conclusions that have been derived from the earlier chapters and some recommendations for the future study.

2. Model design and generation

Ideally the new pavement structure design will reduce the thickness of the asphalt layers of lightly trafficked lanes without compromising the performance of the entire road. Therefore two pavement models, for both the original and new pavement stricture designs, will be established and punished under same circumstances to evaluate and compare their performances.

2.1. Preliminary design

To seek a possible new design for the pavement structure, the traffic data of a specific section of a real motorway is chosen and analysed. Then an original pavement structure can be determined following the current design method and standard. Based on this a potential new design for the pavement structure is proposed.

2.1.1. Traffic data analysis

In the Netherlands, the National Data Warehouse for Traffic Information (NDW) is an organisation that provides an enormous database of both real-time and historical traffic data [29]. In this thesis, 2 types of traffic data files provided by NDW are chosen for analysis:

The first one is an overall look of the traffic distribution on a particular road. It contains not only the total number of the vehicles on both directions, but also the traffic amount on every single lanes. Furthermore, the percentages of passenger cars, light trucks and heavy trucks are also provided in this file.

The second file takes a closer look at the traffic condition of the heavy traffic lanes. The heavy traffic lanes usually are the most outside lanes. For a road containing 5 lanes per direction, the 4th and 5th lane are determined as the heavy traffic lanes. Three sub-sections are included in this file. To begin with, the total amount of vehicles per direction is listed and further classified by tonnage and vehicle category. A 7-class system is used by NDW, where Class 1 represents passenger cars, Classes 2 to 6 represent trucks and Class 7 represents motorcycles. The vehicle tonnages are counted by every 2 tons from 0 to 80 tons with an extra level of over 80 tons. Next, the axle tonnages are summarized. In this section, only axle tonnages that are bigger than 1 ton are counted. Here axles are also divided into

three categories, namely single axle, tandem and tridem. Combined with the total number of trucks acquired from the first section, the average axle number per truck can be calculated. In the last section a calculation of the average truck injury factor is performed. In the Dutch design method, a single axle load of 100kN is chosen as the ESAL. Following the given equation the axle loads of all trucks are transferred into ESALs. The ratio between the transferred ESALs and total amount of trucks is average truck injury factor.

In this thesis, the traffic data acquired from an observation point between Exit 3 and 4 on Rijksweg A2 is chosen to be analysed. This observation point is located between Amsterdam and Utrecht which is one of the busiest motorways in the Netherlands. The section between interchanges Holendrecht and Oudenrijn has been expanded to 5 traffic lanes in each direction [30]. It can be very representative of the busiest traffic situation in the Netherlands. Since the future expansion or construction of new road should also be in such areas, the traffic data will provide the current as well as a potential future traffic development that should be the background of this thesis.

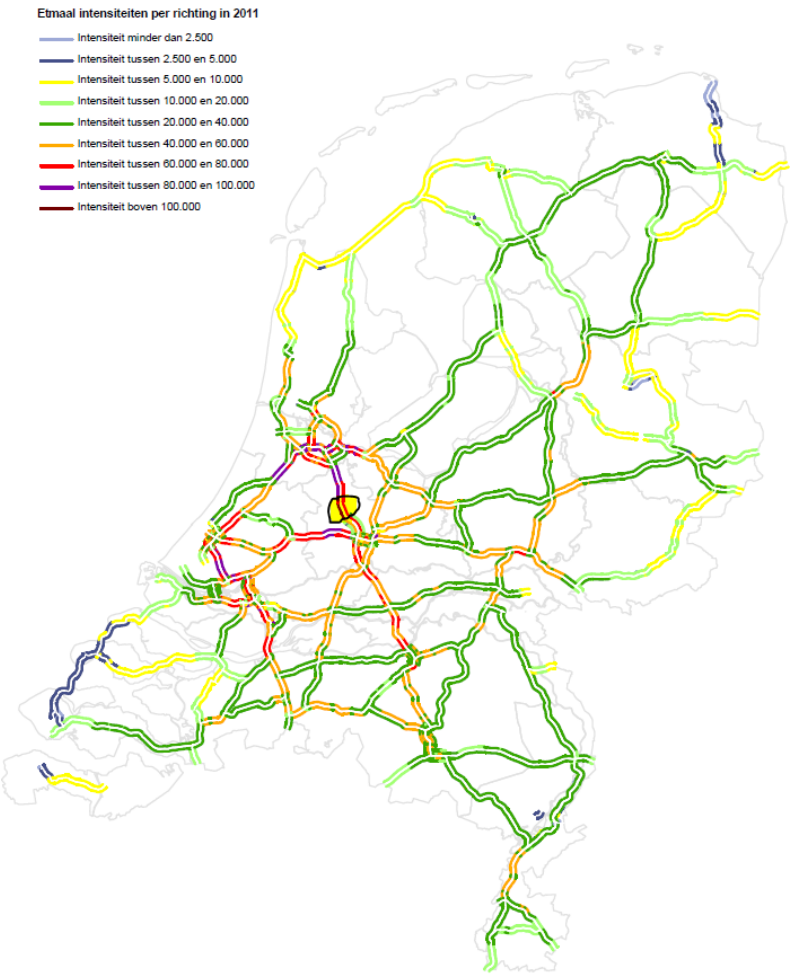

Figure 2.1 Traffic intensities of Dutch motorways in 2011 (black circle is A2 Holendrecht Oude Rijn) [66]

As for the time period, the daily average traffic data of year 2015 (the yearly traffic data analysis was finished in late 2016) is chosen for the overall analysis of the entire road (5 lanes per direction) while the monthly traffic data of January 2015 is used for the analysis of the heavy traffic lanes, namely Lane 4 and 5. (Due to the time limited time and resource, only traffic data of January is analysed in this thesis to investigate the daily traffic distribution. However, future detailed traffic analysis for different month is recommended.)

Direction	Lane No.	Traffic Intensity	Percentage (%)		Amount		Trucks		Passenger Cars	
			Light trucks	Heavy trucks	Light trucks	Heavy trucks	Total number	Percentage (%)	Amount	1/ 10000
R	1	9,416	1.13	0.07	107	6	113	1.49	9,303	1
	2	18,372	1.75	0.12	321	22	343	4.52	18,029	2
	3	22,596	2.51	0.30	567	67	634	8.35	21,962	2
	4	23,183	4.58	1.52	1061	353	1415	18.63	21,768	2
	5	24,982	8.55	11.81	2137	2951	5087	67.01	19,895	2
	Sum						**7593**	100.00	90,956	**9**
L	1	8,065	1.09	0.05	88	4	92	1.18	7,973	1
	2	17,069	1.69	0.09	288	16	304	3.94	16,765	2
	3	23,369	2.16	0.24	505	55	560	7.25	22,809	2
	4	27,530	4.11	1.12	1132	307	1439	18.64	26,091	3
	5	24,696	9.17	12.40	2264	3063	5327	68.99	19,369	2
	Sum						**7722**	100.00	93,007	**9**

Table 2.1 Data analysis for daily traffic flow between Exit 3 and 4 on Rijksweg A2

From the first file it can be easily observed that the traffic flow does not distribute over the lanes evenly. Generally speaking, the outside lanes (Lane 3, 4 & 5) bear more traffic flow than inside ones (Lane 1 & 2). Further calculation shows that different types of vehicles also distribute differently over 5 lanes. To be specific, the majority of heavy trucks run on the most outside lane (Lane 5) while light trucks run mainly on both Lane 4 and 5. On contrary, when considering the "10000 rule", the passenger cars more or less spread evenly over 5 lanes.

In most of the pavement design methods, the impact of the passenger cars to the pavement is usually neglected. It is commonly agreed that the impact of 10,000 passenger cars can be simply considered equal to the impact caused by 1 truck [31]. Even if there are 100,000 passenger cars per day per

direction, when they are transformed into trucks, which is 10 per day, the number is so small that can be neglected comparing to the huge daily truck flow. In the Dutch design method, only axles with a load more than 20kN are counted. Therefore in the second file, the distribution of single axle loads on Lane 4 and 5 is exhibited. For both directions, approximately 75% of the axles are running on the Lane 5 while the other 25% are taken by Lane 4.

Direction	Lane No.	ESALs	Percentage
R	4	302,281	**24.05%**
	5	954,741	**75.95%**
	Total	1,257,022	
L	4	346,456	**24.91%**
	5	1,044,552	**75.09%**
	Total	1,391,008	

Table 2.2 Daily ESALs distribution on lane 4 and 5 between Exit 3 and 4 on Rijksweg A2

2.1.2. Thickness design by the Dutch standard software

Ontwerpinstrumentarium asfaltverhardingen (OIA) is the latest standard software for asphalt pavement design in the Netherlands based on the new design code of Rijkswaterstaat [32]. It is widely used by Dutch contractors to evaluate new designed pavements. OIA will provide an adequate thickness design for all the layers in the pavement structure based on a given input. As discussed earlier in chapter 1.2.4, in OIA, when there are more than 3 lanes in each direction, in this case 5 lanes, the right hand lane will be chosen as design lane and assigned 90% of the total traffic volume. To reduce the thickness of lower traffic lanes, the pavement thickness design should be performed individually for each lane. With the traffic data analysed in chapter 2.1.1, the thickness design for each lane can be addressed via OIA according to its own traffic volume. The results are shown below and indicate that there is indeed a great potential of reduction in asphalt layers' thickness.

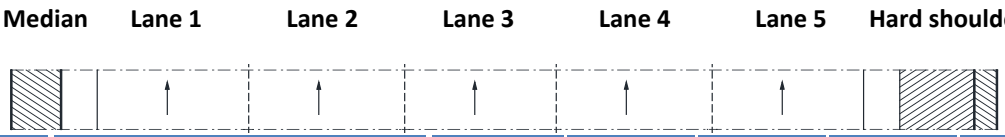

Direction	Lane No.		1	2	3	4	5
R	Truck amount		113	343	634	1415	5087
	Percentage		1.49%	4.52%	8.35%	18.63%	67.01%
	Thickness (mm)	PA layer	50	50	50	50	50
		AC layer 1	55	70	80	55	70
		AC layer 2	59	74	81	60	80
		AC layer 3	0	0	0	71	79
		Unbound base	300	300	300	300	300
		Total	464	494	511	536	579
L	Truck amount		92	304	560	1439	5327
	Percentage		1.18%	3.94%	7.25%	18.64%	68.99%
	Thickness (mm)	PA layer	50	50	50	50	50
		AC layer 1	55	70	80	55	70
		AC layer 2	54	70	78	60	80
		AC layer 3	0	0	0	71	81
		Unbound base	300	300	300	300	300
		Total	459	490	508	536	581

Table 2.3 Thickness design for individual lanes by OIA

A stair-step shaped design can be easily established based on the individual lane layer thickness calculations. To ensure an even surface, a reversed stair structure is proposed by accordingly increasing the thickness of unbound base layer of each lane. However, it can also be easily predicted that a severe stress concentration may occur at the edges (see the red circles in figure 2.2). Ideally smoother (curved) transitions should be placed between two lanes, however this solution is neither practicable nor economical from the construction perspective. Therefore, a slope shaped design is proposed in this thesis.

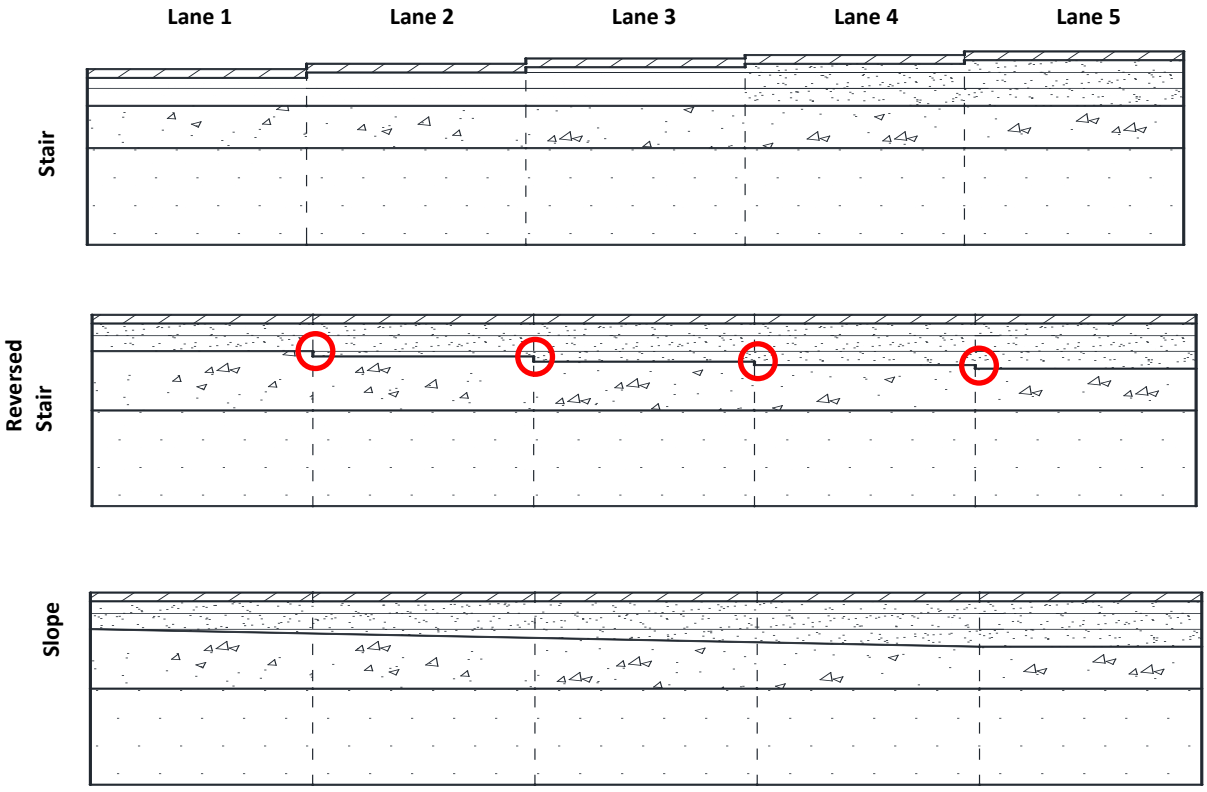

Figure 2.2 Development of the new pavement structural design

2.2. Model design

As discussed in chapter 1, all the current pavement design methods are based on a parallel multi-layer structure assumption, so is the design software. In section 2.1, a slope shaped new design has been proposed, which contains un-parallel layers. Hence traditional design methods are no longer applicable here. As a result, a finite element method (FEM) is introduced in this thesis. A FEM software, CAPA-3D, is used for the strain and stress calculation as well as long-term deformation simulations.

CAPA-3D is a three dimensional finite elements based research tool [33]. Like all the FEM software, the run time and the calculation precision are highly influenced by the dimension and fineness of the mesh. The bigger and finer a mesh is, the longer run time it will take and produce a more precise result. Therefore a proper model has to be established to gain a balance between time consumption and precision of the results.

2.2.1. Number of lanes and dimensions

The Handboek wegontwerp is a design manual published by CROW. It provides guidelines for traffic facilities design outside urban areas in the Netherlands. In its first part, Basiscriteria, a standard layout of a stroomweg (Dutch motorway) is presented, which contains 2 lanes per direction with 1 emergency lane [34].

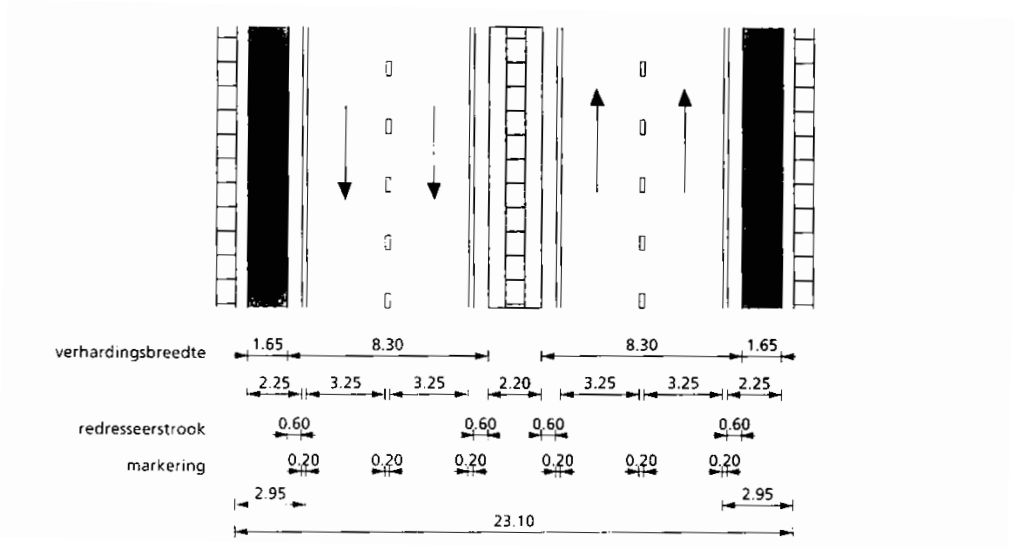

Figure 2.3 Typical dimension design for a Dutch 2×2 motorway [34]

In the previous chapter the traffic data of a 2×5-lane road was used for analysis. However, the scale of a 2×5-lane road plus 1 additional emergency lane can be too time consuming for the finite elements analysis, also the 5-lane motorways do exist in the Netherlands but they are not the standard. Instead, a 2×3-lane layout is proposed. This model not only represents the light and heavy truck traffic lanes, but also provides an overall view of the strain and stress condition along the entire road cross section by adding a passenger car lane and emergency lane. The total transverse width of the model is 15 metres.

A road can be seen as an infinite structure in the longitudinal direction. Thus for a finite element model the length ceiling also should be limited. In addition, a minimum length also has to be determined to minimize the edge effect. Several simple trials were performed during the preliminary research. The results show that for a typical tyre print the influence area for strain and stress of under layers is within 5 metres diameter. Therefore a model with the length of 6 metres in the direction of traffic was selected such that one full passage of the truck on the pavement can be achieved to obtain a complete longitudinal tensile strain response curve including the expected compression-tension-compression sequence [35] which will be further discussed in the next chapter.

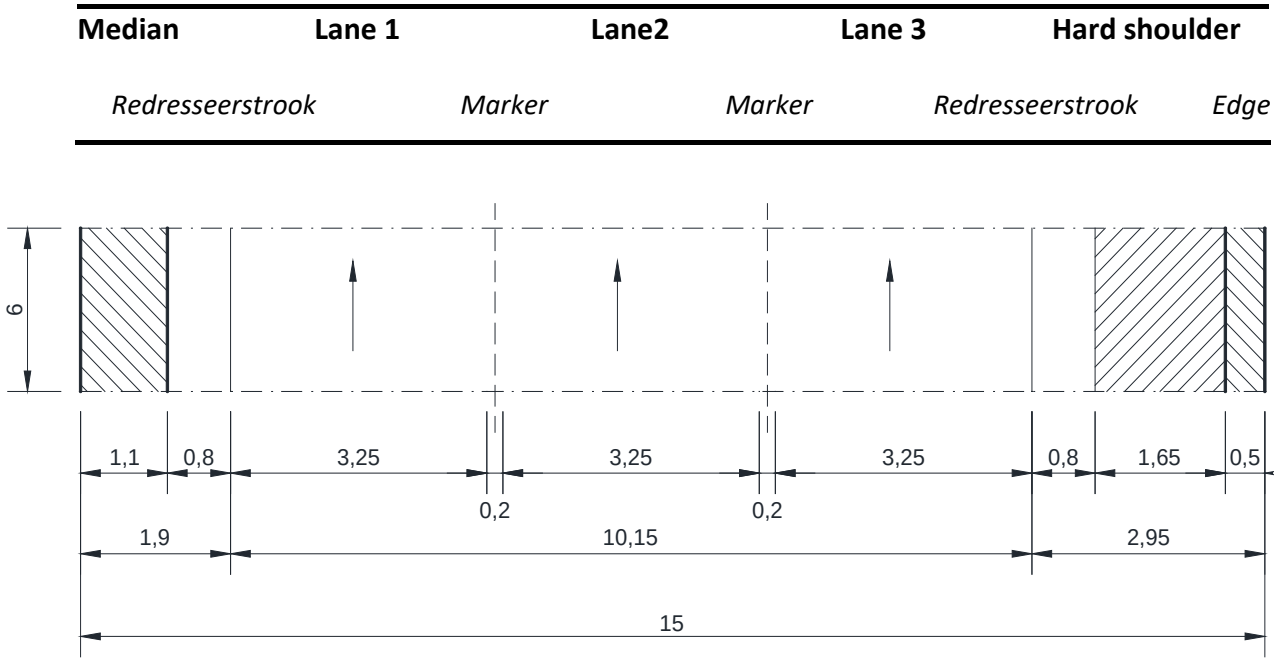

Figure 2.4 Dimension design of the model (Top view, m)

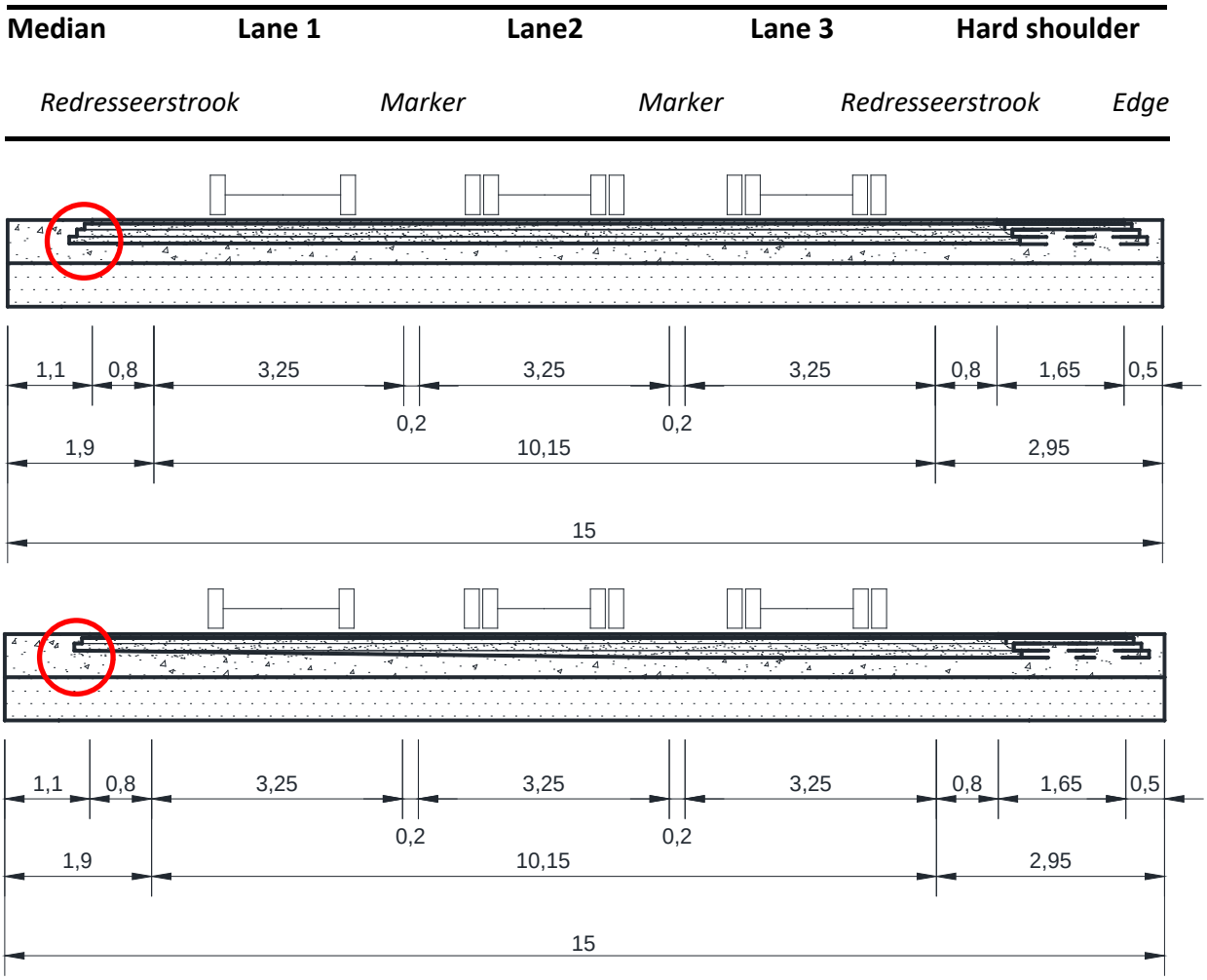

Figure 2.5 Original (up) and New (down) dimension design of the model (Cross section, m)

As for the thickness design, since the number of lanes is reduced, the vehicles running on the 5-lane road are re-distributed on 3 lanes. The previous traffic data analysis in chapter 2 indicates that the axle load gross ratio between the heavier traffic lane and the lighter traffic lane is around 3:1, in other words 75% and 25% respectively. However, the axle load analysis only include the trucks of the 4th and 5th lane, therefore in this thesis, an adjustment has been applied to the traffic distribution. The result is shown in table below.

Traffic Distribution	Daily Amount	Lane No.	Percentage	Amount
Original	7800	3	75%	5850
		2	25%	1950
Adjusted		3	**73%**	**5694**
		2	**27%**	**2106**

Table 2.4 Adjusted daily truck traffic distribution

Comparing the new traffic data to the original data used in the software design, an approximation of the asphalt layer thickness can be estimated. The final thickness design for the heavy traffic lane is composed of one PA layer (50mm), three AC layers (75mm, 80mm and 80mm), one unbound subbase layer (300mm) and one subgrade layer.

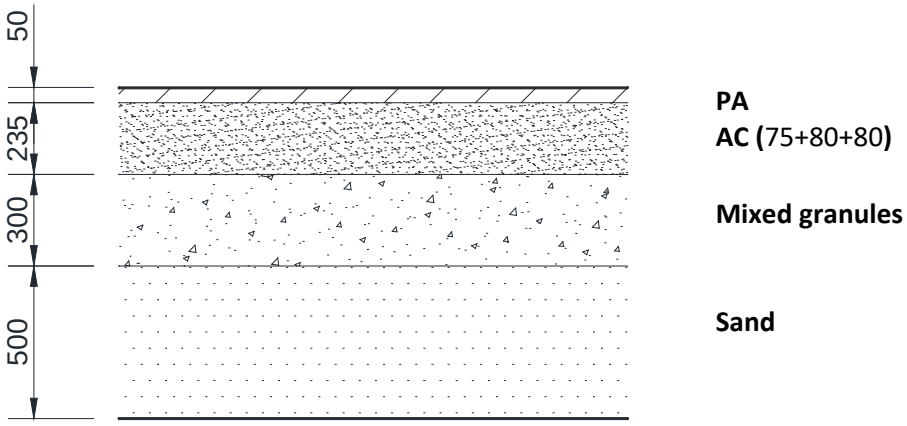

Figure 2.6 Pavement layer thickness design (mm)

The boundary conditions are also required to be determined in advance. It is assumed that there is neither vertical nor horizontal movement at the bottom of the finite elements model, hence the bottom of the model was completely restrained. As to the four vertical surfaces, their horizontal movement perpendicular to the perimeters is also restrained whilst the remaining two directions were considered free, in other words each vertical surface is given two degrees of freedom. In total there are 7 restraints applied to the model. According to the Dutch design method [23], all the layers in the pavement are considered fully bounded, which means the interfaces between different layers are assumed to be tied together without any relative movement.

To optimize a balance between time consumption and result precision, a reasonably refined mesh should be found. The model is divided into several finer mesh parts close to the loading area and coarser mesh parts away from it. Analogously, the area required to produce more output data is also finer than others, for instance, the upper layers, namely the asphalt layers, are divided into more sub layers than the lower substructure.

The final model has a dimension of 15 m × 6 m × 1.085 m with a mesh of 46,000 elements (66 super elements). By calculation the new pavement structure will save approximately 10% of the AC material.

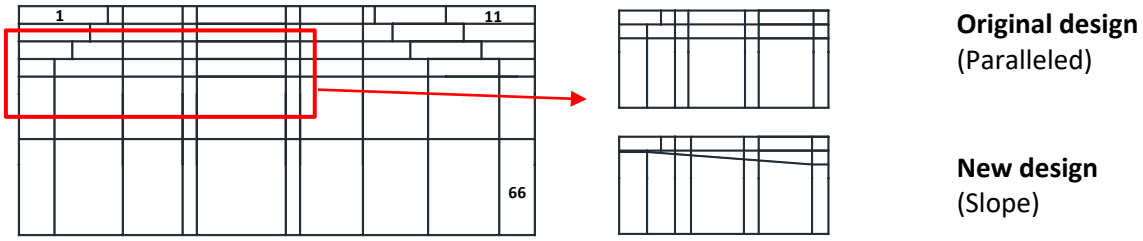

Figure 2.7 Super elements and slope creation

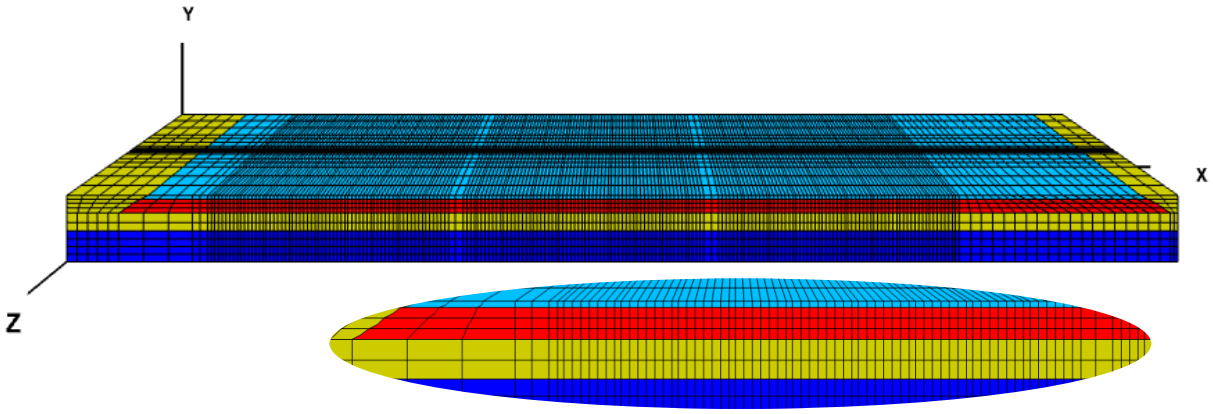

Figure 2.8 Final mesh of original design

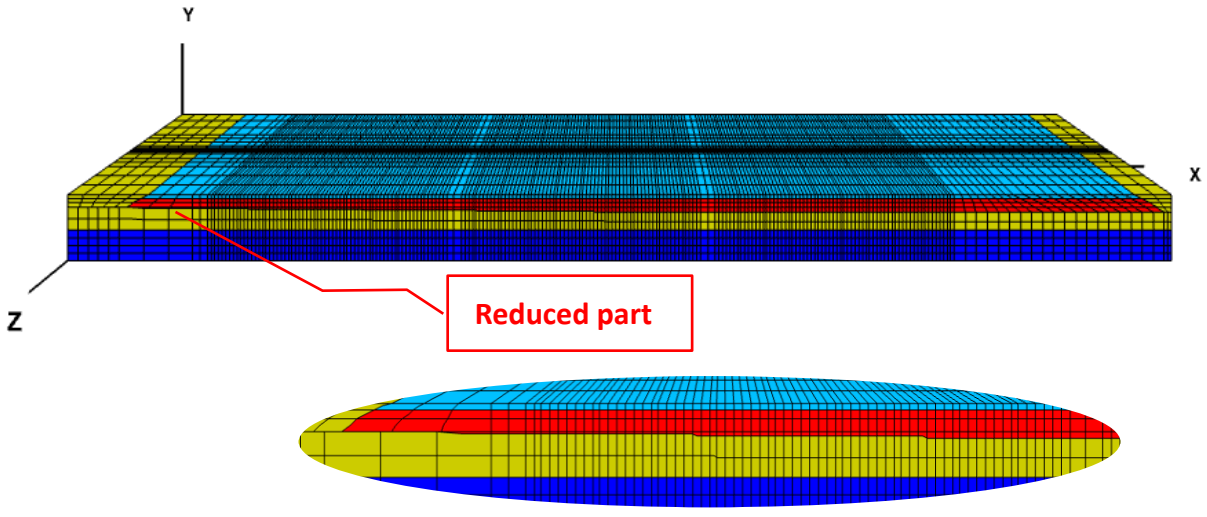

Figure 2.9 Final mesh of new design

2.2.2.Materials

In the Dutch design method, all construction materials are treated as elastic solids, including asphalt [23], although in reality asphalt materials behave viscoelastically. Many pavement analysis methods

have been developed based upon the viscoelastic characterization of asphalt material to calculate strain response and deformation. In this thesis, a rutting calculation following the American standard (Mechanistic-Empirical Pavement Design Guide, MEPDG) is performed for comparison. It requires the introduction of viscoelasticity to the asphalt material.

The viscoelasticity of asphalt can be simply seen as a time-dependent behaviour between stress and strain. The key to simulate the real behaviour of asphalt materials is a proper model of their stress-strain relationship, which can be simulated by a mechanical model consisting of elastic components (spring) and viscous components (dashpot). In CAPA-3D, a Generalized Maxwell model, also known as Wiechert model [36], is employed. It is composed of one single spring and multiple Maxwell components connected in parallel as shown in figure 2.10. Each spring is assigned a relaxation modulus E while each dashpot is assigned a frictional resistance η. The modulus of the Generalized Maxwell model can be expressed as below.

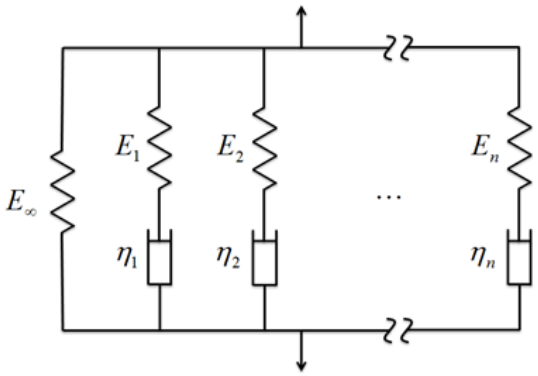

Figure 2.10 Generalized Maxwell model [37]

$$G'(\omega) = G_\infty + \sum_{i=1}^{N} \frac{\omega^2 \tau_i^2 G_i}{\omega^2 \tau_i^2 + 1} \tag{2.1}$$

Where,

$G'(\omega)$ = Storage modulus (Pa)

G_∞ = Long term modulus (Pa)

N = Relaxation modes (-)

ω = Angular frequency (rad/s)

τ_i = Relaxation time (s)

G_i = Prony coefficients (Pa)

Equation 2.1 is also known as Prony series [38]. In this thesis, two viscoelastic materials are used, namely porous asphalt (PA) and asphalt concrete (AC). Both materials are tested in the laboratory and translated into stiffness master curves. In CAPA-3D, the Prony series are converted into 4 parameters to represent the material properties.

$$\mu = G^* \tag{2.2}$$

$$\lambda = \frac{2\nu}{1-2\nu} G^* \tag{2.3}$$

$$\eta = \tau E = 2\tau G^* (1+\nu) \tag{2.4}$$

$$\eta_{vol} = \eta_{dev} = \frac{4}{9}\eta \tag{2.5}$$

Where,

μ, G^* = Shear modulus (Pa)

λ = Lamé's first parameter (Pa)

ν = Poisson's ratio (-), set to 0.35

τ = Relaxition time (s)

η, η_{vol} & η_{dev} = Viscosity parameters (Pa·s)

By substituting the data into equation 2.1 to 2.5, the Prony series of the two materials can be obtained.

i	τ (s)	G_i (Pa)	ν (-)	μ (Pa)	λ (Pa)	E (Pa)	η (Pa·s)	η_d (Pa·s)	η_v (Pa·s)
1	2.12E-01	3.50E+09	3.50E-01	**1.32E+09**	**3.09E+09**	3.58E+09	7.57E+08	**3.36E+08**	**3.36E+08**
2	2.18E-04	2.44E+09	3.50E-01	**5.45E+09**	**1.27E+10**	1.47E+10	3.21E+06	**1.43E+06**	**1.43E+06**
3	3.96E-06	2.44E+09	3.50E-01	**2.99E+09**	**6.97E+09**	8.07E+09	3.19E+04	**1.42E+04**	**1.42E+04**
4	2.12E-07	2.44E+09	3.50E-01	**2.99E+09**	**6.97E+09**	8.07E+09	1.71E+03	**7.62E+02**	**7.62E+02**
5	5.92E-03	2.10E+09	3.50E-01	**2.74E+09**	**6.40E+09**	7.40E+09	4.38E+07	**1.95E+07**	**1.95E+07**
∞		7.10E+03	3.50E-01	**2.95E+02**	**6.87E+02**	7.95E+02			

Table 2.5 Material parameters (Prony series) of porous asphalt (PA)

i	τ (s)	G_i (Pa)	ν (-)	μ (Pa)	λ (Pa)	E (Pa)	η (Pa·s)	η_d (Pa·s)	η_v (Pa·s)
1	2.44E-02	2.44E+09	3.50E-01	**2.44E+09**	**5.70E+09**	6.60E+09	1.61E+08	**7.15E+07**	**7.15E+07**
2	4.19E-03	2.44E+09	3.50E-01	**2.44E+09**	**5.70E+09**	6.60E+09	2.77E+07	**1.23E+07**	**1.23E+07**
3	1.19E-01	2.44E+09	3.50E-01	**2.44E+09**	**5.70E+09**	6.60E+09	7.88E+08	**3.50E+08**	**3.50E+08**
4	2.23E-01	2.10E+09	3.50E-01	**2.10E+09**	**4.89E+09**	5.66E+09	1.26E+09	**5.62E+08**	**5.62E+08**
5	1.38E-02	1.56E+09	3.50E-01	**1.56E+09**	**3.65E+09**	4.22E+09	5.85E+07	**2.60E+07**	**2.60E+07**
6	4.19E-03	8.83E+06	3.50E-01	**8.83E+06**	**2.06E+07**	2.38E+07	9.99E+04	**4.44E+04**	**4.44E+04**
∞		4.28E+09	3.50E-01	**4.28E+10**	**1.00E+11**	1.16E+11			

Table 2.6 Material parameters (Prony series) of asphalt concrete (AC)

A static creep test is done in CAPA-3D. The specimen is a 100×100×100 mm^3 cube. A 200 MPa load is applied onto the specimen for 1 hour. At the end of that 1 hour, the load is removed to allow the specimen to rebound for 10 minutes [39]. The creep test results are shown in figure 2.11–2.14. It can be witnessed that the two material models do show a time-dependent strain-stress behaviour and are capable of representing the viscoelasticity of the asphalt materials.

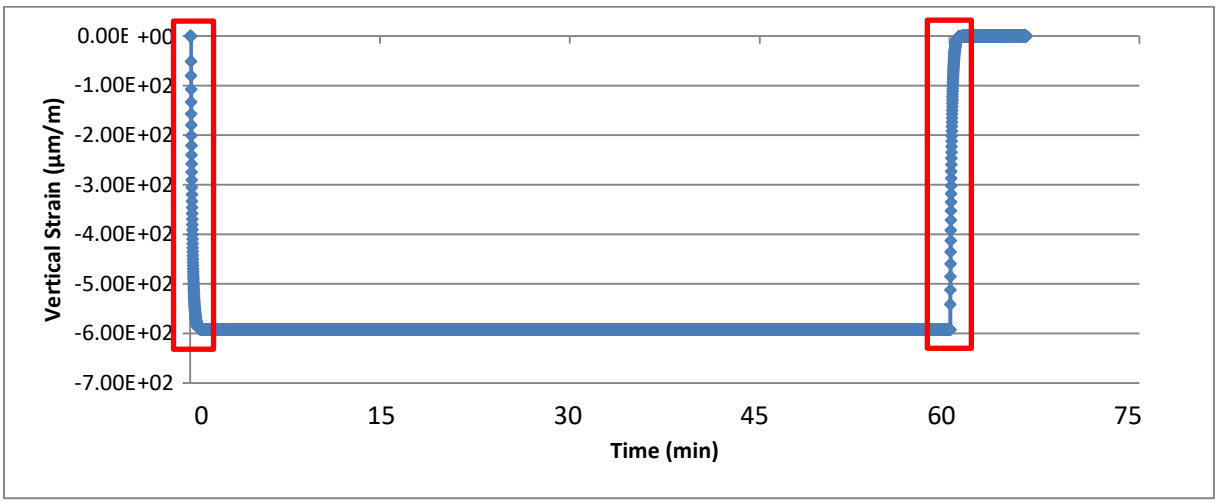

Figure 2.11 1-hour static creep test of porous asphalt (PA)

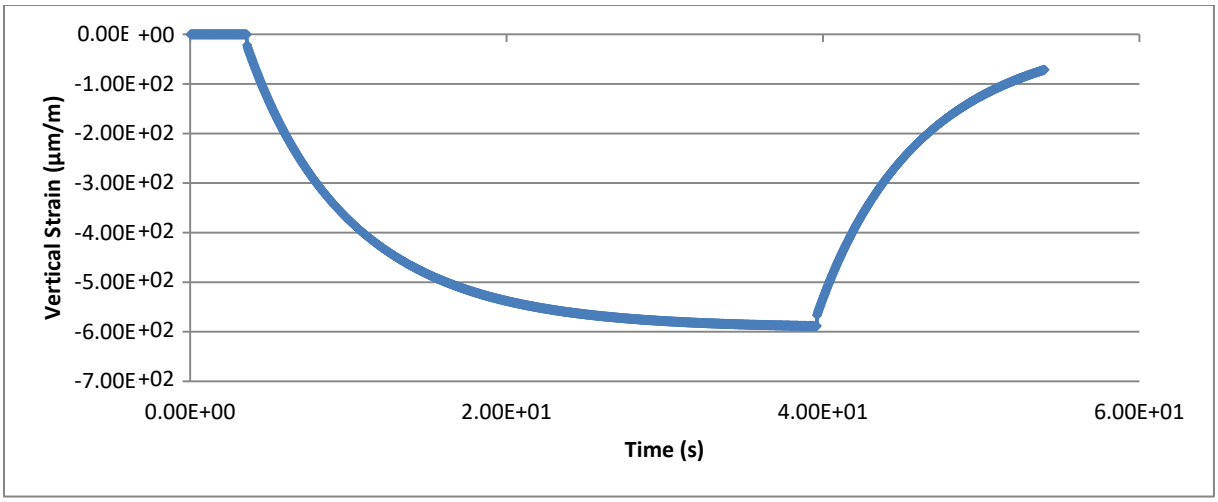

Figure 2.12 First 40 seconds of loading and first 14 seconds of unloading of figure 2.10 (PA)

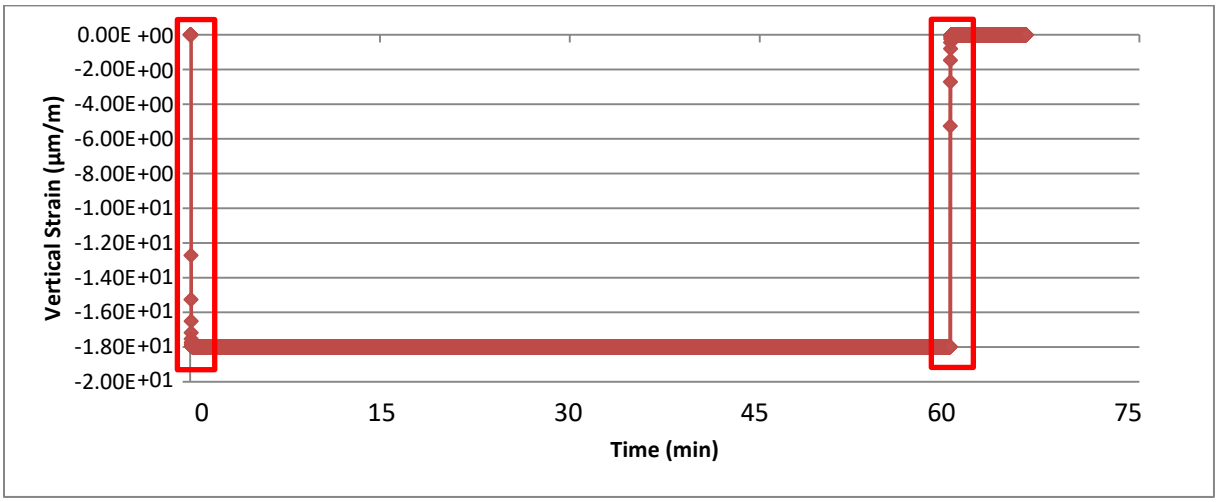

Figure 2.13 1-hour static creep test of asphalt concrete (AC)

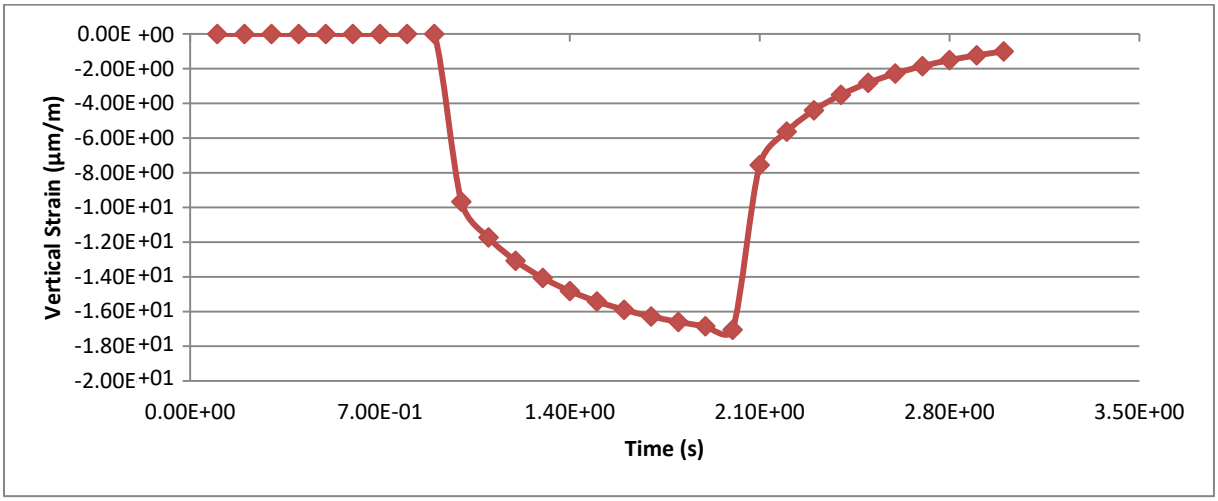

Figure 2.14 First 2 seconds of loading and first 1 second of unloading of figure 2.12 (AC)

2.2.3.Tire prints

In The Dutch design method, four types of tires can be used for design calculation, namely single tire (EL), dual tire (DL), broadband (BB) and super broadband (SB). The nominal dimensions of the contact area of these four tires are determined. The dimension of a tire print depends on the load that is exerted on it. For all the different loads, the width of the tire print remains substantially constant while the length changes correspondingly [23]. The following procedure is used to determine the rectangular contact area of a tire under a certain load. In OIA, the rectangular contact area is then converted into an equivalent circular area for the strain calculation. However, in CAPA-3D, a rectangular shaped load is much easier to apply and more accurate to the real contact condition. Therefore in this thesis the last step of conversion is abandoned.

$$A_{band} = \beta \cdot 1000 \cdot {}^{F_{normal}}/_{\sigma_{normal}} \tag{2.6}$$

Where,

A_{band} = Contact area of the tire (mm^2)

β = Factor depending on the load

F_{normal} = Normal tire load (kN)

σ_{normal} = Normal pressure (MPa)

	Single tire (EL)	Dual tire (DL)	Broadband (BB)	Super Broadband (SB)
Normal axle load (kN)	70	120	100	115
Normal wheel load (kN)	35	30	50	57.5
Wheel width (mm)	200	200	300	400
Normal contact pressure (MPa)	0.75	0.8	0.85	0.95
Centre-to-centre distance (mm)		315		

Table 2.7 Tire types and contact area data

The actual load of individual tire for single tire (EL), broadband (BB) or super broadband (SB) is determined using equation 2.7:

$$F_{band} = 0.5 \cdot F_{axle,i} \tag{2.7}$$

Where,

F_{band} = Actual tire load (kN)

$F_{axle,i}$ = Design value of the single axle load of axle load class i (kN)

The actual load of individual tire for dual tire (DL) is determined using equation 2.8:

$$F_{band} = 0.25 \cdot F_{axle,i} \tag{2.8}$$

Where,

F_{band} = Actual tire load (kN)

$F_{axle,i}$ = Design value of the single axle load of axle load class i (kN)

The factor β is determined by equation 2.9:

$$\beta = 1 + 0.59454 \cdot B_{eq} - 0.10182 \cdot {B_{eq}}^2 \tag{2.9}$$

Where,

β = Factor determined by the load (-)

B_{eq} = Equivalent load (-)

For the determination of equivalent load:

$$B_{eq} = \frac{F_{band}}{F_{normal}} - 1 \tag{2.10}$$

Where,

B_{eq} = Equivalent load (-)

F_{band} = Actual tire load (kN)

F_{normal} = Normal tire load (kN)

Hence the contact pressure can be determined:

$$\sigma_{band} = \frac{F_{band}}{A_{band}} \tag{2.11}$$

Where,

σ_{band} = Actual contact pressure (MPa)

F_{band} = Actual tire load (kN)

A_{band} = Contact area of the tire (mm^2)

OIA provides several standard axle load spectra according to the Dutch road design guide, as well as tire band spectra. For the motorway design, the heavy axle load spectrum of Rijkswaterstaat has been

chosen for the analysis [32]. All the axle loads are divided into 10 tonnage classes. A standard tire type spectrum is also chosen, in which only 3 out of 4 tire types occur.

Range	Calculation value	%
20-40	30	15.60
40-60	50	27.10
60-80	70	28.10
80-100	90	14.60
100-120	110	8.75
120-140	130	4.60
140-160	150	1.04
160-180	170	0.13
180-200	190	0.08
200-220	210	0.00

Table 2.8 Axle load spectrum

Tire type	%
Single tire (EL)	39.00
Dual tire (DL)	38.00
Broadband (BB)	23.00
Super Broadband (SB)	0.00

Table 2.9 Tire type spectrum

As a result, there are a total of 30 different tire prints that are used in this thesis. An additional single tire (EL) print for passenger cars is also determined. A summary form is displayed down below.

Design value (kN)			Singe tire (EL)			Dual tire (DL)			Broadband (BB)		
per axle	per tire (EL/BB)	per tire (DL)	A (mm^2)	σ (MPa)	L (mm)	A (mm^2)	σ (MPa)	L (mm)	A (mm^2)	σ (MPa)	L (mm)
30	15	7.5	29261	**0.51**	**146.30**	18631	**0.40**	**93.15**	31408	**0.48**	**104.69**
50	25	12.5	38352	**0.65**	**191.76**	23195	**0.54**	**115.98**	39840	**0.63**	**132.80**
70	35	17.5	46667	**0.75**	**233.33**	27547	**0.64**	**137.74**	47793	**0.73**	**159.31**
90	45	22.5	54206	**0.83**	**271.03**	31688	**0.71**	**158.44**	55266	**0.81**	**184.22**
110	55	27.5	60970	**0.90**	**304.85**	35616	**0.77**	**178.08**	62261	**0.88**	**207.54**
130	65	32.5	66957	**0.97**	**334.79**	39331	**0.83**	**196.66**	68776	**0.95**	**229.25**
150	75	37.5	72169	**1.04**	**360.85**	42835	**0.88**	**214.18**	74813	**1.00**	**249.38**
170	85	42.5	76606	**1.11**	**383.03**	46127	**0.92**	**230.63**	80370	**1.06**	**267.90**
190	95	47.5	80266	**1.18**	**401.33**	49206	**0.97**	**246.03**	85448	**1.11**	**284.83**
210	105	52.5	83151	**1.26**	**415.75**	52074	**1.01**	**260.37**	90047	**1.17**	**300.16**
7.5	3.75	1.875	18106	**0.21**	**90.53**						
Tread width (mm)			**200**			**200**			**300**		

Table 2.10 Tire prints summary

2.2.4. Axle tracks

Axle track is the distance between the centreline of two wheels (for dual tire the centreline in the middle of one dual tire set is used) on the same axle. It varies with the vehicle types, loads and in some cases the position (front or rear track) of the axle. For the traffic input a standard axle track need to be determined.

In Handboek wegontwerp the average dimensions of different vehicle classes are specified for the purpose of road design [34]. The average axle track of a passenger car is 1.50 m whilst a truck holds a larger axle track of 2.15 m (figure 2.14).

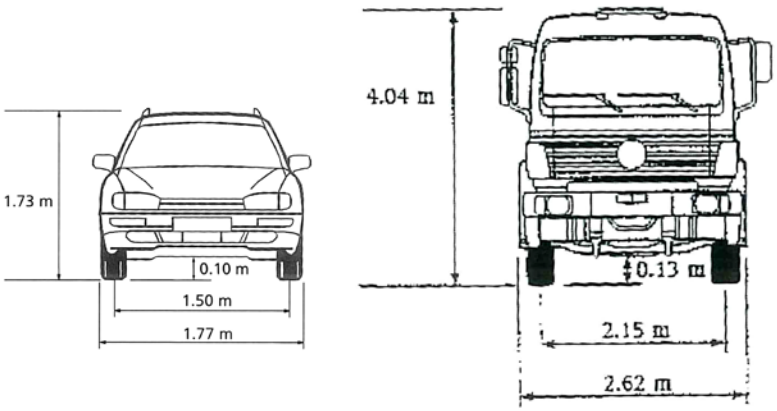

Figure 2.15 Average dimensions of passenger cars (r) and trucks (l) [34]

However, the trucks used for pavement design, as discussed in the section 2.2.3, are equipped with three tire types which will result in different axle tracks. The Handboek wegontwerp also provides a standard width of a truck (2.62m). Hence the axle tracks of three tire types can be determined. The results are shown in table 2.11.

	Passenger car	Truck		
		EL	DL	BB
Axle track (mm)	1500	2100	1785	2000

Table 2.11 Axle tracks

2.2.5. Time interval

In most situations, vehicles apply moving, dynamic load onto the pavement. Obviously it is a continuous process. However, in finite element software, this continuous process is simulated by a series of patterns gradually shifted according to time. It takes a fixed time for a wheel to pass a certain distance, in this case 6 metres, at a certain speed. Therefore the more steps there are, the shorter interval it will need, and obviously the simulation will be closer to a continuous moving load. On the other hand, the more steps, the more computing time. Thus an optimized balance between running time and result precision should also be found. 5 tests with different time intervals were performed during the preliminary research. It is set that for a test with 2N time steps, the wheel centre will come to the position right on the output point at the $(N+1)^{th}$ step. The results are shown down below. The red bold values are the maximum strain values occurred in each test.

PA layer					
Total time steps	Output time step	Time (s)	Strain (µm/m)		
			xx	yy	zz
10	5	1.29E-01	-1.84E+01	6.83E+00	2.49E+00
	6	**1.54E-01**	**-4.42E+01**	**-1.22E+02**	**-4.50E+01**
20	10	1.28E-01	-3.33E+01	2.13E+01	-1.66E+01
	11	**1.41E-01**	**-4.74E+01**	**-9.45E+01**	**-4.66E+01**
	12	1.54E-01	-4.02E+01	-1.52E+01	-2.43E+01
40	20	1.29E-01	-3.76E+01	-3.58E+01	-1.89E+01
	21	1.35E-01	**-4.27E+01**	**-8.76E+01**	-3.84E+01
	22	1.41E-01	-4.18E+01	-4.89E+01	**-4.58E+01**
	23	1.48E-01	-3.67E+01	-1.80E+01	-2.42E+01
80	40	1.29E-01	-4.05E+01	-6.64E+01	-3.55E+01
	41	1.32E-01	-4.26E+01	-8.33E+01	-4.12E+01
	42	1.35E-01	**-4.30E+01**	**-1.01E+02**	-3.27E+01
	43	1.38E-01	-4.19E+01	-5.92E+01	**-4.44E+01**
	44	1.41E-01	-4.01E+01	-2.65E+01	-3.26E+01
160	80	1.29E-01	-4.16E+01	-7.27E+01	-3.92E+01
	81	1.30E-01	-4.25E+01	-8.12E+01	-4.14E+01
	82	1.32E-01	-4.30E+01	-8.94E+01	-4.13E+01
	83	1.33E-01	**-4.30E+01**	-9.88E+01	-3.43E+01
	84	1.35E-01	-4.27E+01	**-1.03E+02**	-3.06E+01
	85	1.37E-01	-4.20E+01	-6.66E+01	**-4.29E+01**
	86	1.38E-01	-4.11E+01	-3.76E+01	-4.07E+01
	87	1.40E-01	-4.01E+01	-2.88E+01	-3.32E+01

Table 2.12 Peak strain values for different time intervals (PA layer, Broadband, 210 kN axle load)

AC layer					
Total time steps	Output time step	Time (s)	Strain (µm/m)		
			xx	yy	zz
10	5	1.29E-01	1.58E+01	-6.71E+00	-3.07E+00
	6	**1.54E-01**	**4.40E+01**	**-4.30E+01**	**4.51E+01**
20	10	1.28E-01	3.05E+01	-2.13E+01	1.19E+01
	11	**1.41E-01**	**4.68E+01**	**-4.49E+01**	**4.56E+01**
	12	1.54E-01	3.69E+01	-2.63E+01	1.82E+01
40	20	1.29E-01	3.62E+01	-3.16E+01	2.79E+01
	21	**1.35E-01**	**4.21E+01**	**-4.05E+01**	**4.10E+01**
	22	1.41E-01	4.01E+01	-3.50E+01	3.26E+01
80	40	1.29E-01	3.97E+01	-3.72E+01	3.62E+01
	41	1.32E-01	4.19E+01	**-4.02E+01**	**4.07E+01**
	42	1.35E-01	**4.20E+01**	-3.93E+01	3.94E+01
	43	1.38E-01	4.02E+01	-3.51E+01	3.30E+01
160	80	1.29E-01	4.08E+01	-3.89E+01	3.88E+01
	81	1.30E-01	4.17E+01	-4.00E+01	4.04E+01
	82	**1.32E-01**	**4.21E+01**	**-4.01E+01**	**4.06E+01**
	83	1.33E-01	4.19E+01	-3.92E+01	3.93E+01

Table 2.13 Peak strain values for different time intervals (AC layer, Broadband, 210 kN axle load)

It can be observed that the value of the interval and the time steps indeed have an influence on the stress result. When the time steps are larger than 40, the results of the maximum strain value becomes stable. The strain plots, surface strain particularly, also show that when the number of time steps is larger than 40, the shapes of the longitudinal strain curves of top layer (PA layer) become similar and start to show the preferable triple V shape with three compression strain peaks. This triple V shape was also observed in many filed tests and FEM simulations before [40]. Unfortunately, more time steps also leads to an issue that the peak strain value of each direction occurs at different time step.

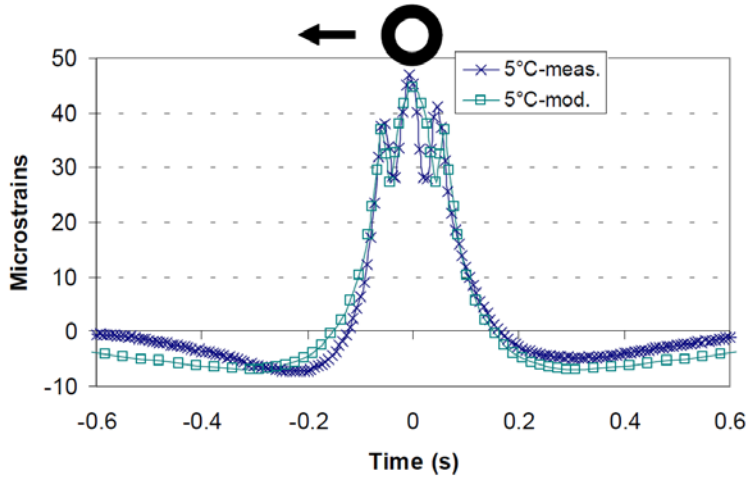

Figure 2.16 Field test measured and modelled (elastic linear) strain signals near to the surface [40][1]

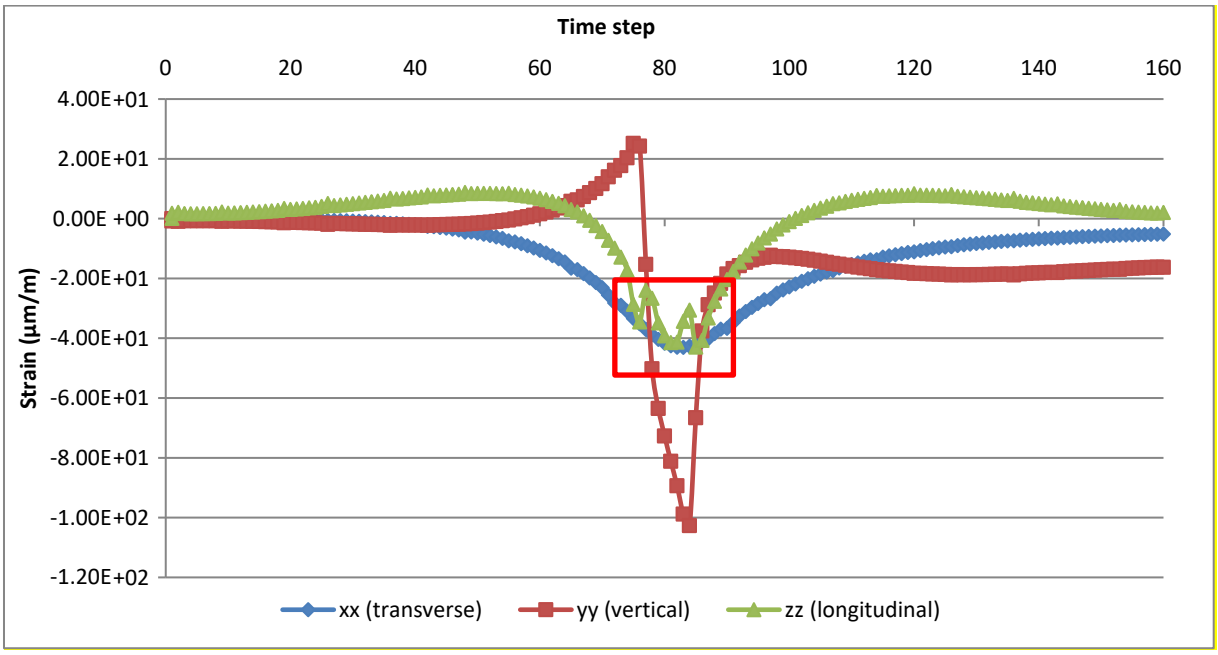

Figure 2.17 Time-strain curves for 160 time steps at the centre of PA layer (Broadband, 210 kN)

[1] In paper [40] the compressive strain is set to be positive.

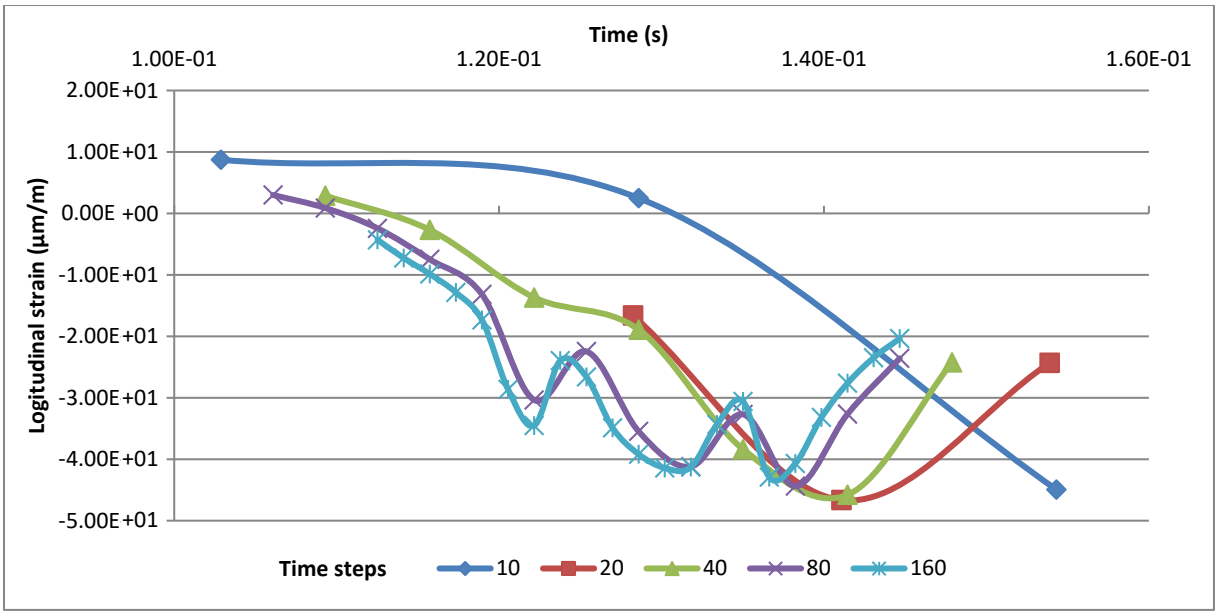

Figure 2.18 Peak part of longitudinal strain curves at the centre of PA layer for different time steps

In this thesis however, the accurate simulation of the strain curve shape, especially the triple V shape of the strain plot of PA layer, is not the priority since the bottom of AC layer is the main focus. That is the determination of the maximum strain to fulfil the fatigue calculation. It can be seen in table 2.12 and 2.13 that the results of peak strain of all the five tests, although not identical, are still within a small range and close enough for the fatigue prediction. Considering the time assumption, the 20 time steps interval is chosen for the peak strain and stress calculation while the 10 time steps interval is used in the real-life and platooning simulation.

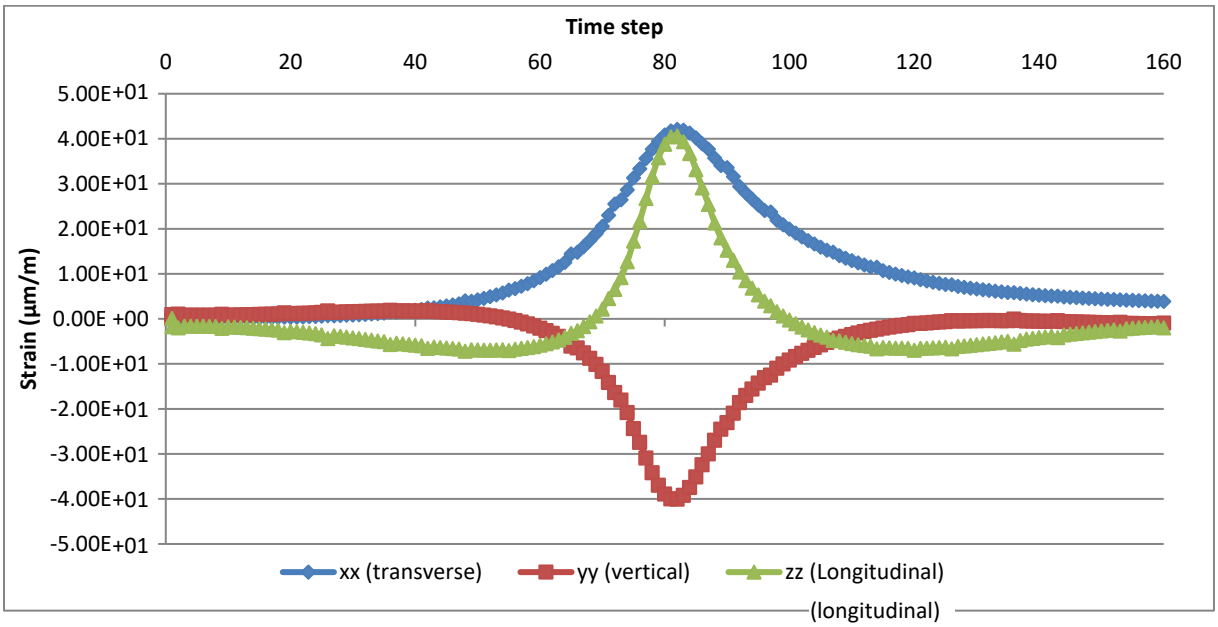

Figure 2.19 Time-strain curves of 160 time steps at the bottom of AC layer (Broadband, 210 kN)

3. Performance analysis

3.1. Strain plot analysis (individual wheel)

Typical curves of the time-strain relationship for an axle load of 210 kN with dual tire at the centre of one tire and the bottom of the asphalt layer are shown below (positive strain represents tensile strain while negative strain represents compressive strain). Normal strain along three different directions, namely vertical, transverse and longitudinal, are drawn separately.

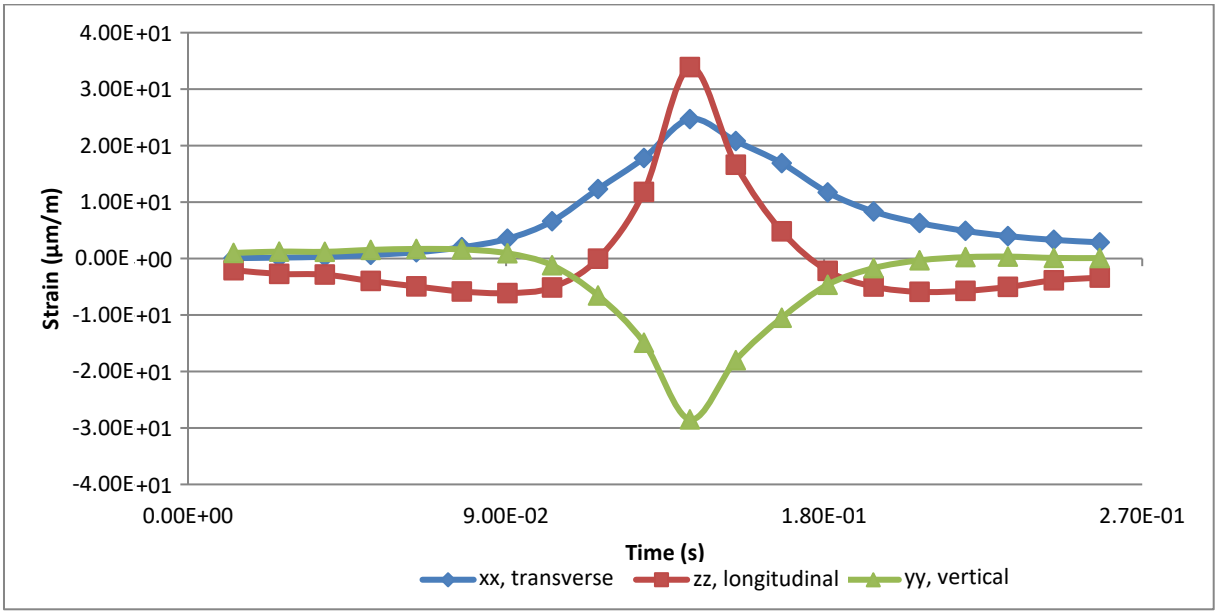

Figure 3.1 Time-strain curves at the bottom of AC layer (Dual tire, 210 kN axle load)

For the vertical strain, the pavement suffers three different phases during the entire pass. As the wheel approaches the observation point, a small tensile strain is generated. After that, the strain decreases and becomes compressive as the wheel comes closer to the observation point. The maximum compressive strain occurs when the wheel reaches the observation point. When the wheel leaves the observation point, the compression strain starts to decline and eventually turns back into tensile strain. As the wheel continues to be driven away from the observation point, the vertical strain approaches to zero.

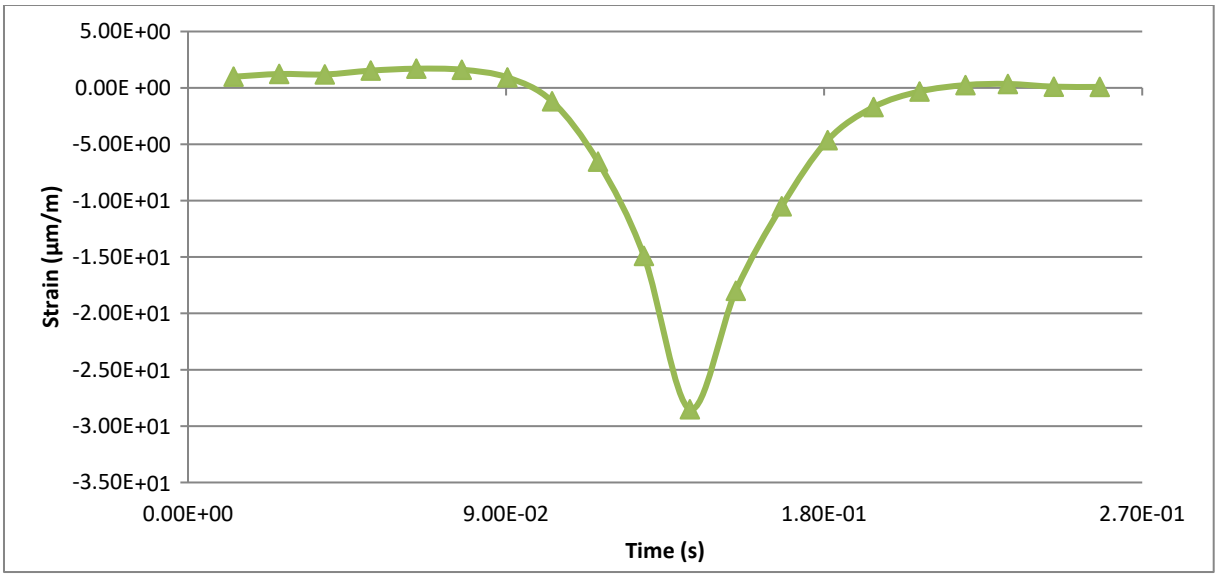

Figure 3.2 Time-vertical strain curve at the bottom of AC layer (Dual tire, 210 kN)

For the longitudinal strain, a similar pattern can be obtained, only the directions of the strain are reversed. Instead, a compression-tension-compression pattern is observed [41]. Also these three segments of the curve are more distinctive with a larger deviation between the tensile and compressive strain comparing to the vertical strain curve. This pattern was investigated by Sebaaly and Mamlouk [42]. They developed a pavement structural model that takes into account the inertial forces. The result shown that the vertical acceleration of a point within the pavement changes from positive to negative as the axle loading passes over. There is also a simpler explanation that the compressive longitudinal strain is a result of the combination of bending stresses and horizontal shear stresses.

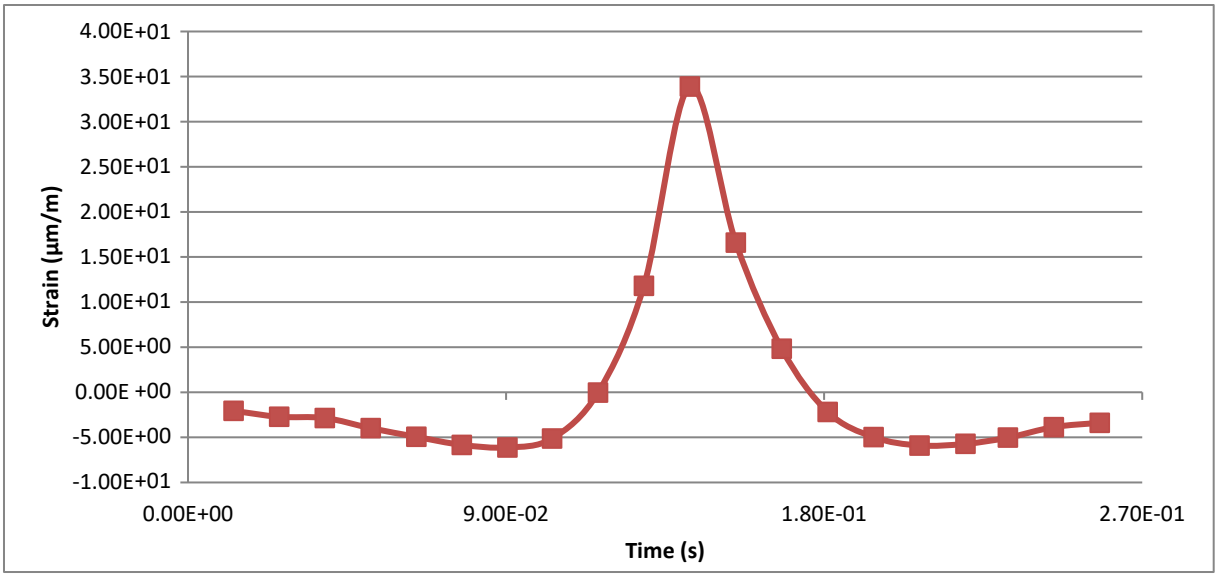

Figure 3.3 Time-longitudinal strain curve at the bottom of AC layer (Dual tire, 210 kN)

For transverse strain, unlike the other two directions, the variation with time at the bottom of asphalt layer only experiences tensile strain. A tensile strain starts to emerge as the wheel is driven closer and peaks when the wheel reaches the top of the observation point. When the wheel leaves the observation point, the tensile strain starts to decline with a lower rate.

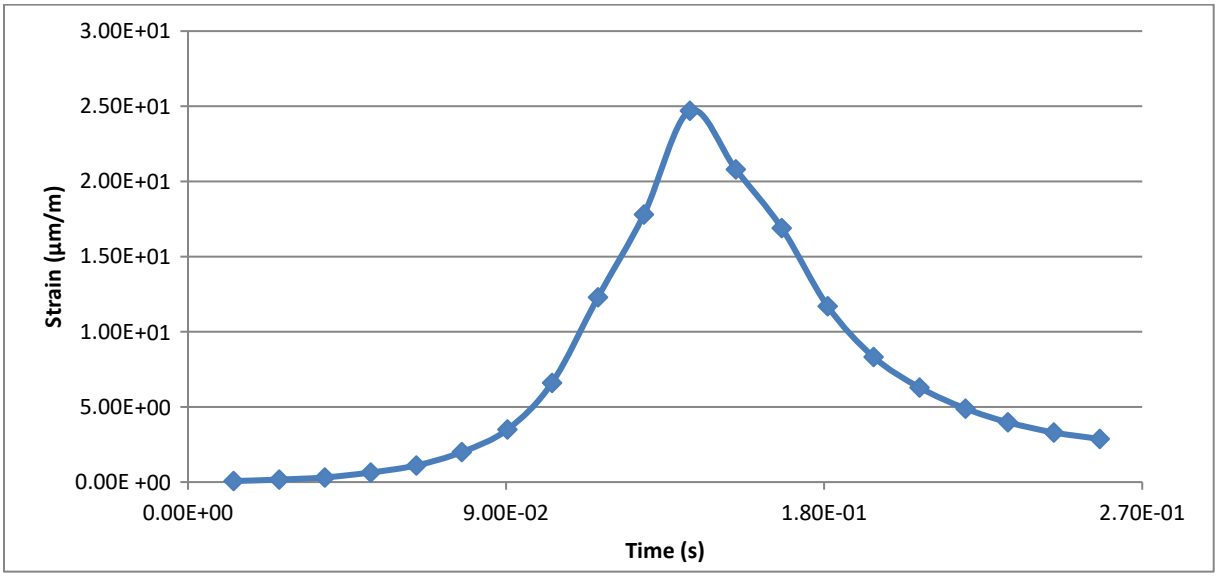

Figure 3.4 Time-transverse strain curve at the bottom of AC layer (Dual tire, 210 kN)

Several field tests confirmed the observations obtained from the simulation [40]. Transverse strains stay tensile throughout the entire loading whilst longitudinal strains contain compressive strain sections before and after each tensile strain pulse.

It is worth noting that due to the viscosity of the material, several special features can be observed in the plot. The strain curves are not symmetrical. The decline rate of the strain is usually lower than its increase rate. In horizontal directions, the strains remain non-zero for a longer period after the wheel being driven far away from the observation point. There should be a delay between the strain peak time and the stress peak time. However, since the chosen time interval (20 time steps) is bigger than the delay time, in this simulation two peaks are merged at the same output time point. This delay can be observed when the time steps number is more than 80 (Table 2.11 & 2.12).

3.2. Strain plot analysis (cross section)

Traditionally pavement design only focuses on a single lane, the design lane. In the early days, the calculation only considered the loading of one wheel (or one set of dual wheels). Since in reality, all axles contain at least two wheels, the influence to the strain caused by the wheel loading at the other

end of the axle should be considered. Modern motorways always consist of more than one lane, thus logically the strain condition of one lane will be influenced by the loading on other lanes. In some severe cases, i.e. vehicles running shoulder by shoulder, the distance between two adjacent wheels of two vehicles is even smaller than their own axle track. Hence this phenomenon is also worth investigating especially to find out whether there will be any fluctuation in the new design. Three comparison tests are conducted to investigate this problem. The first two use the original design, whereas the third one uses the new design.

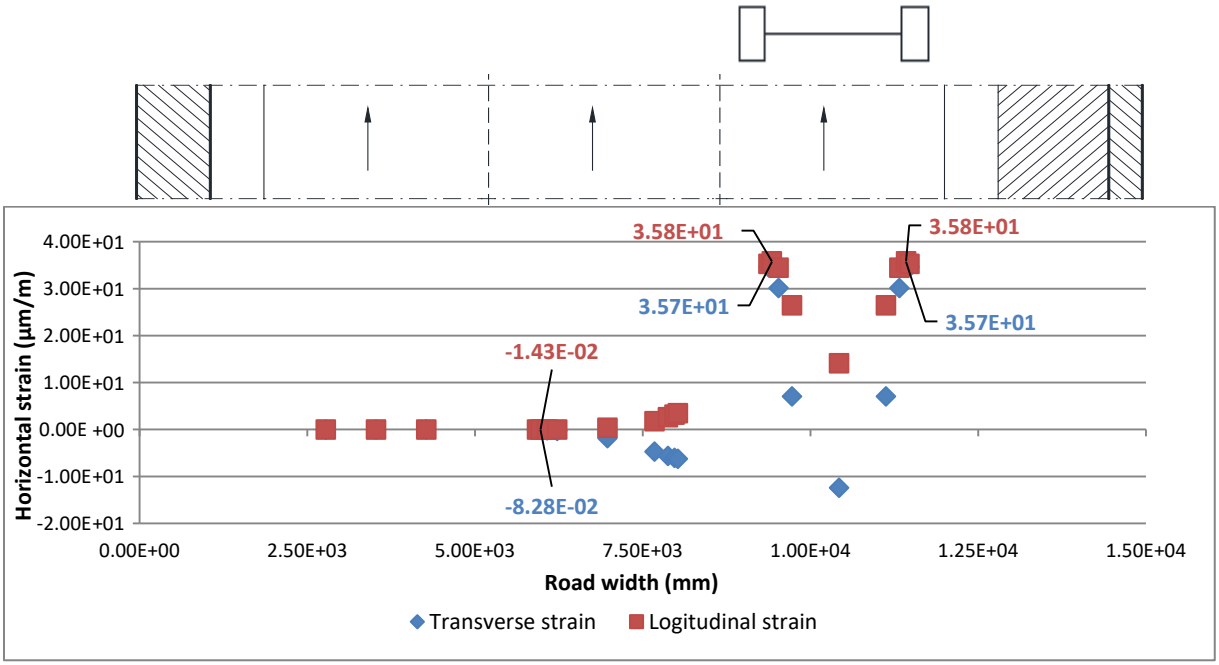

Figure 3.5 Horizontal strains under single axle load (Original design, Broadband, 80km/h, AC bottom)

The first plot shows the horizontal strain situation when only one single axle loads the heavy traffic lane. It is clear in this plot that the strain distribution on the load bearing lane is symmetrical. The load on the heavy traffic lane does produce an influence on its neighbour lane with a limited effect radius. To be specific, the strain caused by the load on the heavy traffic lane has a noticeable influence at the adjacent wheel position on the light traffic lane. However, this influence diminishes so rapidly with the increase of the distance away from the loading position that at the middle of the un-trafficked lane it has already dropped to less than 1% of the maximum strain value. As a result, the influence on the far wheel of the axle on the un-trafficked lane caused by the heavy traffic on the right-hand lane is so small that it can be considered negligible.

Later simulation indicates that the strain caused by a standard passenger car is around 10% of the strain caused by the maximum axle load of a truck which is used here. This means that for the passenger car lane the horizontal strain at bottom of the AC layer caused by the truck running on the adjacent lane may cause equal or even worse damage to the passenger car lane than the passenger car itself.

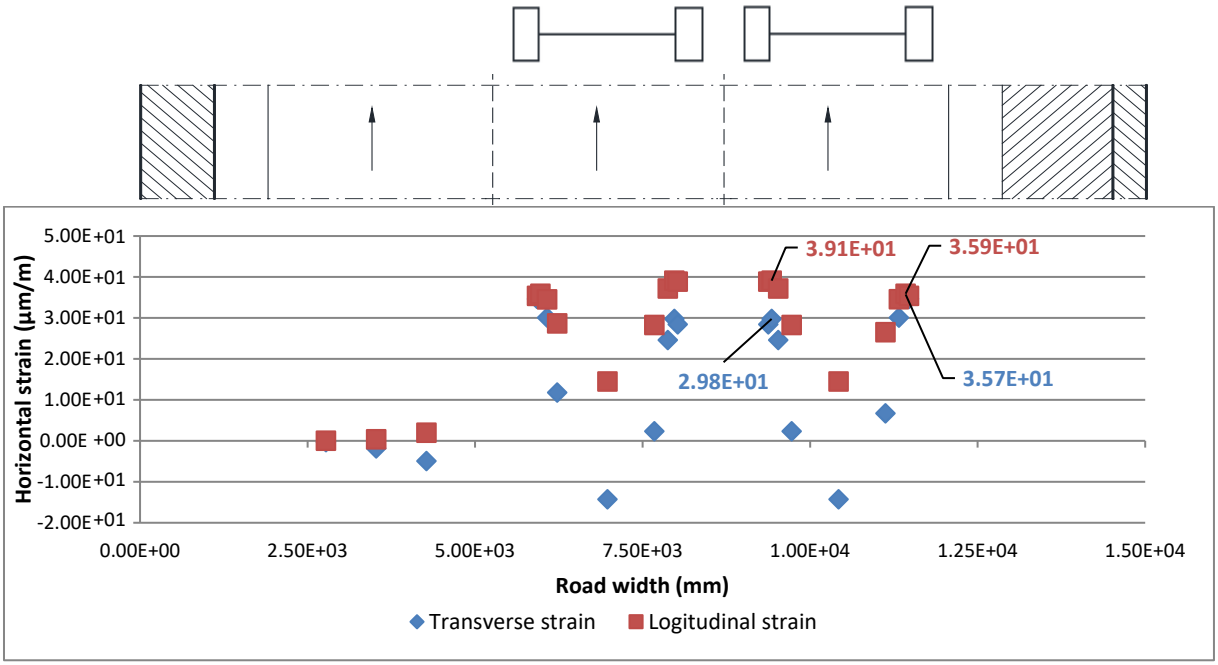

Figure 3.6 Horizontal strains under double axle loads (Original design, Broadband, 80k/h, AC bottom)

The second plot confirms the conclusions obtained from the first test. In this test two single axle loads are placed on both light and heavy traffic lanes. The strain values at the far end of the axle remains the same as the values when only one axle loading is applied which proves that the influence caused by the load on one lane to the far end of another lane is negligible. On contrast, the strain values at the near end do experience variations. For the longitudinal strain there is an increase while for the transverse train there is a decline. These variations are the result of the different influences caused by the load on the other lanes. Although right under the centre of a wheel the horizontal strains in both directions are tensile, the signs of their effective strains on the adjacent wheel are opposite to each other. The first test has indicated that the loading on one lane will cause a tensile longitudinal strain and a compressive transverse strain at the adjacent wheel position of the other lane.

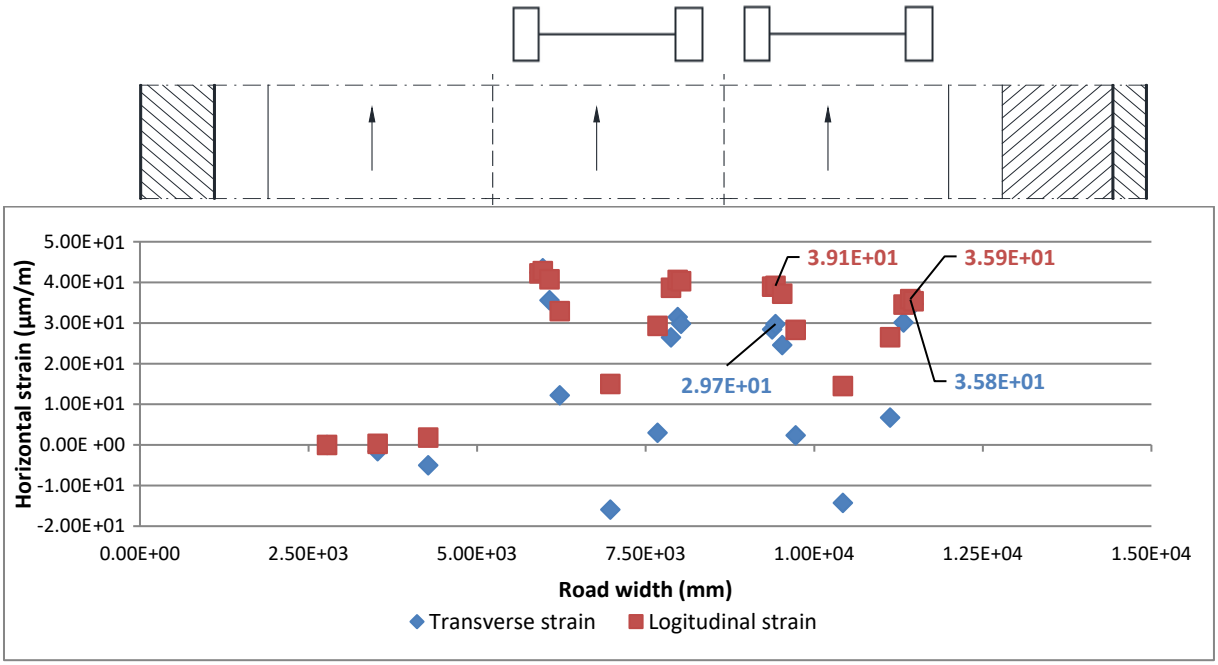

Figure 3.7 Horizontal strains under double axle loads (New design, Broadband, 80km/h, AC bottom)

The third plot is used to compare with the second plot. The comparison indicates that with the new design, the thickness reduction of the light traffic lane to be specific, does not lead to a negative influence on the heavy traffic lane. Strain values of both near and far ends of the axle almost remain the same comparing to the original design. Thus the new design is able to reduce the thickness of the lighter traffic lanes without negatively effecting the performance of the heavy traffic lane whose thickness remains the same.

The latter two plots illustrate that when two vehicles running shoulder by shoulder on two lanes, the longitudinal strains at the near ends of the axles will increase while the transverse strains will decrease. Hence it is suggested that for the fatigue evaluation the negative effect of longitudinal strain should be noticed and discussed.

These tests also provide a possibility of simplifying the strain calculation procedure. Since the new design hardly has any changes in strain condition of the heavy traffic lane, all the necessary data, namely the horizontal strains at the bottom of certain layers and vertical strains at top of both reduced and unchanged lanes, can be obtained from a single test on the new design instead of running two tests on both original and new design models. By doing this the test time can be dramatically reduced.

Additionally, strain plots for different vehicle speeds are also proceeded. It can be easily observed that vehicle with lower speed will produce larger strain response and lead to more severe damage to the pavement structure.

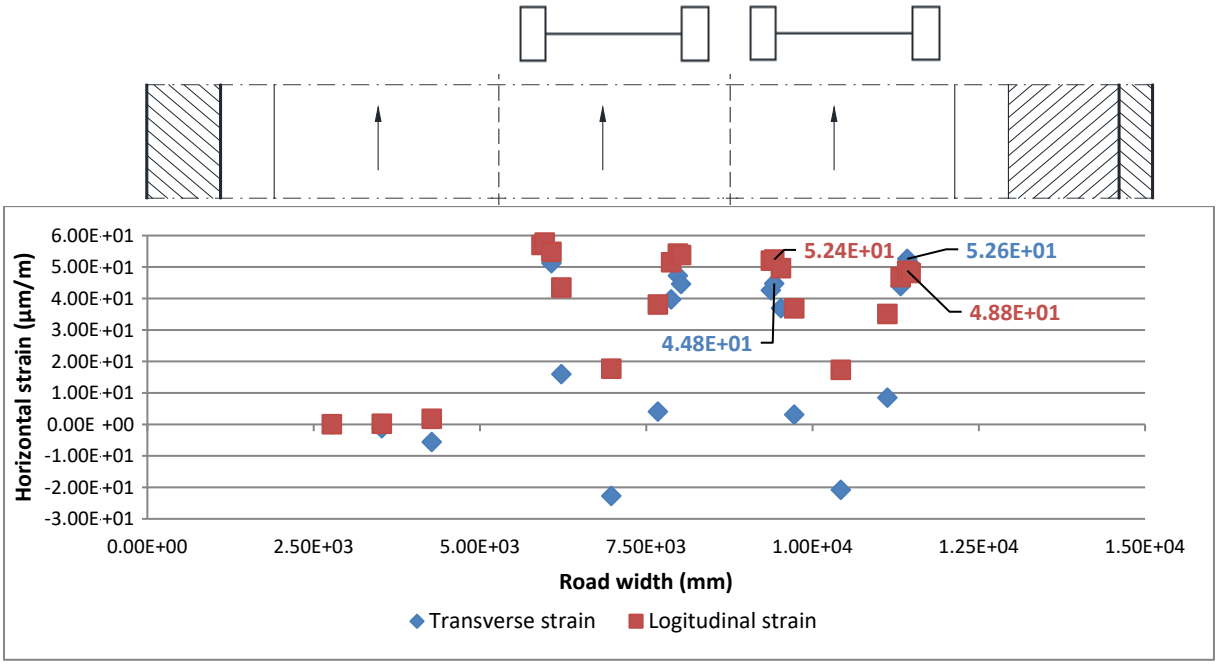

Figure 3.8 Horizontal strains under double axle loads (New design, Broadband, 10km/h, AC bottom)

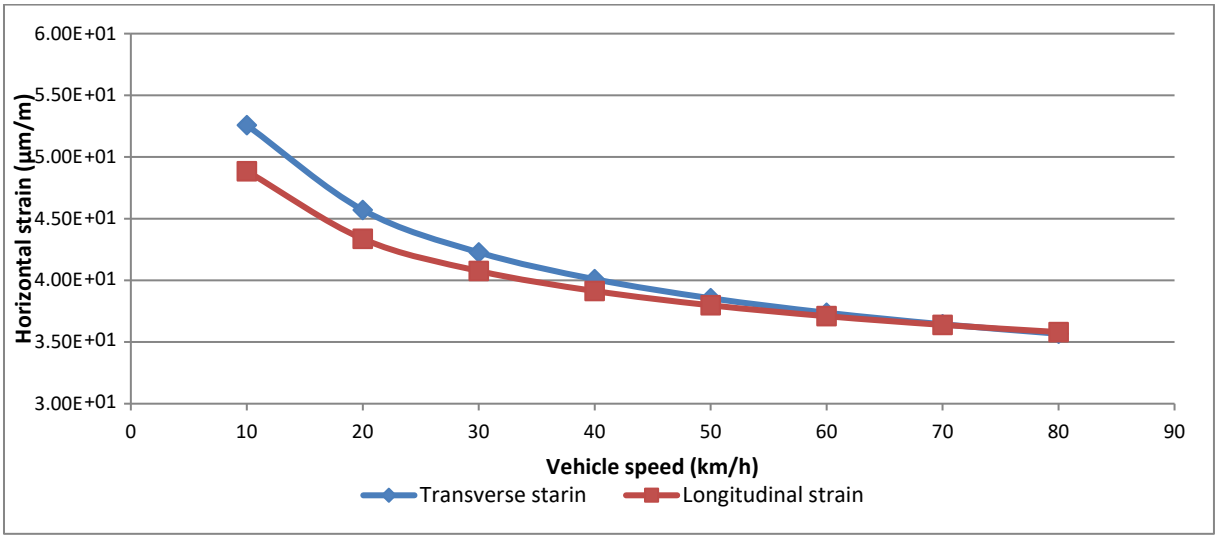

Figure 3.9 Maximum horizontal tensile strains at the bottom of AC layer under different vehicle speeds (Original design, Broadband)

Figure 3.9 indicates that as the vehicle speed decreases, both transverse and longitudinal strains increase. The increase rates of the two directions are not the same therefore in this case at the lower speed range the transverse strains become larger than longitudinal strains. Furthermore, the increase rates also rise noticeably when the vehicle speed is lower than 40 km/h. Hence the traffic load with a lower speed will cause more severe damages to the pavement. In practice traffic speed should be maintained above a certain value.

3.3. Longitudinal strain versus Transverse strain

In the Dutch design method, the rectangular tire prints are converted into equivalent circular prints [23]. Plus the basic assumption that all the layers are homogenous, isotropic and horizontally infinite, the horizontal strains calculated from the software are therefore also isotropic.

However in reality, although the shape of a tire print is not an ideal rectangle, it is far more different from a circle [43]. As a result the longitudinal and transverse strain are hardly the same. Many field tests have proved this difference. In a NCAT research, the strains of two orientations were investigated to determine which, or both, should be considered in the fatigue prediction models [44]. To compare the two responses, the maximum transverse reading was plotted against the maximum longitudinal reading for each pass, shown in figure 3.10. There is quite a bit of scatter in the data since it was pooled over a wide range of conditions, however, generally speaking the strain was higher in the longitudinal direction rather than the transverse. Al-Qadi et al. also observed that the longitudinal strain was higher than the complimentary transverse strain [45]. Some design methods suggest to consider the two strains using an average value, though it can be clearly seen that an average value would falsely reduce the strain value. In this NCAT research, it was decided to use the most severe response in its analysis. To stay consistent throughout the procedure, only the longitudinal strain was considered in its development of the fatigue functions in this NCAT research.

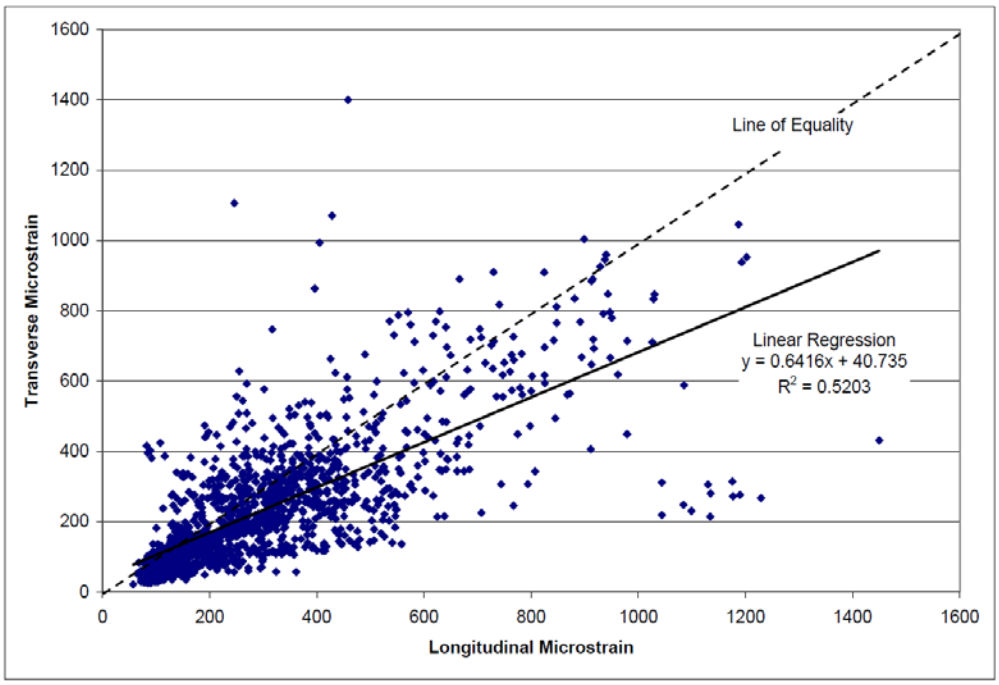

Figure 3.10 Transverse vs. Longitudinal Strain [44]

In this thesis, both longitudinal and transverse strains with different tire types as well as loadings are listed in the forms down below. Since the dimensions of the tire prints change with the different loadings and tire types, the higher value between longitudinal and transverse strain also shifts. Based on the available data, in general, when the length of the tire print is bigger than the width, the transverse strain will be bigger than the longitudinal strain, and vice versa. In the case of a dual tire, the length of the tire print should be compared with twice the width plus the gap in-between. The calculated strain results reveal that for a dual tire and a broadband, the longitudinal strains are almost always the dominant values regardless the weights of the loading. For a single tire, the transverse strains are in most cases bigger than their longitudinal counterparts with few exceptions only when the load is very light. Considering the substantial percentage of the single tires in the prediction model, both transverse and longitudinal strains are taken into account for fatigue analysis in this thesis.

The results of horizontal strains at the bottom of AC layer as well as vertical strains at the surfaces of unbound base and subgrade are shown in table 3.1 and 3.2.

Axle Load (kN)	Single tire (EL)				Dual tire (DL)				Broadband (BB)			
	Original design		New design		Original design		New design		Original design		New design	
	ε_{xx} (μm/m)	ε_{zz} (μm/m)	ε_{xx} (μm/m)	ε_{zz} (μm/m)	ε_{xx} (μm/m)	ε_{zz} (μm/m)	ε_{xx} (μm/m)	ε_{zz} (μm/m)	ε_{xx} (μm/m)	ε_{zz} (μm/m)	ε_{xx} (μm/m)	ε_{zz} (μm/m)
30	6.38E+00	6.38E+00	7.97E+00	7.89E+00	3.58E+00	5.31E+00	4.44E+00	6.42E+00	5.69E+00	6.32E+00	6.99E+00	7.78E+00
50	1.04E+01	1.02E+01	1.30E+01	1.26E+01	5.96E+00	8.79E+00	7.38E+00	1.06E+01	9.44E+00	1.04E+01	1.16E+01	1.27E+01
70	1.45E+01	1.38E+01	1.80E+01	1.68E+01	8.44E+00	1.23E+01	1.05E+01	1.47E+01	1.33E+01	1.45E+01	1.64E+01	1.77E+01
90	1.85E+01	1.71E+01	2.29E+01	2.07E+01	1.09E+01	1.58E+01	1.35E+01	1.90E+01	1.68E+01	1.81E+01	2.07E+01	2.20E+01
110	2.22E+01	2.03E+01	2.76E+01	2.44E+01	1.30E+01	1.87E+01	1.61E+01	2.24E+01	2.05E+01	2.17E+01	2.51E+01	2.63E+01
130	2.62E+01	2.32E+01	3.25E+01	2.78E+01	1.53E+01	2.19E+01	1.89E+01	2.61E+01	2.41E+01	2.51E+01	2.96E+01	3.04E+01
150	2.99E+01	2.61E+01	3.70E+01	3.11E+01	1.83E+01	2.58E+01	2.22E+01	3.07E+01	2.77E+01	2.85E+01	3.40E+01	3.43E+01
170	3.36E+01	2.88E+01	4.15E+01	3.43E+01	1.99E+01	2.80E+01	2.46E+01	3.32E+01	3.14E+01	3.18E+01	3.84E+01	3.82E+01
190	3.72E+01	3.16E+01	4.60E+01	3.76E+01	2.22E+01	3.09E+01	2.75E+01	3.66E+01	3.48E+01	3.50E+01	4.26E+01	4.19E+01
210	4.09E+01	3.45E+01	5.05E+01	4.09E+01	2.47E+01	3.39E+01	3.04E+01	4.01E+01	3.82E+01	3.82E+01	4.68E+01	4.56E+01

Table 3.1 Horizontal strains at the bottom of AC layer (Original & New design)

Axle Load (kN)	Single tire (EL)				Dual tire (DL)				Broadband (BB)			
	Original design		New design		Original design		New design		Original design		New design	
	ε_{base} (μm/m)	ε_{subg} (μm/m)	ε_{base} (μm/m)	ε_{subg} (μm/m)	ε_{base} (μm/m)	ε_{subg} (μm/m)	ε_{base} (μm/m)	ε_{subg} (μm/m)	ε_{base} (μm/m)	ε_{subg} (μm/m)	ε_{base} (μm/m)	ε_{subg} (μm/m)
30	-1.94E+01	-3.44E+01	-2.37E+01	-3.86E+01	-1.52E+01	-3.27E+01	-1.81E+01	-3.62E+01	-1.87E+01	-3.44E+01	-3.85E+01	-3.85E+01
50	-3.17E+01	-5.69E+01	-3.85E+01	-6.39E+01	-2.52E+01	-5.44E+01	-3.00E+01	-6.03E+01	-3.10E+01	-5.73E+01	-3.74E+01	-6.41E+01
70	-4.37E+01	-7.95E+01	-5.30E+01	-8.93E+01	-3.55E+01	-7.67E+01	-4.22E+01	-8.51E+01	-4.37E+01	-8.13E+01	-5.26E+01	-9.08E+01
90	-5.54E+01	-1.02E+02	-6.71E+01	-1.15E+02	-4.60E+01	-9.98E+01	-5.46E+01	-1.11E+02	-5.50E+01	-1.03E+02	-6.62E+01	-1.15E+02
110	-6.67E+01	-1.24E+02	-8.06E+01	-1.39E+02	-5.48E+01	-1.19E+02	-6.50E+01	-1.32E+02	-6.67E+01	-1.26E+02	-8.02E+01	-1.40E+02
130	-7.80E+01	-1.47E+02	-9.41E+01	-1.65E+02	-6.45E+01	-1.41E+02	-7.64E+01	-1.56E+02	-7.82E+01	-1.48E+02	-9.40E+01	-1.66E+02
150	-8.89E+01	-1.69E+02	-1.07E+02	-1.90E+02	-7.64E+01	-1.66E+02	-9.02E+01	-1.84E+02	-8.96E+01	-1.71E+02	-1.08E+02	-1.91E+02
170	-9.96E+01	-1.91E+02	-1.20E+02	-2.14E+02	-8.35E+01	-1.84E+02	-9.87E+01	-2.04E+02	-1.01E+02	-1.94E+02	-1.21E+02	-2.17E+02
190	-1.10E+02	-2.13E+02	-1.33E+02	-2.39E+02	-9.29E+01	-2.06E+02	-1.10E+02	-2.28E+02	-1.12E+02	-2.16E+02	-1.34E+02	-2.42E+02
210	-1.21E+02	-2.35E+02	-1.46E+02	-2.63E+02	-1.03E+02	-2.28E+02	-1.21E+02	-2.53E+02	-1.23E+02	-2.38E+02	-1.47E+02	-2.66E+02

Table 3.2 Vertical strains at the surfaces of unbound base and subgrade (Original & New design)

3.4. Pavement performance prediction

The background report of OIA provides an outline of the Dutch design method. With the strain values obtained from CAPA-3D, a series of performance predictions in the OIA software can be recreated manually following the instructions.

3.4.1. Basic parameters

3.4.1.1. Traffic data

When evaluating the performance of the pavement it is assumed that each passage of a vehicle axle will cause certain damage to the pavement structure. The number of the passing axles, the axle load spectrum and the tire spectrum of the passing vehicles are the most important and fundamental

parameters for identifying the traffic load. The axle load spectrum is the frequency distribution of the weight of the axle loadings whilst the tire spectrum is the frequency distribution of the number of axles with various types of tires. Both spectrums have been chosen in Chapter 2, which leaves only one parameter to determine: the total number of the passing axles.

The total number of load repetitions in the design period can be specified by equation 3.1:

$$n_{total} = A \cdot a \cdot W \cdot O \cdot F_R \cdot F_{source} \tag{3.1}$$

Where,

n_{total} = Total number of load repetitions during the design service life (-)

A = The daily intensity of trucks in each direction (-/day)

a = Average number of axles per truck (-); in the software the system default value is 3.5 [32]

W = The user specified number of working days per year (day/year); in this thesis the traffic data is not based on working days but all weekdays, thus this value is set to 365

O = Corrected design service life with the growth factor (year)

F_R = Correction factor for number of lanes (-); in this thesis all lanes are design individually, hence even though it is a three-lane road, the correction factor is still 1

F_{source} = Correction factor for the origin of the traffic (-); in this thesis the traffic data comes from a standard selection of RWS primary roads, hence the correction factor is 1.75 [32]

For the determination of the design period, a 20 years period has been chosen as the design lifetime. Ideally the traffic flow is continuously growing as time goes by. The density of trucks at the beginning of a design period tends to be lower than it is at the end. This increase can be represented by an average annual growth of the truck density:

$$O = \frac{\left(1+\frac{g}{100}\right)^t - 1}{\frac{g}{100}} \tag{3.2}$$

Where,

O = Corrected design service life with the growth factor (year)

g = Average annual growth of the truck density (%)

t = Design service life (year)

3.4.1.2. Adjustment for lateral wander

Trucks cannot, in practice, all move in the same perfect straight line on the road [46]. The position of a wheel set shifts within a certain range along the transverse direction. This phenomenon is called lateral wander. When considering the lateral wander, the vehicles are no longer driven on the same track line, but in a certain bandwidth around the middle of the track line. The lateral wander can dramatically affect the performance predictions of the designed pavement since the loadings are no longer concentrated at the same position. Hence it is important to introduce a factor for lateral wander in the design procedure.

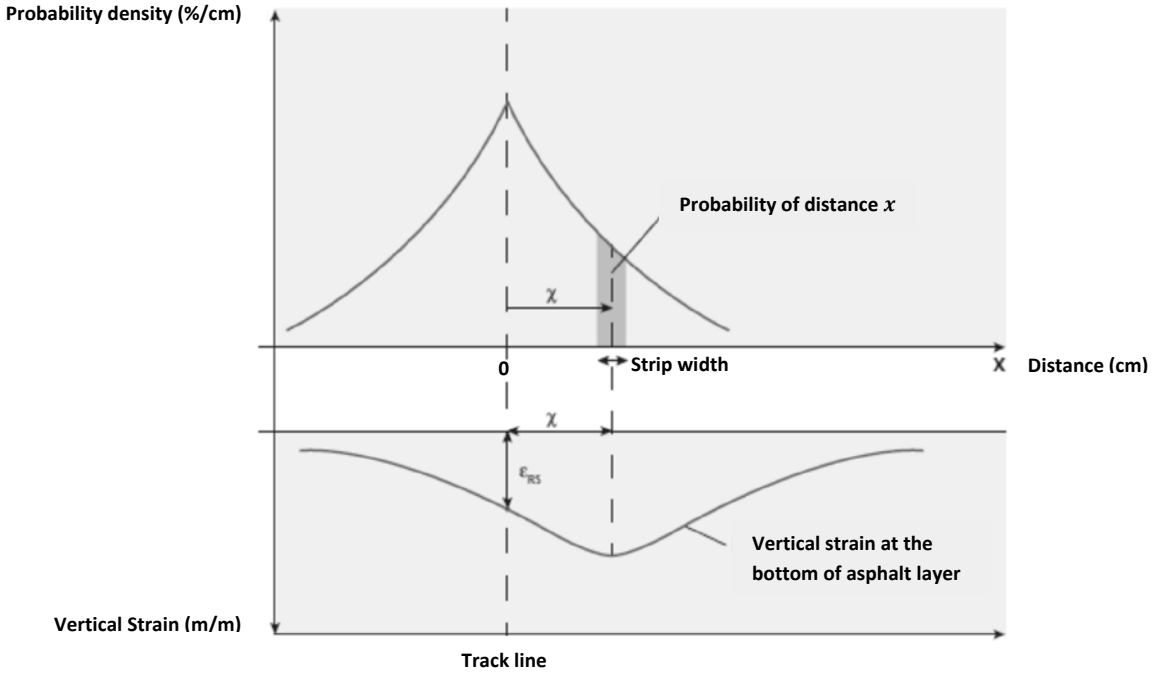

Figure 3.11 Probability density and vertical strain distribution caused by a wheel [32]

The lateral wander factor mainly depends on lane width, vehicle width, vehicle speed and extent of rutting. The distribution of the wheel position along the transverse direction is assumed to be a Laplace distribution. The probability density function of the Laplace distribution is:

$$f(i) = \frac{1}{2\lambda} \cdot e^{-\frac{|x-\mu|}{\lambda}} \tag{3.3}$$

Where,

$f(i)$ = Probability density (%/cm)

x = Distance from the centre of the track line (cm)

μ = Average value (cm)

λ = Scale parameter (cm)

For the lateral wander factor, the centre of the track line is taken as the reference point. The value of μ is therefore 0. The scale parameter indicates the shape of the distribution curve. A small value indicated a narrow distribution which means a limited lateral wander range.

Equation 3.4 shows the relationship between scale parameter and standard deviation.

$$\lambda = \frac{\sigma}{\sqrt{2}} \tag{3.4}$$

Where,

λ = Scale parameter (cm)

σ = Standard deviation (cm)

The standard deviation of the lateral wander is described by the following settings:

$$\sigma_b = b_0 + b_1 \cdot R_{edge} \tag{3.5}$$

Where,

σ_b = Standard deviation of lateral wander (cm)

b_0 , b_1 = Model coefficients based on tire types, allowed maximum rutting depth and vehicle speed (cm)

R_{edge} = Edge width class, varies from 1 to 6 (-)

The edge width is defined as the distance between the tire print edge and the edge of the lane. The determination of the edge width class is dependent on the lane width, the truck width as well as the truck type. Light trucks have smaller width with an average from 2.00 m to 2.25 m while heavy trucks have an average width between 2.25 m to 2.50 m [32]. In this thesis the truck width (distance between tires outside edges) is set to a fixed value of 2.30 m. The edge width class can be obtained by the following formula：

$$R_{edge} = {(b_{lane} - 2.75)}/{0.25} \tag{3.6}$$

Where,

R_{edge} = Edge width class, varies from 1 to 6 (-)

b_{lane} = Width of the lane (m)

In OIA the model coefficients in equation 3.5 are determined based on the data of the class whose rutting depth is less than 10 mm. The vehicle speed has been set to a fixed value of 80 km/h.

There are 4 kinds of tires listed in the Dutch design method, 3 of them are used in the chosen spectrum. However the lateral wander calculation is not performed for all these types. Controlled research showed that the calculated lateral wander factors for solo tire type, namely single tire, broad band and super broad band, did not differ much. Therefore in the Dutch design method the lateral wander factor calculation is only determined for the broad band tire. An additional calculation for the dual tire will be performed separately.

In addition, the calculation is not performed for all axle load classes. Controlled research also showed that the lateral wander factor did not change much for different axle loads. Hence in OIA the calculation is only performed with certain axle loadings, which are 100 kN and 120 kN for broadband and dual tire respectively [32].

The calculated parameters are listed in the table down below.

	Broadband (BB)	Dual tire (DL)
b_0 (cm)	10.14	10.26
b_1 (cm)	3.12	2.49
b_{lane} (m)	3.5	3.5
R_{edge} (-)	3	3
σ_b (cm)	19.5	17.73
λ (cm)	**13.789**	**12.537**

Table 3.3 Calculated parameters for lateral wander

The probability density function will come close to zero, but will never become zero as the distance increases to infinite. For this reason an upper limit of distance should be set to terminate the calculation. In the Dutch design method this limit is set to the distance where at least 95% of the wandering traffic is included in the calculation.

The Laplace distribution is easy to integrate due to the use of the absolute value function. Its cumulative distribution function can be written into [47]:

$$F(x) = \int_{-\infty}^{x} f(u)du = 0.5 \cdot \left\{1 + sgn(x-\mu) \cdot \left(1 - e^{\frac{-|x-\mu|}{\lambda}}\right)\right\} \quad (3.7)$$

Notice that the cumulative distribution function gives the output between negative infinity to the target distance. For lateral wander the wheel is assumed to be driven in a symmetrical area with a centre track line. Hence the lateral wander distribution area should be determined with an additional step:

$$F(x)' = \int_{-x}^{x} f(u)du = 2 \cdot [F(x) - 0.5]$$

$$= 2F(x) - 1 \tag{3.8}$$

Where,

$F(x)$ = Cumulative probability from distance $-\infty$ to x (%)

$F(x)'$ = Cumulative probability from distance $-x$ to x (%)

$f(u)$ = Probability density at u (-)

x = Distance from the centre of the track line (m)

μ = Average value (m)

λ = Scale parameter (-)

The lateral wander areas for both broadband and dual tire are listed in table 3.4:

Broadband (BB)			Dual tire (DL)		
x (cm)	$F(x)$	$F(x)'$	x (cm)	$F(x)$	$F(x)'$
0	50.00%	0.00%	0	50.00%	0.00%
2.5	58.29%	16.58%	2.5	59.04%	18.08%
7.5	70.98%	41.95%	7.5	72.51%	45.02%
12.5	79.80%	59.61%	12.5	81.55%	63.10%
17.5	85.95%	71.89%	17.5	87.62%	75.24%
22.5	90.22%	80.44%	22.5	91.69%	83.38%
27.5	93.20%	86.39%	27.5	94.42%	88.85%
32.5	95.26%	90.53%	32.5	96.26%	92.52%
37.5	96.71%	93.41%	37.5	**97.49%**	**94.98%**
42.5	**97.71%**	**95.41%**	42.5	98.31%	96.63%

Table 3.4 Lateral wander area for broadband and dual tire

Once the lateral wander area is determined, it will be divided into several strips with a certain width to continue the calculation of the correction factor for lateral wander. Due to the dimension design of the mesh, the strip width is fixed to 5 cm as shown in table 3.4. For each strip the allowable number of

load repetitions is determined. The formulas used here are same as the ones calculating the allowable number of load repetitions of different construction layers on the basis of the horizontal strain or vertical deformation at the certain position. To determine the lateral wander factor, firstly the damage factor when all traffic is driven right on the track line is calculated by equation 3.9:

$$D_0 = \frac{1}{N(0)} \tag{3.9}$$

Where,

D_0 = Damage factor when 100% of the traffic runs right on the track line (-)

$N(0)$ = Permissible number of load repetitions (-)

Then the damage factor when lateral wander occurs is also determined. The damage factors of all strips are calculated separately and summed up by equation 3.10:

$$D_V = \frac{f[0]}{N[0]} + 2 \cdot \sum_{i=1}^{n_{strip}-1} \frac{f[i]}{N[i]} \tag{3.10}$$

Where,

D_V = Summed damage factor of all strips (-)

$f[0]$ = Percentage of traffic runs right on the central strip (%)

$N[0]$ = Permissible number of load repetitions on the central strip (-)

n_{strip} = Number of strips (-)

$f[i]$ = Percentage of traffic runs on strip i (%)

$N[i]$ = Permissible number if load repetitions on strip i (-)

After obtaining the damage factors under two different circumstances, the final lateral wander factor can be easy determined by equation 3.11:

$$F_S = \frac{D_V}{D_0} \tag{3.11}$$

Where,

F_S = Correction factor for lateral wander (-)

D_V = Summed damage factor when lateral wander occurs (-)

D_0 = Damage factor when all traffic is driven right on the track line (-)

The results are shown in the form.

Tire type	Broadband (BB)		Dual tire (DL)	
Direction	Longitudinal	Transverse	Longitudinal	Transverse
D_V	1.10E-08	3.06E-08	2.71E-09	1.87E-08
D_0	2.35E-08	4.90E-08	3.15E-09	2.42E-08
F_S	**0.468**	**0.624**	**0.861**	**0.774**

Table 3.5 Correction factors for lateral wander

3.4.1.3. Material properties

In the Dutch design method the fatigue performance evaluation for asphalt layers is mainly based on the material stiffness. To determine the stiffness, asphalt temperature plays an important role. In OIA this design temperature is set fixed to 20℃. Equation 3.12 shows the relationship between temperature and stiffness modulus of asphalt. There are four regression coefficients introduced in that equation. They vary by asphalt mixture types and the load frequency.

$$\ln(E_a) = c_1 + c_2 \cdot T_a + c_3 \cdot {T_a}^2 + c_4 \cdot {T_a}^3 \tag{3.12}$$

Where,

E_a = Stiffness modulus of asphalt mixture (MPa)

T_a = Asphalt temperature (℃)

$c_1 \sim c_4$ = Regression coefficients (-), see table 3.6

c_1	See equation 3.13
c_2	-0.0184
c_3	-0.001098
c_4	0

Table 3.6 Regression coefficients for asphalt stiffness modulus determination

$$c_1 = \ln\left(E_{a,250} - \Delta E_{a,250}\right) + 0.80734 \tag{3.13}$$

Where,

$E_{a,250}$ = Stiffness modulus of asphalt according to test 62 of the Standard RAW Provision 2010 (MPa)

$\Delta E_{a,250}$ = Stiffness reduction depending on the test load distribution and repetition number of the tests (MPa), in this thesis the stiffness reduction is set to 1285 MPa [32]

In test 62 of the Standard RAW Provision 2010, the stiffness modulus of asphalt material is only required at a single temperature (20℃) and load frequency (8 Hz) [32]. In practice there are obviously various vehicle speeds. A different load speed can be converted to an equivalent load frequency and then to a fictive temperature, which is used in equation 3.12 to calculate the stiffness modulus.

$$T_{fict} = \frac{1}{\frac{1}{T_a+273} - \frac{\log\left(\frac{f_{test}}{f}\right)}{C}} - 273 \tag{3.14}$$

Where,

T_{fict} = Fictive temperature for the determination of the asphalt stiffness (℃)

T_a = Design temperature (℃), 20 ℃ in this case

f_{test} = Load frequency used in the standard test (Hz), 8 Hz in this case

f = Load frequency of the design traffic speed (HZ);

C = Experimentally determined constant (K), 11242 K in this case [32]

The traffic speed can be converted into the frequency of a sinusoidal load by equation 3.15:

$$\log(f_{eq}) = -0.6 - 0.5 \cdot h_a + 0.94 \cdot \log(V) \tag{3.15}$$

Where,

f_{eq} = Equivalent load frequency of the design traffic speed (Hz)

h_a = Asphalt layer thickness (m)

V = Design traffic speed (km/h)

In conclusion, the effect of a moving load at a certain speed is firstly converted into a load frequency. Then on the basis of the master curve a corresponding fictive temperature of asphalt can be obtained. With these parameters the stiffness modulus of the asphalt can be finally determined by the equation 3.12.

3.4.2.Fatigue analysis

In the Dutch design method the evaluation criterion for the fatigue analysis is mainly the surface cracks caused by the horizontal strain at the bottom of asphalt layers. A fatigue line is used to predict the fatigue performance of asphalt layers. This fatigue line is a function obtained from laboratory tests for the determination of the fatigue life of asphalt based on the horizontal strain at a certain asphalt layer and the stiffness modulus of asphalt tested under design conditions. The equation is described by a polynomial whose form is fixed but the regression coefficients vary by asphalt mixture:

$$\ln(N_{fatigue}) = c_1 + c_5 \cdot \{\ln(\varepsilon_{horizontal}) + c_2 \cdot \ln^2(E_a) + c_3 \cdot \ln(E_a) + c_4\}^2 \qquad (3.16)$$

Where,

$N_{fatigue}$ = Permissible number of load repetitions for fatigue prediction (-)

E_a = Stiffness modulus of asphalt for selected design traffic speed and temperature (MPa)

$\varepsilon_{horizontal}$ = Horizontal strain at the bottom of asphalt layer (μm/m)

$c_1 \sim c_5$ = Regression coefficients (-), obtained directly from the OIA report as listed in table 3.7

c_1	45.596584	c_4	-0.142729
c_2	-0.064449	c_5	-0.222478
c_3	1.404363	**Healing factor**	2.00

Table 3.7 Fatigue related coefficients

In this section a healing factor is also introduced to represent the self-healing ability of the asphalt material. The micro cracks that result from the fatigue of asphalt layer may heal up to some extent during the rest (non-loaded) period. The exact mechanism behind this phenomenon has not been clearly discovered. The healing factor here is defined as the ratio between laboratory tested lifetimes with and without rest periods expressed in numbers of permissible load repetitions. In this case the healing factor is set to 2.0 (according to the OIA input file), which means the calculated permissible number of load repetitions by equation 3.16 should be doubled for the final fatigue evaluation.

3.4.3.Permanent deformation analysis

In the Dutch design method the deformation at the surface of the unbound layers is considered as the primary reason for the permanent deformation of a pavement. A relationship between unbound layer deformation and vertical strain at the top of the layer has been determined. This relationship is converted into a function and displayed down below:

$$\log(N_{deform}) = c_1 + c_2 \cdot \log(\varepsilon_{vertical}) \tag{3.17}$$

Where,

N_{deform} = Permissible number of load repetitions for permanent deformation prediction (-)

$\varepsilon_{vertical}$ = Vertical strain at the top of the targeted unbound layer (μm/m)

c_1 & c_2 = Regression coefficients (-), $c_1 = 17.289$, $c_2 = -4.00$

3.4.4.Performance prediction results

Following the fatigue and permanent deformation analysis procedure discussed in the former chapters, the allowable numbers of load repetitions can be determined under all different load conditions and tire prints. Then the ratio of fatigue or permanent deformation resistance of each axle load and tire type combination is calculated. This rate is defined as the predicted number of axle passes of a certain axle load and tire type divided by the allowed number of load repetitions for the pavement under the same combination. Finally sum the ratios of fatigue or permanent deformation resistance of all the combinations, considering several correction factors such as lateral wander, to evaluate the performance of the designed pavement structure. This summation can be expressed as equation 3.18:

$$\sum_{NL}^{NL}\sum_{NT}^{NT}\frac{n_{ij}}{N_{ij}} = M_t \tag{3.18}$$

Where,

n_{ij} = Design number of load repetitions of axle load class i and tire type j (-)

N_{ij} = Fatigue or permanent deformation resistance (allowed number of load repetitions) of axle load class i and tire type j (-)

NL = Number of axle load classes (-)

NT = Number of tire types (-)

M_t = Damage fraction (Miner's rule) (-)

Here the Miner's rule is used to evaluate the pavement performance. The relationship between structural damage and the Miner number is listed in table 3.7 [23].

Structural damage	Strength fatigue	Miner number
5%	32%	0.32
10%	43%	0.43
15%	**54%**	**0.54**
20%	64%	0.64
25%	74%	0.74

Table 3.8 Relationship between asphalt structural damage and Miner number

Rijkswaterstaat stipulates a maximum permissible structural damage ratio of 15% for fatigue evaluation, whose Miner number is 0.54 according to the table. For the permanent deformation evaluation the maximum permissible Miner number is equal to 1. Therefore when the calculated Miner number for fatigue is larger than 0.54 or for permanent deformation larger than 1, the designed pavement structure will be considered to have failed and need to be re-designed.

Performance	Miner number
AC layer fatigue	**0.54**
Unbound base deformation	- (≈0)
Subgrade deformation	**0.08**

Table 3.9 Performance prediction by OIA (Miner number)

The calculated results for both original and new designs are listed in the table 3.10 and 3.11. For lane 3 the values remain the same since the thickness design of lane 3 remains the same.

	Lane 2		Lane 3	
Truck axle distributions	27%		73%	
	1.14E+08		3.09E+08	
Direction	Transverse	Longitudinal	Transverse	Longitudinal
$M_{Original}$	0.006	0.009	**0.016**	**0.024**
M_{New}	**0.016**	**0.021**		

Table 3.10 Fatigue performance prediction (Miner number)

	Lane 2		Lane 3	
Truck axle distributions	27%		73%	
	1.14E+08		3.09E+08	
Layer	Unbound base	Subgrade	Unbound base	Subgrade
$M_{Original}$	0.003	0.048	**0.009**	**0.13**
M_{New}	**0.007**	**0.074**		

Table 3.11 Deformation performance prediction (Miner number)

3.4.5.Performance prediction analysis

Several conclusions can be drawn from the results:

- For fatigue analysis the Miner numbers in two directions, longitudinal and transverse, are indeed different. The Miner number in the longitudinal direction is larger than it in the transverse direction. Therefore the longitudinal direction should be considered as the dominant direction for the simplicity of the calculation in the future.
- For permanent deformation the Miner number of the subgrade is larger than that of unbound base. This observation is a match with the OIA calculated result.
- For the original design, the huge difference of the traffic amounts between the light traffic lane and heavy traffic lane does produce two different damage fractions. It is indicated that there is indeed a possibility to optimize the thickness design of the light traffic lanes.

- For the new design, since the thickness of asphalt layer is reduced, the calculated Miner numbers all increase compared to the numbers of original design. Even so, these new Miner numbers are still below the permissible values, which indicate that the new design is a proper pavement structure according to the Dutch standard.

It is worth noticing that the fatigue Miner numbers calculated with the horizontal strain results obtained from the viscoelastic materials are quite small compared to the results of the original OIA reports. Ideally the fatigue damage fraction of the heavy traffic lane should be close to the upper limits (0.54) since its thickness design comes from the OIA design results with a 100% fatigue failure for the asphalt layer. To look into this problem closer, a comparison test is executed in which the two viscoelastic asphalt materials are substituted by two elastic materials with the E modulus used in the original OIA calculation. Since all the materials in the comparison test are non-time related elastic materials, the required strain results for all 30 circumstances (10 axle load classes and 3 tire types) can be easily obtained from one run that contains 30 static load simulations. Then on this basis the pavement performance evaluation, namely fatigue and permanent deformation, can be processed following the same procedures. The results are listed in the table 3.12.

	Lane 2		Lane 3	
Truck axle distributions	27%		73%	
	1.14E+08		3.09E+08	
Direction	**Transverse**	**Longitudinal**	**Transverse**	**Longitudinal**
$M_{Original}$	0.13	0.20	**0.36**	**0.54**
M_{New}	**0.34**	**0.50**		

Table 3.12 Fatigue performance prediction of elastic model (Miner number)

The comparison test provides a more desirable result. The dominant Miner number, which is the fatigue damage fraction of the heavy traffic lane in longitudinal direction, is exactly 0.54. The other Miner numbers are all below the permissible value, which proves that both original and new design are eligible for the performance evaluation. Focusing on the light traffic lane, it can be clearly observed that with the new design the Miner number of the longitudinal direction remarkably increases from 0.20 to 0.50, which is close to the 0.54 limit. As a matter of fact, in both longitudinal and transverse directions the fatigue damage fractions of the new design's light traffic lane are close to the fractions

of heavy traffic lane. This result is very meaningful since it shows that the new design causes the light and heavy traffic lane to have a similar material utilization.

The comparison test indicates that the finite element model is able to provide proper results for the pavement design. The small strain value issue is mainly because of the use of the viscoelastic material. In general, the strain responses calculated from the viscoelastic model is around 50% of the strain values calculated from the elastic model. After the Miner number calculation the difference becomes even bigger.

Numerically it can be explained. The creep test for the AC material shows that within the short loading time used in the moving load simulation the stiffness of the AC can be still very high compared to the 10000 MPa value used in the elastic simulation, which will lead to smaller strain responses.

4. Long-term run analysis

As discussed in the earlier chapters, although the finite element software is capable of calculating the strain response of a pavement structure in a more direct way, the evaluation for the performance is still on the basis of a series of empirical equations. Fortunately the finite element software is also able to carry out a long-term simulation. With the introduction of the viscoelasticity or damage factor of a material, the software can predict the pavement's condition after thousands even millions of axle loads passing by. It provides another perspective to evaluate the performance of pavement structures.

4.1. Real-life simulation

In most studies, there are mainly two ways of realizing a real-life simulation. The first one is converting the moving load into a sinusoidal load applying at one position [48] whilst the second is to calculate the accumulated impact time and punish the model with the same amount of time and load [49].

However, in reality a moving load almost never acts like a sinusoidal load or occurs at constant time intervals. The various dimensions and distances between vehicles result in different strain peaks and recovering time for each axle loads. Although it is definitely impossible to recreate the actual situation on a pavement, there are still some efforts to be made to obtain a more suitable simulation.

4.1.1. Traffic load input

Traffic never distributes evenly during the 24 hours of a day or the 4 seasons of a year. The traffic conditions, namely amount, loading classes or even speed, can be quite different between the rush hours and the off-peak hours [50]. For example, during the rush hours the traffic amount will definitely boost. As a result the time interval between vehicles will decline and lead to a shorter recovery time for the pavement. However, in some statistical researches during the rush hours, the amount of heavy trucks tends to decrease since they prefer to run during the off-peak hours [50]. Obviously it is neither possible nor economical to make a 100% real simulation. Therefore a smart choice of traffic load input is necessary.

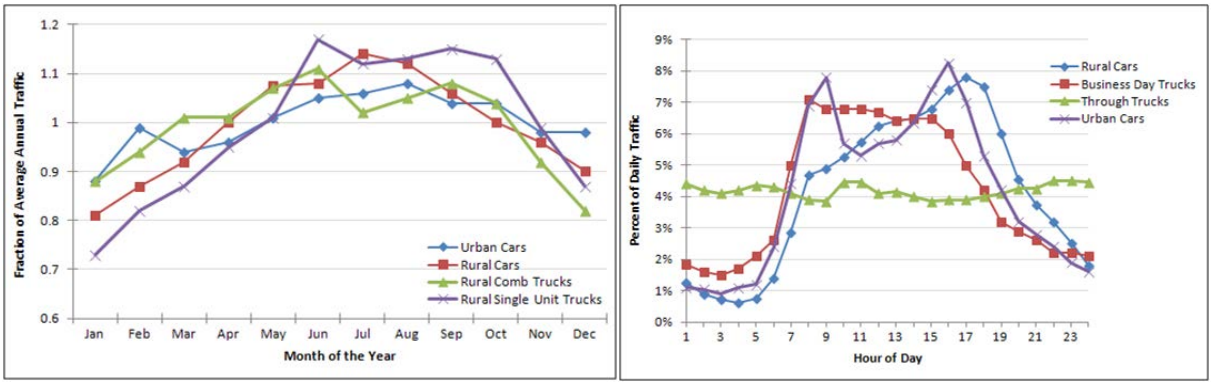

Figure 4.1 Monthly (r) and hourly (l) vehicle volume distributions by classification [50]

In the NDW files the average daily traffic amount is provided. Clearly there are two extreme cases to arrange these vehicles. One case is letting all vehicles run as in the rush hours with a minimum interval for the first few hours until the total daily traffic amount is reached, then let the pavement relax for the rest of the day. The other case is simply dividing 24 hours by the traffic amount to obtain an average time slot for one vehicle and apply this into the simulation. The reality should be a situation inbetween these two cases.

Currently the time consumption for one pass of a moving load simulation is around 30 minutes. This implies that by the end of this research the real-life simulation may not accomplish the vehicle amount even for one day. Thus to obtain some useful information in this limited time period, only the most severe case, the first case, is applied.

In the earlier chapter, 30 combinations of axle load classes and tire types were chosen to represent all the vehicles. Theoretically these combinations should randomly appear in the real-time simulation following their distribution percentages. To simplify the input procedure, in this section all axle load classes are converted into an ESAL of 100 kN. Three tire types remain with a slightly adjusted spectrum ratio (EL: DL: BB = 4:4:2). One loading cycle for 10 axles contains 420 time steps with a time interval of 0.025 s. The time steps for one axle passing is 10 (80 km/h).

As to the time interval between vehicles, for the first case, the safe distance, which is considered as the minimum allowable distance between vehicles, should be determined. In a report published by Conference of European Directors of Roads [51], a 2-second rule is applied in the Netherlands. The basis of the rule is 1 second reaction time and 1 second braking time. However in practice, especially in the rush hours, fewer drivers comply with this rule. In theory, the capacity of one lane per hour is 1800 vehicles whilst in practice, there can be up to 2300 vehicles running on a single lane per hour. Therefore in this case a time interval of 1.6s is applied.

A standard two-axle truck with a front and rear wheelbase of 6.6m is chosen for the simulation [34]. Considering the tire length, the time for one truck passing by is 0.5s. Since in reality most of the front axles are equipped with single tire, an order for the three tires' appearance is settled.

Figure 4.2 Typical two-axle truck (VOLVO FL) [65]

To simulate the passing lane's influence to the light traffic lane, a series of passenger cars are assigned onto the passing lane. A 2-axle single-wheel passenger car with a wheelbase of 2.5 m and axle load of 7.5 kN is chosen as the representative model. The speed of passenger cars is set to 120 km/h with the same 1.6 s following distance as trucks'. One loading cycle for each passenger car (2 axles) passing by contains 67 time steps with the same time interval of 0.025 s. The time steps for one axle passing is 7 (120 km/h). The final traffic input is listed in table 4.1.

Lane 1 Passenger cars (120 km/h)				
Car No.	**Start step**	**End step**	**Total steps**	**Tire type**
1	1	7	67	EL
	4	10	67	EL

Lane 2 Trucks (80 km/h)				
Truck No.	**Start step**	**End step**	**Total steps**	**Tire type**
1	1	10	420	EL
	12	21	420	DL
2	85	94	420	BB
	96	105	420	DL
3	169	178	420	EL
	180	189	420	DL
4	253	262	420	EL
	264	273	420	BB
5	337	346	420	EL
	348	357	420	DL

Table 4.1 Traffic input for real-life simulation

4.1.2. Rutting prediction

The real-life simulation not only provides a direct prediction for the deformation of the pavement, but also exports certain strain values of all asphalt and unbound layers which can be used for the calculation of rutting depth following the Guide for Mechanistic-Empirical Design by National Cooperative Highway Research Program (NCHRP) of USA.

4.1.2.1. Background

For decades it has been a convention that the evaluation for the permanent deformation of a pavement is associated to the vertical strains on top of the unbound layers. Even today, many pavement structure design methods, including the Dutch design method used in the former chapters, are still based on this fundamental criterion: by limiting the vertical strains of the unbound layers, the permanent deformation at the surface of the pavement will be controlled to a tolerable level. What happens in the upper asphaltic layers is not relevant in these methods. With the development of the technology and knowledge, it becomes more and more widely accepted that the rutting depth of the pavement is an accumulation of the deformations in all layers, from top to bottom, of the entire pavement structure [52].

Based on this concept, a rutting prediction procedure has been developed by NCHRP in the Mechanistic-Empirical Pavement Design Guide to evaluate the permanent deformation of the pavement considering the rutting performance in all the layers. Different functions are applied to predict the rutting depth for different layers. Generally these functions are all associated with time and traffic repetitions [52].

4.1.2.2. Rutting prediction procedure

For the rutting depth in asphalt layers, the calculation is as equation 4.1:

$$\Delta_{p(HMA)} = \varepsilon_{p(HMA)} \cdot h_{HMA} = \beta_{1r} \cdot k_z \cdot \varepsilon_{r(HMA)} \cdot 10^{k_{1r}} \cdot n^{k_{2r}\beta_{2r}} T^{k_{3r}\beta_{3r}} \quad (4.1)$$

Where,

$\Delta_{p(HMA)}$ = Permanent deformation of asphalt layer (in)

$\varepsilon_{p(HMA)}$ = Accumulated permanent strain in asphalt layer (in/in)

$\varepsilon_{r(HMA)}$ = Resilient strain calculated by the structure response model (in this thesis CAPA-3D) at the mid-depth of each asphalt layer (in/in)

h_{HMA} = Total thickness of all asphalt layers (in)

n = Number of axle load repetitions (-)

T = Design temperature (°F)

$k_{1r} \sim k_{3r}$ = Global field calibration parameters, according to NCHRP 1-40D recalibration (-) [52]

$\beta_{1r} \sim \beta_{3r}$ = Local or mixture field calibration constants (-), for global calibration all three constants are set to 1.0

k_z = Depth confinement factor (-), see equation 4.2 to 4.4

$$k_z = (C_1 + C_2 D) \cdot 0.328196^D \tag{4.2}$$

$$C_1 = -0.1039 \cdot {H_{HMA}}^2 + 2.4868 \cdot H_{HMA} - 17.342 \tag{4.3}$$

$$C_2 = 0.0172 \cdot {H_{HMA}}^2 - 1.7331 \cdot H_{HMA} + 27.342 \tag{4.4}$$

Where,

D = Depth below the surface (in)

H_{HMA} = Total asphalt layer thickness (in)

A summary of the required constants and parameters is shown in table 4.2:

β_{1r}	1.00E+00	k_{1r}	-3.35E+00
β_{2r}	1.00E+00	k_{2r}	4.79E-01
β_{3r}	1.00E+00	k_{3r}	1.56E+00

Original design	inch or F°	m or C°		
H_{HMA}	1.12E+01	2.85E-01	C_1	-2.52E+00
T	6.80E+01	2.00E+01	C_2	1.01E+01
New design	**Inch or F°**	**m or C°**		
H_{HMA}	1.02E+01	2.58E-01	C_1	-2.80E+00
T	6.80E+01	2.00E+01	C_2	1.16E+01

Design	Layer	Thickness (mm)	D		k_z
			(m)	(inch)	
Original	PA	50	0.0250	0.9843	**2.49E+00**
	AC 1	75	0.0875	3.4449	**6.99E-01**
	AC 2	80	0.1650	6.4961	**4.56E-02**
	AC 3	80	0.2450	9.6457	**2.05E-03**
New	PA	50	0.0250	0.9843	**2.87E+00**
	AC 1	75	0.0875	3.4449	**7.99E-01**
	AC 2	80	0.1650	6.4961	**5.21E-02**
	AC 3	53.4	0.2317	9.1220	**3.96E-03**

Table 4.2 Summary of constants and parameters for asphalt layer rutting depth prediction

For the unbound material layers, the rutting depth of subgrade and other unbound layers are calculated separately.

The initial model used to predict the permanent deformation of unbound layers was proposed by Tseng and Lytton in 1989 [53]. The basic relationship is:

$$\Delta_{p(unbound)} = \left\{\left[\varepsilon_0 \cdot e^{-\left(\frac{\rho}{N}\right)^{\beta}}\right] \cdot \beta_1 \cdot \left(\frac{\varepsilon_v}{\varepsilon_r}\right)\right\} \cdot h = \beta_1 \cdot \left(\frac{\varepsilon_0}{\varepsilon_r}\right) \cdot e^{-\left(\frac{\rho}{N}\right)^{\beta}} \cdot \varepsilon_v \cdot h \quad (4.5)$$

Where,

$\Delta_{p(unbound)}$ = Permanent deformation of unbound layer (in)

ε_0, β & ρ = Material properties (-)

N = Number of axle load repetitions (-)

ε_r = Resilient strain imposed in laboratory test to obtain the above listed material properties (in/in)

ε_v = Average vertical resilient strain in the unbound layer as obtained from the primary response model (in/in)

h = Thickness of the unbound layer (in);

β_1 = Calibration factor for the unbound materials (-)

The ratio is estimated upon the type of the material. Many models have been developed and modified to derive this ratio. For the upper unbound layers, the final chosen approach is shown in a series of equations:

$$\log \beta = -0.61119 - 0.017638 \cdot W_c \quad (4.6)$$

$$\left(\frac{\varepsilon_0}{\varepsilon_r}\right) = \frac{\left(e^{\rho\beta} \cdot a_1 \cdot E_r^{b_1}\right) + \left(e^{\left(\frac{\rho}{10^9}\right)^{\beta}} \cdot a_9 \cdot E_r^{b_9}\right)}{2} \quad (4.7)$$

$$C_0 = \ln\left[\frac{(a_1 \cdot E_r^{b_1})}{(a_9 \cdot E_r^{b_9})}\right] \quad (4.8)$$

$$\rho = 10^9 \left[\frac{C_0}{1-(10^9)\beta}\right]^{\frac{1}{\beta}} \quad (4.9)$$

$$W_c = 51.712 \cdot \left[\left(\frac{E_r}{2555}\right)^{\frac{1}{0.64}}\right]^{-0.3586 \cdot GWT^{0.1192}} \quad (4.10)$$

Where,

a_1, b_1 & a_9, b_9 = Traffic level related parameters (-), solved for N=1 and N=10^9 respectively. Here, $a_1 = 0.15, b_1 = 0.0,\ a_9 = 20.0, b_9 = 0.0$ [52]

W_c = Water content (%)

E_r = Resilient modulus of the unbound material (psi)

GWT = Ground water table depth (ft). In the Netherlands the ground water level varies from 0.5 to 1.0 metre below the surface in the western part of the country, while in the higher area from 1.0 to 20.0 metres [54]. In this thesis a GWT of 1.0 metre is chosen for the calculation

The subgrade of the pavement usually possesses very large depth and in some cases, for example the Dutch design method, is considered to be a semi-infinite layer. Therefore the procedure of the determination of permanent deformation in the upper unbound layers is no longer applicable. An alternative method has been developed to evaluate the plastic strain for an infinite layer as noted down below:

$$\varepsilon_p(z) = (\varepsilon_{p,z=0}) \cdot e^{-kz} \tag{4.11}$$

Where,

$\varepsilon_p(z)$ = Plastic vertical strain at depth z ((in/in)), measured from the top of the subgrade

$\varepsilon_{p,z=0}$ = Plastic vertical strain at the top (z=0) of the subgrade (in/in)

z = Depth measured from the top of the subgrade (ft)

k = Constant obtained from regression (-)

The resilient strains at the top of the subgrade and at the depth of 6 inches from the top of the subgrade can be obtained from the real-life simulation. The requisite parameters, $\left(\frac{\varepsilon_0}{\varepsilon_r}\right)$, β and ρ, at the two depth can be calculated separately using the procedure mentioned earlier for unbound materials. Then the plastic vertical strain for both depth can be computed as:

$$\varepsilon_p = \left(\frac{\varepsilon_0}{\varepsilon_r}\right) \cdot e^{-\left(\frac{\rho}{N}\right)^{\beta}} \cdot \varepsilon_v \tag{4.12}$$

Where,

ε_v = Resilient strain output from the real-life simulation (in/in)

N = Number of axle load repetitions (-)

Using these two data points, the regression constant can be solved as:

$$\mathrm{k} = \frac{1}{6}\ln\left(\frac{\varepsilon_{p,z=0}}{\varepsilon_{p,z=6}}\right) \tag{4.13}$$

Where,

$\varepsilon_{p,z=0}$ = Plastic vertical strain at the top (z=0) of the subgrade (in/in)

$\varepsilon_{p,z=6}$ = Plastic vertical strain at the 6 inches below the surface of the subgrade (in/in)

Finally the total permanent deformation of the subgrade can be predicted:

$$\Delta_{p(subgrade)} = \varepsilon_{p,z=0} \cdot \int_0^{h_{bedrock}} e^{-kz} dz = \left(\frac{1 - e^{-kh_{bedrock}}}{k}\right) \cdot \varepsilon_{p,z=0} \quad (4.14)$$

Where,

$\Delta_{p(subgrade)}$ = Permanent deformation of the subgrade (in)

$h_{bedrock}$ = Depth to the bedrock (ft), since the subgrade is considered to be semi-infinite, in this thesis the distance from the top of the subgrade to the imaginary bedrock is 500mm which is used in the CAPA-3D model

The calculated parameters for unbound base and subgrade are listed in table 4.3.

	Subgrade 6 inch	Subgrade surface	Unbound base
GWT (m)	8.48E-01	1.00E+00	1.30E+00
E_r (MPa)	1.00E+02	1.00E+02	4.00E+02
GWT (ft)	2.78E+00	3.28E+00	4.27E+00
E_r (psi)	1.45E+04	1.45E+04	5.80E+04
W_c (%)	1.72E+01	1.69E+01	6.46E+00
β	1.22E-01	1.23E-01	1.88E-01
C_0	-4.89E+00	-4.89E+00	-4.89E+00
ρ	9.35E+05	7.40E+05	5.12E+03
$\varepsilon_0/\varepsilon_r$	**3.07E+01**	**3.02E+01**	**2.21E+01**

Table 4.3 Summary of constants and parameters for unbound layer and subgrade rutting depth prediction

The resilient strains for each layer under different tire types can be obtained from the strain plots output from the real-time simulation. One example is shown in figure 4.4:

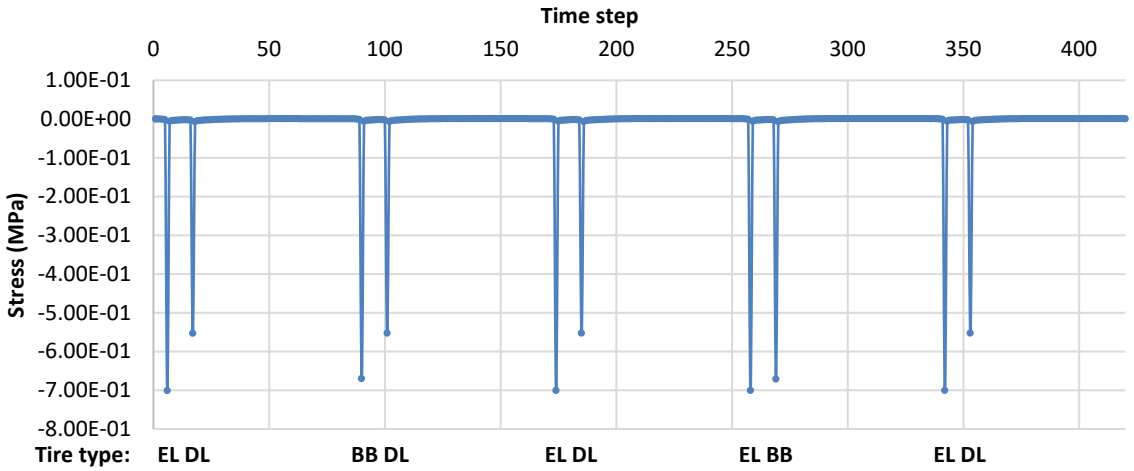

Figure 4.3 Vertical stress plot at the centre of AC layer of real-life simulation

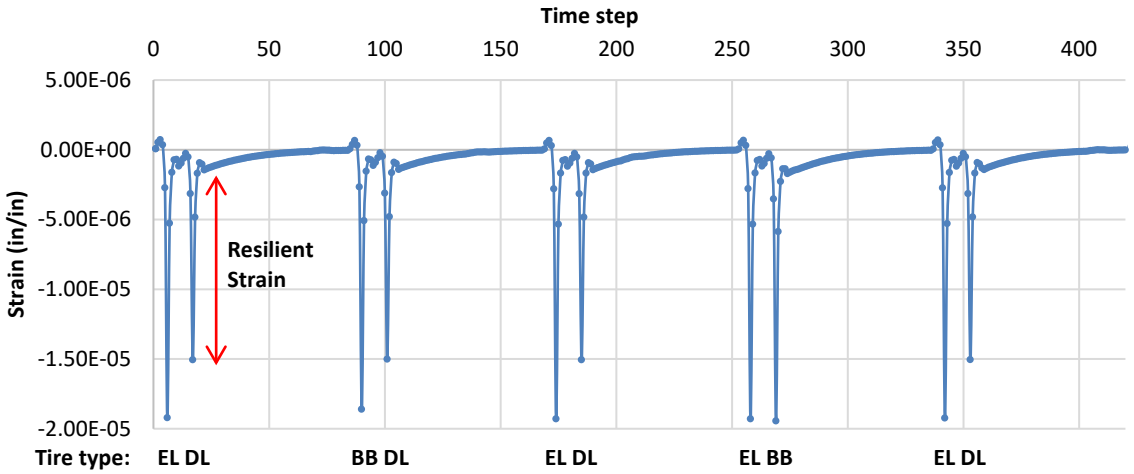

Figure 4.4 Vertical strain plot at the centre of AC layer of real-life simulation

4.1.2.3. Rutting prediction results

By far, the procedures for the prediction of permanent deformation for all three types of layers have been discussed. Since the rutting depth calculation uses a non-linear method, the total rutting depth cannot be simply summed up by percentage of each tire types. Therefore the rutting depth under all three tire types are calculated separately. The results for both original and new designs are listed in tables below:

Single tire (EL)									
Design	Original				New				Δ%
Layer	ε_r (in/in)	Δ_p		%	ε_r (in/in)	Δ_p		%	
		(inch)	(mm)			(inch)	(mm)		
PA	7.91E−05	0.3220	**8.1800**	**82.67%**	7.54E-05	0.3530	**8.9700**	**82.39%**	**9.68%**
AC 1	1.03E-05	0.0117	0.2980	3.01%	8.49E-06	0.0111	0.2810	2.58%	-5.72%
AC 2	1.25E-05	0.0009	0.0236	0.24%	1.37E-05	0.0012	0.0296	0.27%	25.66%
AC 3	1.58E-05	0.0001	0.0013	0.01%	1.98E-05	0.0001	0.0033	0.03%	142.89%
AC		0.0127	**0.3230**	**3.26%**		0.0123	**0.3140**	**2.88%**	**-2.81%**
Asphalt		0.3350	**8.5000**	**85.93%**		0.3650	**9.2800**	**85.27%**	**9.20%**
Unbound base	4.84E-05	0.0112	**0.2830**	**2.86%**	5.63E-05	0.0141	**0.3590**	**3.30%**	**26.65%**
Subgrade z=0	1.14E-04	0.0026	0.0656		1.29E-04	0.0029	0.0743		
Subgrade z=6	1.04E-04	0.0024	0.0596		1.17E-04	0.0026	0.0671		
k		0.0159				0.0169			
Subgrade		0.0436	**1.1100**	**11.21%**		0.0490	**1.2400**	**11.43%**	**12.23%**
ΣΔ		**0.3890**	**9.8890**			**0.4280**	**10.8830**		**10.04%**

Table 4.4 Pavement rutting depth prediction under Single tire (EL)

Dual tire (DL)									
Design	Original				New				
Layer	ε_r (in/in)	Δ_p		%	ε_r (in/in)	Δ_p		%	Δ%
		(inch)	(mm)			(inch)	(mm)		
PA	7.16E-05	0.2913	**7.3994**	**82.05%**	6.89E-05	0.3225	**8.1903**	**81.90%**	**10.69%**
AC 1	8.36E-06	0.0095	0.2419	2.68%	7.28E-06	0.0095	0.2409	2.41%	-0.42%
AC 2	9.01E-06	0.0007	0.0170	0.19%	1.02E-05	0.0009	0.0219	0.22%	29.00%
AC 3	1.20E-05	0.0000	0.0010	0.01%	1.50E-05	0.0001	0.0025	0.02%	141.53%
AC		0.0102	**0.2599**	**2.88%**		0.0104	**0.2653**	**2.65%**	**2.06%**
Asphalt		0.3015	**7.6593**	**84.93%**		0.3329	**8.4556**	**84.55%**	**10.40%**
Unbound base	4.41E-05	0.0102	**0.2582**	**2.86%**	5.07E-05	0.0127	**0.3590**	**3.59%**	**39.04%**
Subgrade z=0	1.11E-04	0.0025	0.0636		1.24E-04	0.0028	0.0743		
Subgrade z=6	1.03E-04	0.0023	0.0587		1.14E-04	0.0026	0.0671		
k		0.0133				0.0144			
Subgrade		0.0433	**1.1008**	**12.21%**		0.0481	**1.2220**	**12.22%**	**11.00%**
ΣΔ		**0.3551**	**9.0183**			**0.3937**	**10.0003**		**10.89%**

Table 4.5 Pavement rutting depth prediction under Dual tire (DL)

Broadband (BB)									
Design	Original				New				
Layer	ε_r (in/in)	Δ_p		%	ε_r (in/in)	Δ_p		%	Δ%
		(inch)	(mm)			(inch)	(mm)		
PA	7.86E-05	0.3195	**8.1163**	**82.74%**	7.49E-05	0.3509	**8.9128**	**82.43%**	**9.81%**
AC 1	9.50E-06	0.0108	0.2747	2.80%	7.99E-06	0.0104	0.2643	2.44%	-3.80%
AC 2	1.17E-05	0.0009	0.0221	0.23%	1.30E-05	0.0011	0.0279	0.26%	26.54%
AC 3	1.52E-05	0.0001	0.0013	0.01%	1.91E-05	0.0001	0.0031	0.03%	143.18%
AC		0.0117	**0.2981**	**3.04%**		0.0116	**0.2954**	**2.73%**	**-0.92%**
Asphalt		0.3313	**8.4144**	**85.78%**		0.3625	**9.2081**	**85.16%**	**9.43%**
Unbound base	4.86E-05	0.0112	**0.2847**	**2.90%**	5.67E-05	0.0127	**0.3612**	**3.34%**	**26.88%**
Subgrade z=0	1.14E-04	0.0026	0.0655		1.29E-04	0.0142	0.0741		
Subgrade z=6	1.04E-04	0.0023	0.0597		1.17E-04	0.0029	0.0670		
k		0.0156				0.0166			
Subgrade		0.0437	**1.1104**	**11.32%**		0.0490	**1.2434**	**11.50%**	**11.98%**
ΣΔ		**0.3862**	**9.8095**			**0.4257**	**10.8127**		**10.23%**

Table 4.6 Pavement rutting depth prediction under Broadband (BB)

4.1.3. Rutting prediction comparison

The rutting depth results of all three tire types share the same pattern. For the total rutting depth, the new designed pavement structure indeed suffers a more severe deformation. However this increase is not as significant as the boost of fatigue prediction. The new design leads to a roughly 10% increase for all three tire types.

When zooming into the rutting depth of each layer respectively, the top layer (PA layer) undoubtedly hold the dominant position with a nearly 82% contribution of the total rutting depth. In the new design the resilient strain of the PA layer increases. Since the thickness of this layer remains the same, a 10% increase of the rutting depth is produced.

For the AC layer, although the resilient strains fluctuate due to the thickness change, the reduction of the thickness in this layer to some extent neutralizes the strain increase. As a result the original and new design almost share the same rutting depth in the AC layer.

On the contrary, in the unbound base layer, the reduction of the AC layer leads to an increase of the resilient strain. Plus the extra thickness assigned to this layer, the unbound base layer suffers the biggest increase percentage around 26%.

Finally the subgrade has the same change pattern as the PA layer. With increased resilient strains and non-changed layer thickness, a 12% rise is witnessed in the rutting depth of the subgrade.

It is also worth noticing that although the rutting depth prediction of the new design indeed increases, which indicates a positive result in material cost-efficiency, there is still a significant gap to the rutting depth prediction of the heavy traffic lane. If the pavement is evaluated solely based on this criterion, there is still more potential for reduction of thickness in the light traffic lanes.

4.1.4. Real-life simulation deformation output

The deformation plots of the real-life simulation are shown below.

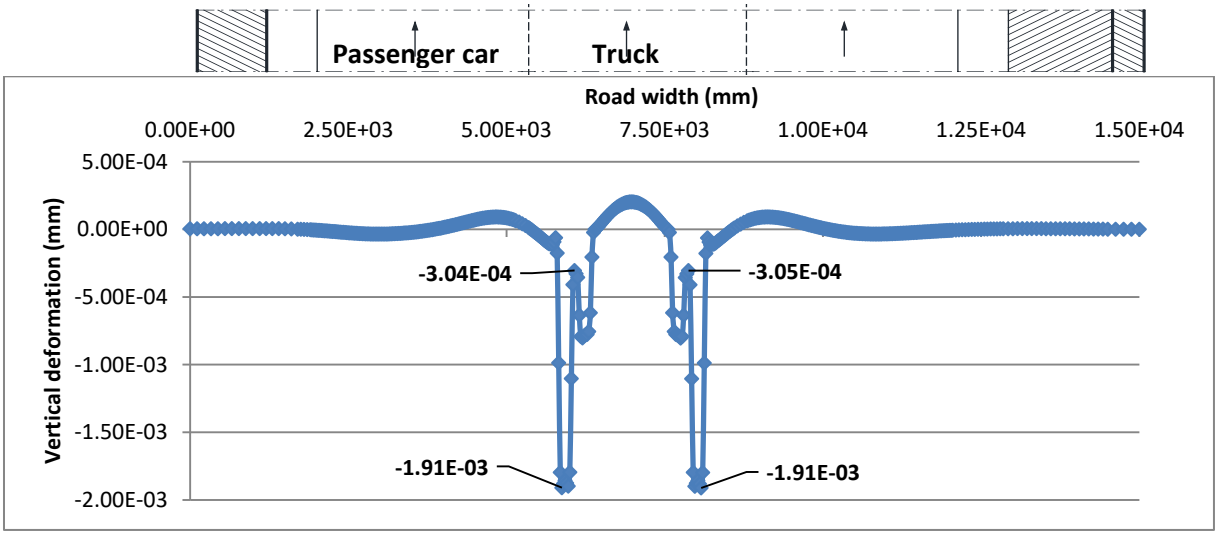

Figure 4.5 Vertical deformation at pavement surface (Original design, 384th step, 1st cycle)

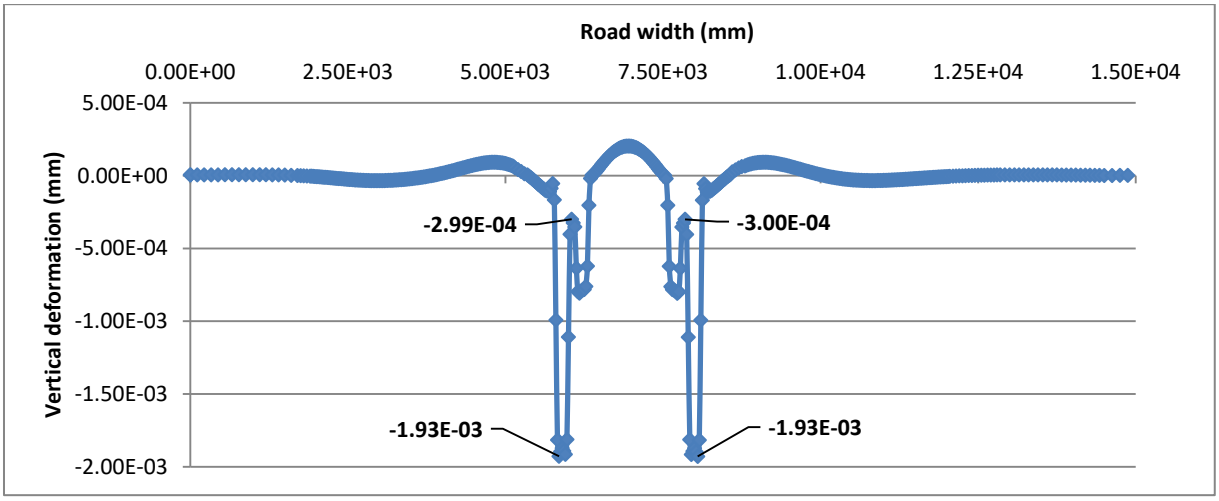

Figure 4.6 Vertical deformation at pavement surface (Original design, 384th step, 132nd cycle)

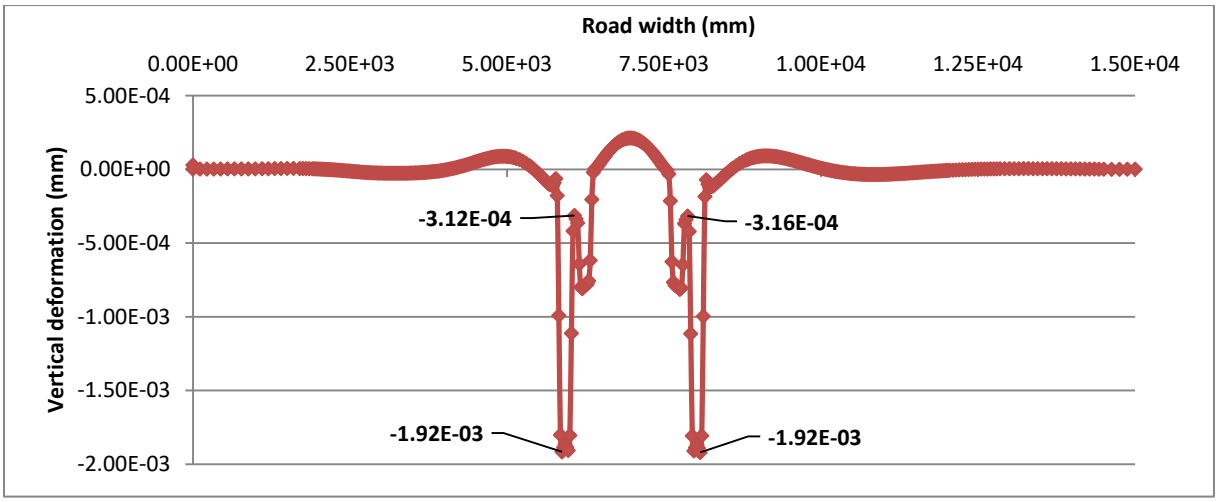

Figure 4.7 Vertical deformation at pavement surface (New design, 384th step, 1st cycle)

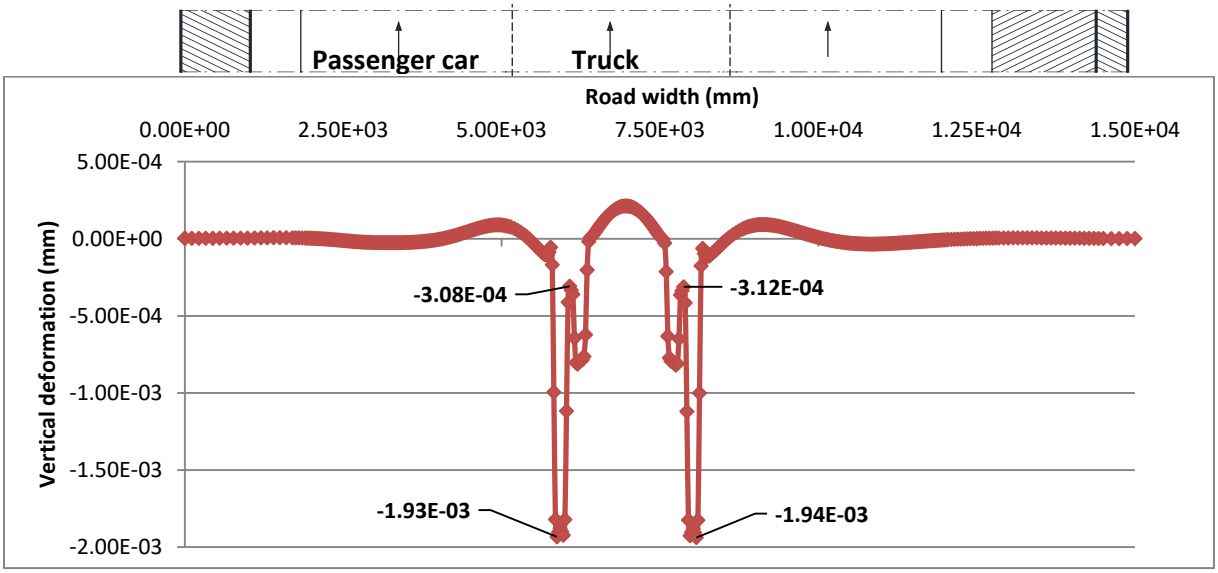

Figure 4.8 Vertical deformation at pavement surface (New design, 384th step, 132nd cycle)

Figure 4.5 & 4.6 and 4.7 & 4.8 show the vertical deformation at the surface of the pavement of the 1st load cycle and the 67th cycle for both original and new design. As time goes by, the accumulated vertical deformation indeed occurs in both cases. As predicted the new design produces larger deformation than the original design since the thickness of asphalt layer is reduced in the outer and middle lanes (left two lanes). Moreover, the slope structure design in the new design indeed affects the vertical deformation distribution across the pavement. However this influence is limited which will not negatively affect the driving experience on this lane. Both original and new designs share the same growth rates.

	Position	Deformation (mm)		Growth value	Growth rate
		1st cycle	132nd cycle		
Original design	Tire edge 1	-1.91E-03	-1.93E-03	1.77E-05	**0.93%**
	Gap centre 1	-3.04E-04	-2.99E-04	4.47E-06	**1.47%**
	Gap centre 2	-3.05E-04	-3.00E-04	4.48E-06	**1.47%**
	Tire edge 2	-1.91E-03	-1.93E-03	1.77E-05	**0.93%**
New design	Tire edge 1	-1.92E-03	-1.93E-03	1.77E-05	**0.92%**
	Gap centre 1	-3.12E-04	-3.08E-04	4.49E-06	**1.44%**
	Gap centre 2	-3.16E-04	-3.12E-04	4.48E-06	**1.42%**
	Tire edge 2	-1.92E-03	-1.94E-03	1.77E-05	**0.92%**

Table 4.7 Vertical deformation growth at critical positions (Original vs New design)

Figures below show the vertical deformation at the surface of each structural layer in the pavement.

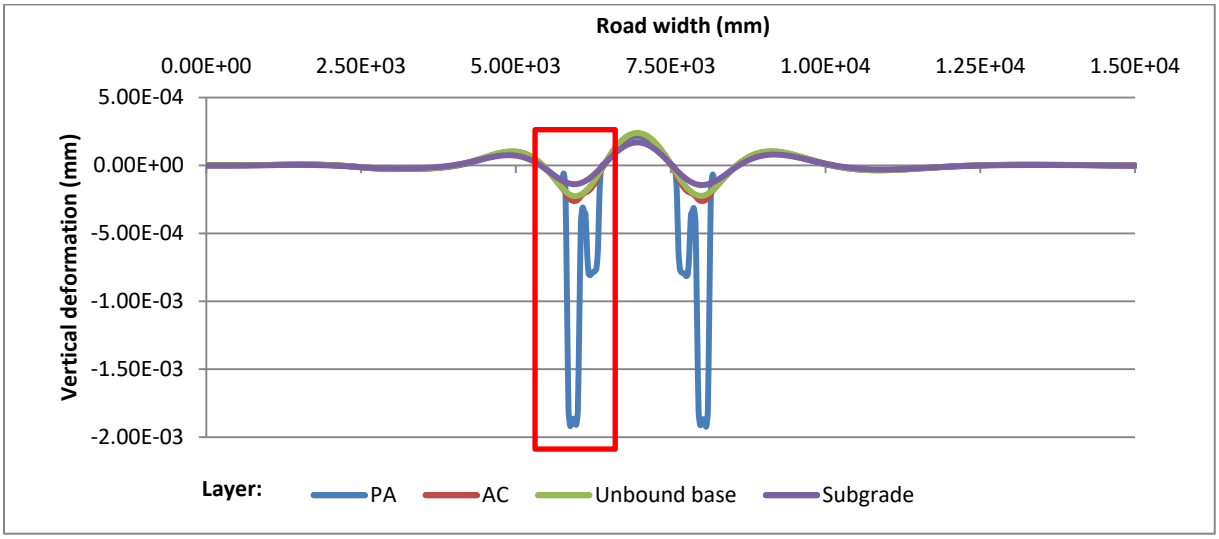

Figure 4.9 Vertical deformation at surface of different layers (New design, 384th step, 1st cycle)

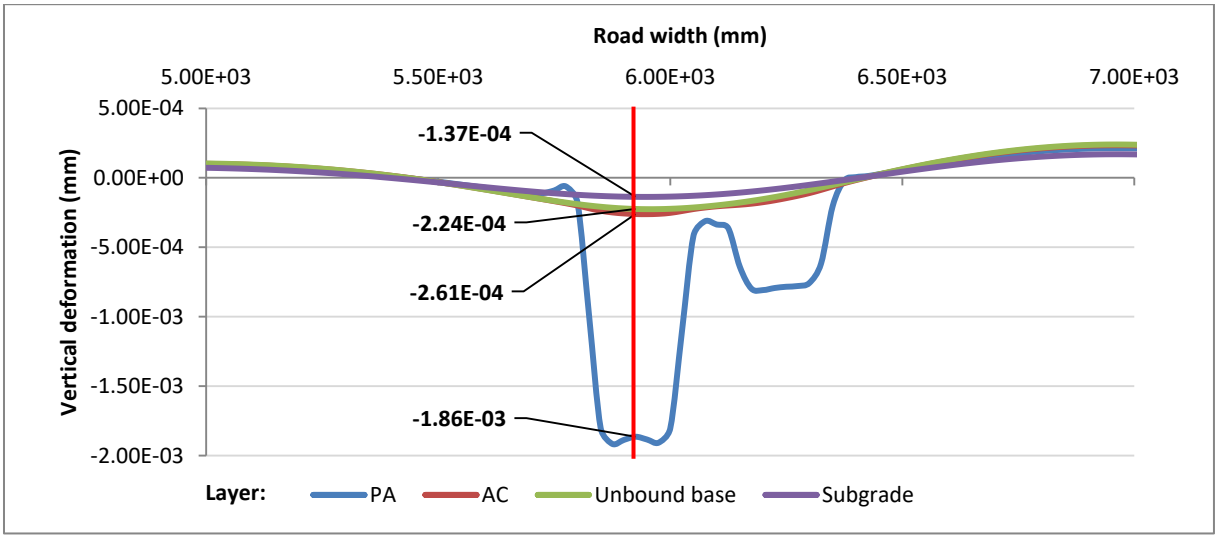

Figure 4.10 Partial enlargement of figure 4.9

Figure 4.10 is a partial enlargement of the vertical deformation condition under one dual set. It proves the assumption used in the rutting depth calculation in the earlier sections. The top PA layer contributes the most to the total vertical deformation, followed by the subgrade, the unbound base and the AC layer.

Layer	Surface positon (mm)	Total deformation (mm)	Deformation per layer (mm)	Percentage	Calculated percentage
PA	1.09E+03	-1.86E-03	-1.60E-03	**85.97%**	**82.39%**
AC	1.04E+03	-2.61E-04	-3.70E-05	**1.99%**	**2.88%**
Unbound base	8.28E+02	-2.24E-04	-8.70E-05	**4.67%**	**3.30%**
Subgrade	5.00E+02	-1.37E-04	-1.37E-04	**7.37%**	**11.43%**

Table 4.8 Vertical deformation contribution of each layer

The results support the concept that the rutting depth of the pavement is an accumulation of the deformations in all layers, from top to bottom, of the entire pavement structure. Therefore it is recommended that for the future pavement structure design the permanent deformation evaluation should consider the rutting condition in all the layers rather than only focusing on the subgrade or unbound layers.

4.1.5. Criticism on the deformation analysis

In the previous sections both MEPDG calculation and real-life simulation output indicated that the top PA layer would produce the largest vertical deformation. However, in practice it is hardly the case.

Porous asphalt (PA) uses an open-graded aggregate to obtain high air voids which provide the ability of quickly removing the water from the pavement surface. Meanwhile open-graded aggregate also leads to a coarse granular skeleton with more stone-on-stone contact since there is limited fine aggregate or asphalt binder comparing to AC (figure 4.11). The skeleton of larger stones resists traffic loads by transmitting them through stone-on-stone contact and eventually to the layers below. As a result, the deformation or rutting resistant capacity of PA is better than AC [67].

However in both MEPDG method and the finite element models, the materials are considered to be isotropic and homogeneous. So does the Dutch design software OIA. The strain response as well as deformation are calculated almost solely based on the stiffness. Since the stiffness of PA is smaller than AC, the top layer is predicted to produce the largest vertical deformation.

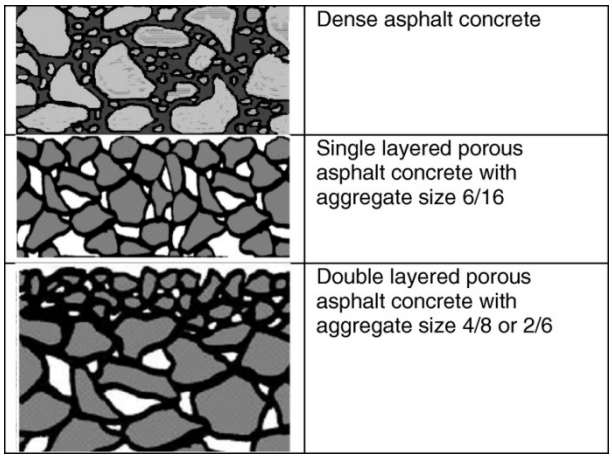

Figure 4.11 Schematic presentation of pavement materials commonly used I the Netherlands [68]

Furthermore, theoretically the deformation plots here can never be the “permanent” deformation. In the real-life simulation the axle loads are constantly passing by on the pavement. For example figure 4.9 shows the 384th time step in the 1 loading cycle. It means the plot represents the deformation situation after the last axle passing by during the 348th to 357th time step. Hence the pavement is still recovering from the deformation causing by the past axle load. In fact since in the simulation all materials are elastic or viscoelastic (generalized Maxwell model), if the pavement is given long enough time to relax, in the end all the deformation will disappear. As a result here figure 4.8 shows more likely the instant deformation under the passing loads (or primary deformation) rather than the permanent deformation.

4.2. Platooning

In Europe, truck platooning has become a hot research topic and industrial opportunity. A truck platoon consist of several trucks driven closely one by one with the help of a modern communicating and navigating system. Since the distance between the trucks is relatively smaller, the different strain condition in the pavement is worth studying [55].

With the proper traffic, pavement geometry and material parameter input, almost any traffic condition can be simulated and compared by using the established model in CAPA-3D. In this section a simple simulation and comparison of truck platooning on the pavement structure is executed.

4.2.1. Background

Truck platooning comprises a row of trucks equipped with an advanced driving support system which enables the trucks to follow each other with a much closer safe distance. As mentioned in the former chapter, in many countries, including the Netherlands, the regulated minimum safe distance between vehicles is defined by two parts in the form of time: reaction time and braking time. In a truck platoon, with a zero reaction thanks to the system, the following trucks are able to brake immediately which can help improve traffic safety with even a shorter safety distance. Platooning also has the potential of cost saving since trucks are driven closer to each other at a same speed which will lower the fuel consumption as well as the CO_2 emissions. Lastly, platooning also efficiently enhances the traffic flows resulting in a reduction of traffic jams [56].

All the advantages mentioned above are almost all based on the fact that truck platooning will lead to a more frequent, constant loading on the pavement with a shorter relaxing time. This may cause a different strain reaction of the pavement structure and lead to a different performance prediction. Hence it is worth investigating it with the help of the finite element model.

4.2.2.Data Input

Since in most of the present platooning field tests the trucks in a platoon hold the same specifications, and also to simplify the input, only one type of axle load, which is dual tire with a vertical load of 100 kN, is applied in this platooning simulation. A longer truck model with a wheelbase of 11 metres is applied to mimic the standard shipping container truck used in the field test hence the time interval between the front and rear axles is 0.5 second [34]. The following distance between trucks in platooning is smaller than the regulated safe distance of 2.0 second. European Automobile Manufacturers' Association (ACEA) set 0.5 second as a minimum following distance for the truck manufacturers [55]. Finally four trucks are set for one platoon in this simulation.

As for the control test the same truck models are used with a regulated safe distance of 2.0 second. The total amount of trucks in both tests should be the same. It takes 10 seconds for 4 trucks to pass by in the normal case, therefore the time interval between two truck platoons is set to 6.5 seconds.

The input data for both cases is listed in figure 4.12.

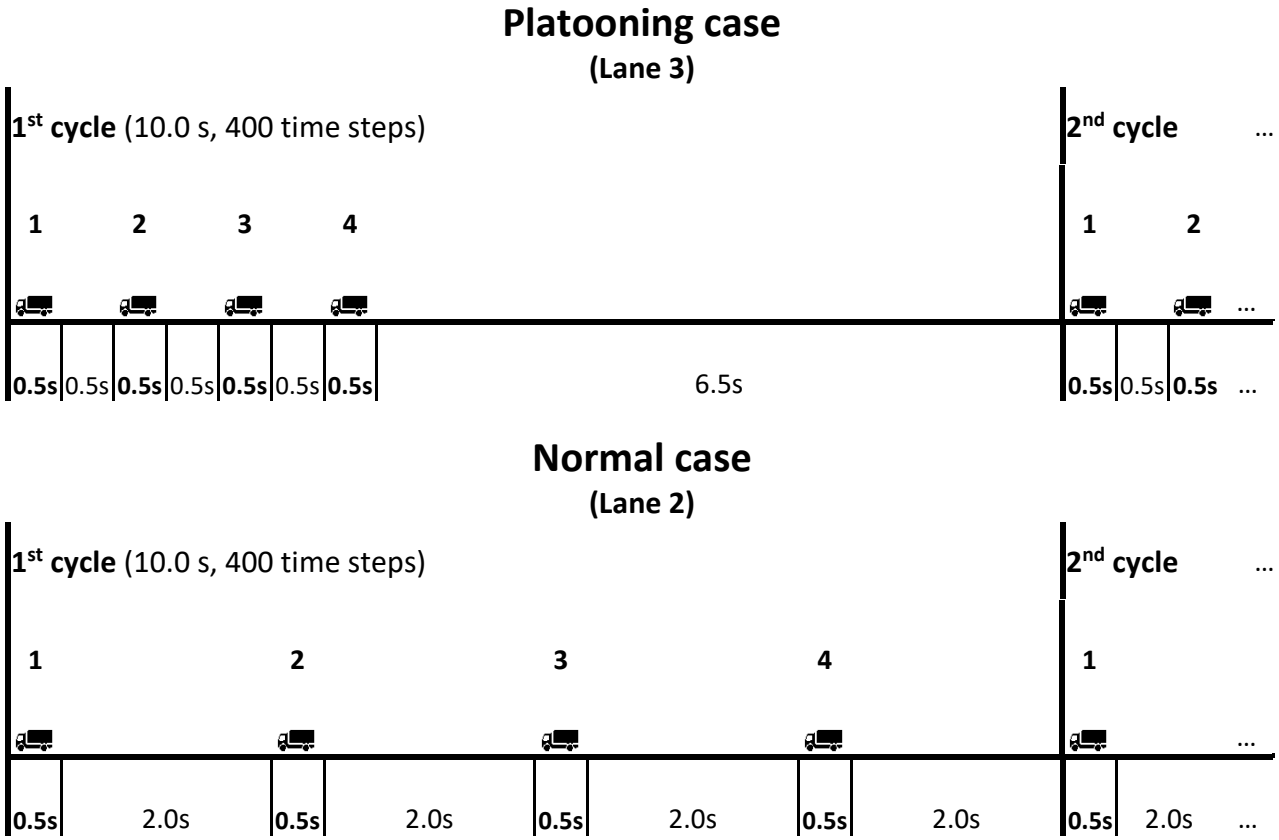

Figure 4.12 Traffic input for Platooning and Normal case simulation

4.2.3.Data Output and comparison

The plots of horizontal strains at the bottom of the asphalt layer for both normal and platooning cases in one cycle (four trucks) are shown below:

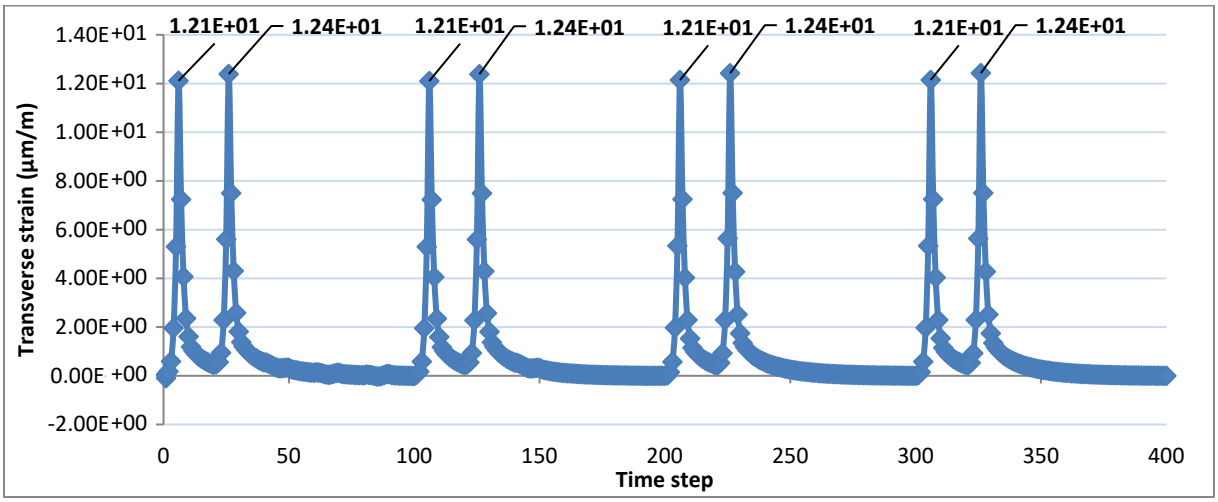

Figure 4.13 Transverse strain at AC layer bottom (Normal case, 1st cycle)

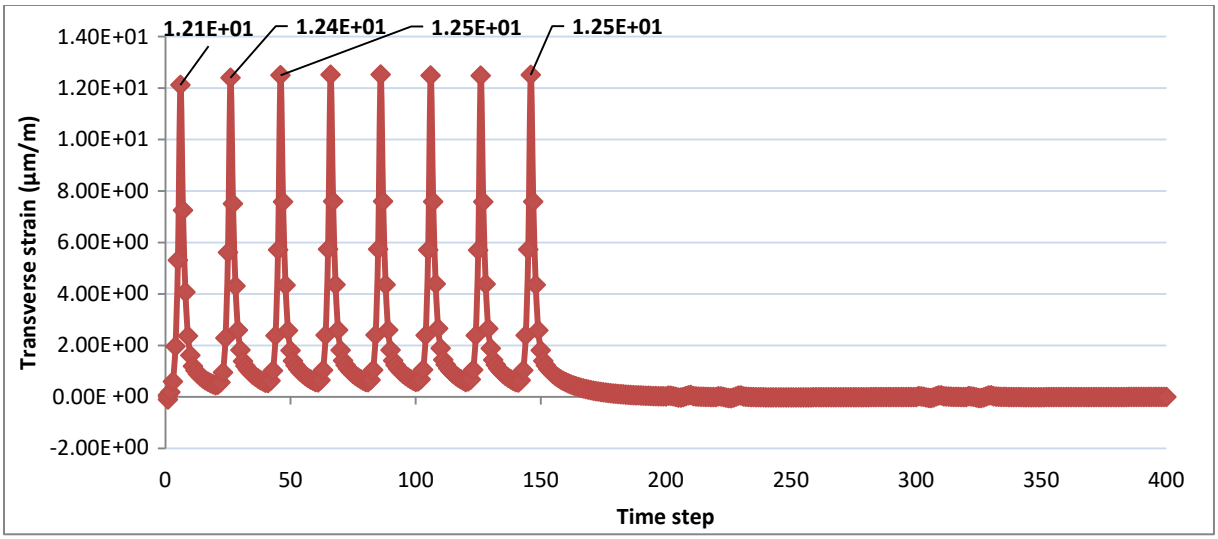

Figure 4.14 Transverse strain at AC layer bottom (Platooning case, 1st cycle)

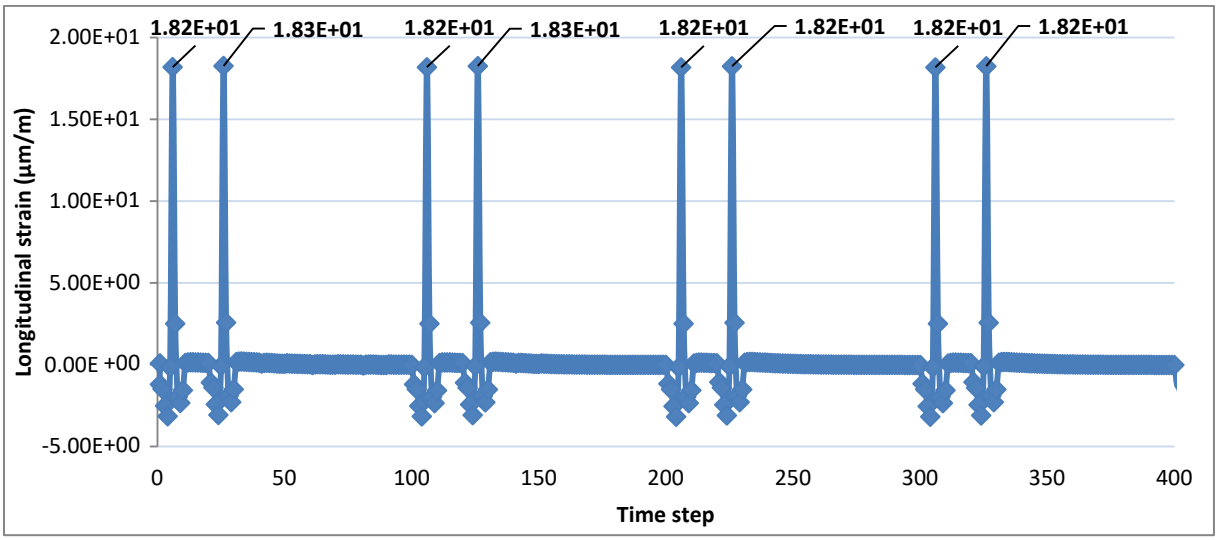

Figure 4.15 Longitudinal strain at AC layer bottom (Normal case, 1st cycle)

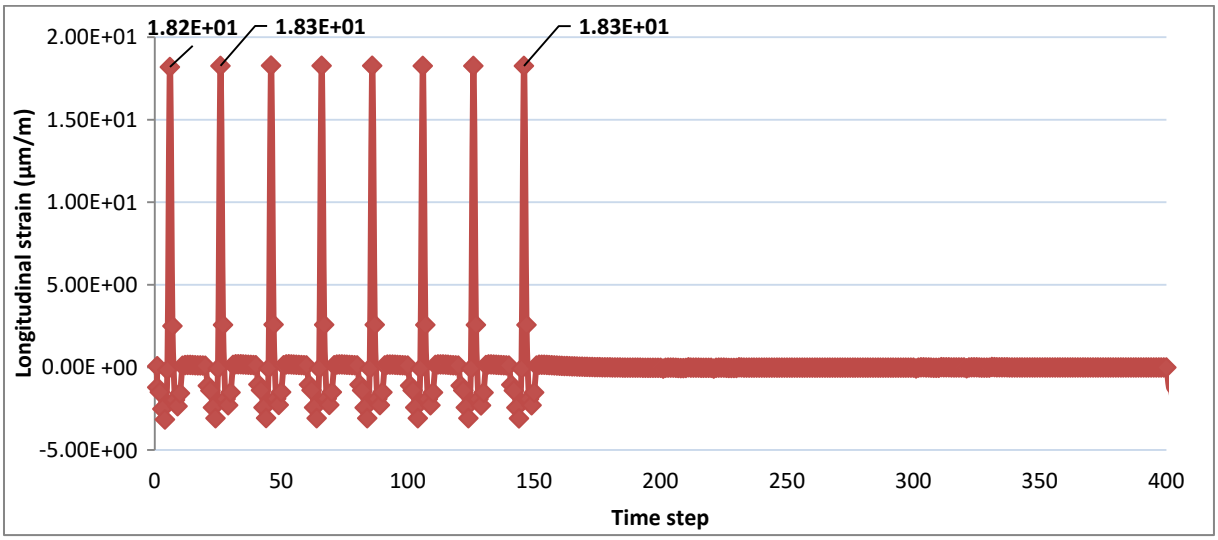

Figure 4.16 Longitudinal strain at AC layer bottom (Platooning case, 1st cycle)

From the plots it can be seen that for the first truck both cases share the same strain pattern. However for the following trucks, the platooning case produce slight higher strain values while the normal case continue to repeat the strain pattern of the first truck. The short following time in the platooning case leaves the pavement a correspondingly shorter recovery time, hence the horizontal strains caused by the following trucks are larger compared to the normal case. Notice that this response is highly influenced by the viscoelasticity of the material.

The larger strain in the platooning case means that by the current fatigue prediction procedure used in chapter 3, the platooning case will cause more severe fatigue problem (larger Miner value) than the normal case. However since in theory the time interval between two platoons is longer than it in the normal case, the effect on the recovery or self-healing of the pavement is worth further studies.

The plots of vertical deformation at the surface of the pavement for both normal and platooning cases at the end of the 1st and 155th cycle are shown below:

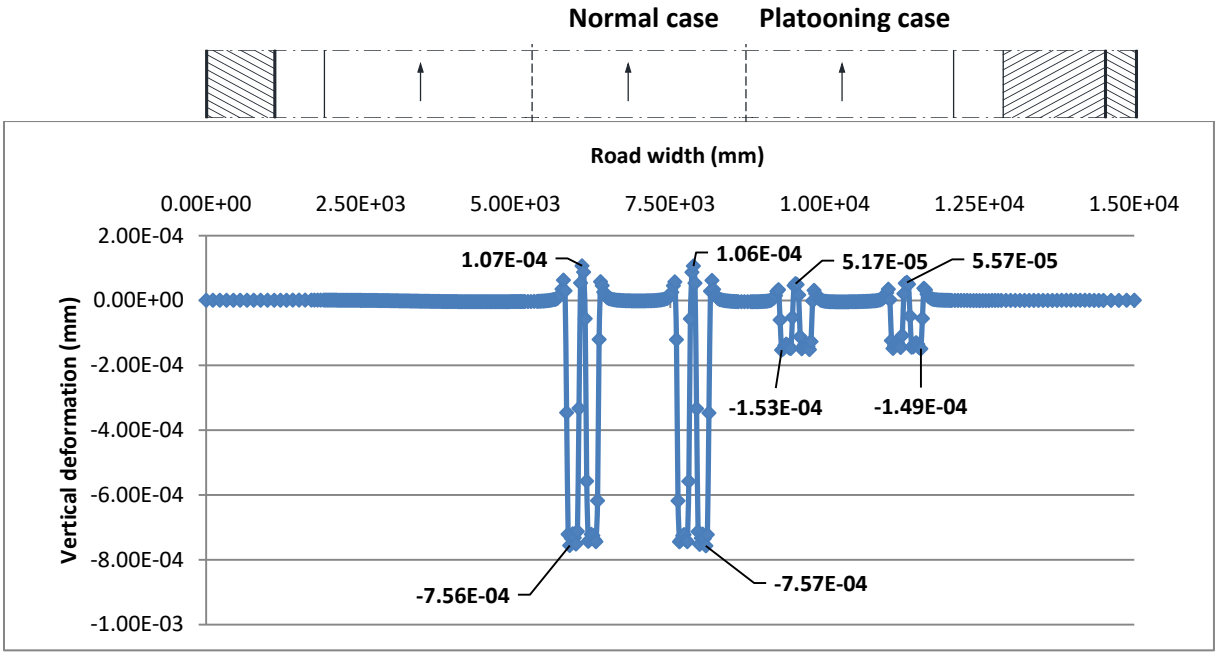

Figure 4.17 Vertical deformation at pavement surface (400th step, 1st cycle)

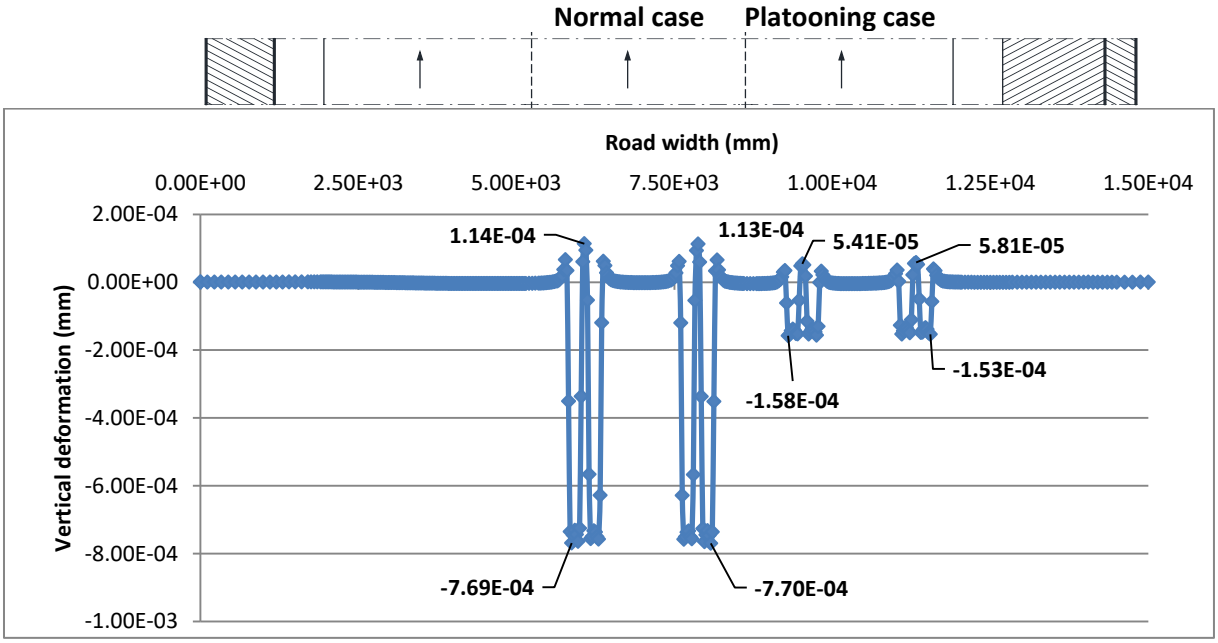

Figure 4.18 Vertical deformation at pavement surface (400th step, 155th cycle)

The comparison of the two plots indicate that as time goes on, there is indeed accumulated vertical deformation in the pavement for both cases. Since the end frame of each cycle is chosen to be displayed here, at this time point the platooning case has longer rest period than the normal case. As a result, in these plots the vertical deformation of the normal case is much larger. However, the intermediate point under the dual tire in the normal case owns the largest deformation growth whilst the platooning case has a bigger growth rate of the maximum vertical deformation. This may imply that the platooning case may cause more permanent deformation problem. Nevertheless, further investigation is required.

	Position	Deformation (mm)		Growth value	Growth rate
		1st cycle	155th cycle		
Normal case	Tire edge 1	-7.56E-04	-7.69E-04	1.27E-05	**1.68%**
	Gap centre 1	1.07E-04	1.14E-04	6.96E-06	**6.52%**
	Gap centre 2	1.06E-04	1.13E-04	6.96E-06	**6.57%**
	Tire edge 2	-7.57E-04	-7.70E-04	1.27E-05	**1.67%**
Platooning case	Tire edge 1	-1.53E-04	-1.58E-04	4.39E-06	**2.87%**
	Gap centre 1	5.17E-05	5.41E-05	2.40E-06	**4.63%**
	Gap centre 2	5.57E-05	5.81E-05	2.41E-06	**4.33%**
	Tire edge 2	-1.49E-04	-1.53E-04	4.37E-06	**2.93%**

Table 4.9 Vertical deformation growth at critical positions (Normal vs Platooning case)

5. Construction advice and practice feasibility

5.1. Construction

Road construction is a relatively mature industry. Systematic procedures have been established for the road construction step by step from scratch. In a way, the road construction industry can be somewhat conservative. Although in the former chapters it has been proven that from the design perspective the new pavement structure design indeed saves asphaltic materials without compromising its performance, its feasibility of construction should also be proved.

At present, varies equipment and machines have been developed for certain tasks in the pavement construction procedure. The road construction is after all a business for both government and contractors. To earn their support the new design has to be cost efficient for both material saving and construction cost. It is in their best interest if the new pavement structure design can be implemented with only the existing equipment and machines.

5.1.1. Existing equipment and machines

The construction of an asphalt pavement has a straightforward procedure to follow. Generally speaking there are three main steps: preparation of the pavement site, spreading the asphalt mixture, and compaction of the asphalt mixture [9]. This section will only focus on the equipment and machines used in each step.

First step: the pavement site should be properly prepared. The subgrade needs to be levelled and usually compacted to the required density by various types of compaction equipment. On top of the subgrade an unbound base is placed. The materials are spread by motor graders or bulldozers (dozers). For drainage purpose the pavement requires a 2% crossfall or crown gradient of the surface. To obtain this crossfall the surface of the subgrade and unbound base should also have the same slope. This slope can be accomplished through the final trimming by motor graders [57].

Figure 5.1 Motor grader (l) and Dozer (r) for pavement site preparation [58]

Second step: the asphalt mixture should be spread onto the base layer with the designed grade, thickness and slope gradient. A mechanical spreader referred as an asphalt paver or finisher is specially designed for this task. The most important part of an asphalt paver is the screed. Its primary function is to lay the asphalt mixture to the designed thickness. Since the screed is able to pivot in a certain range of angles [59], the slope gradient of the pavement surface is also accomplishable.

Figure 5.2 Asphalt paver for asphalt mixture distribution [58]

Third step: the spread pavement material should be compacted to the desired density to gain the strength and smoothness. In fact, during the entire pavement construction, in every step, the subgrade, the unbound base, and the final asphalt mixture all require compaction. Different compactors or rollers have been developed for different materials. For the asphalt layer, four types of rollers are used: static, vibratory, pneumatic and a combination thereof [9]. Since in most cases the standard compaction width of the compactor is smaller than the road width or even the lane width, a rolling pattern with overlaps between passes is applied.

Figure 5.3 Static/vibratory roller (l) and Pneumatic roller (r) for compaction [58]

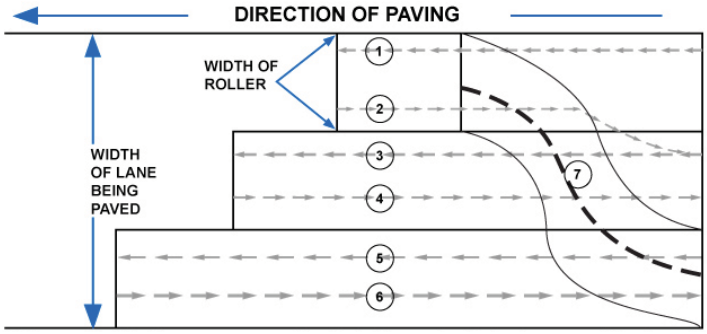

Figure 5.4 Typical rolling pattern [60]

5.1.2. Advice on construction

The cross-section of the new pavement structure design is once again shown in figure 5.5. For a motorway divided into two individual carriageways for each direction, like this project, a single crossfall is applied for water runoff instead of a crown.

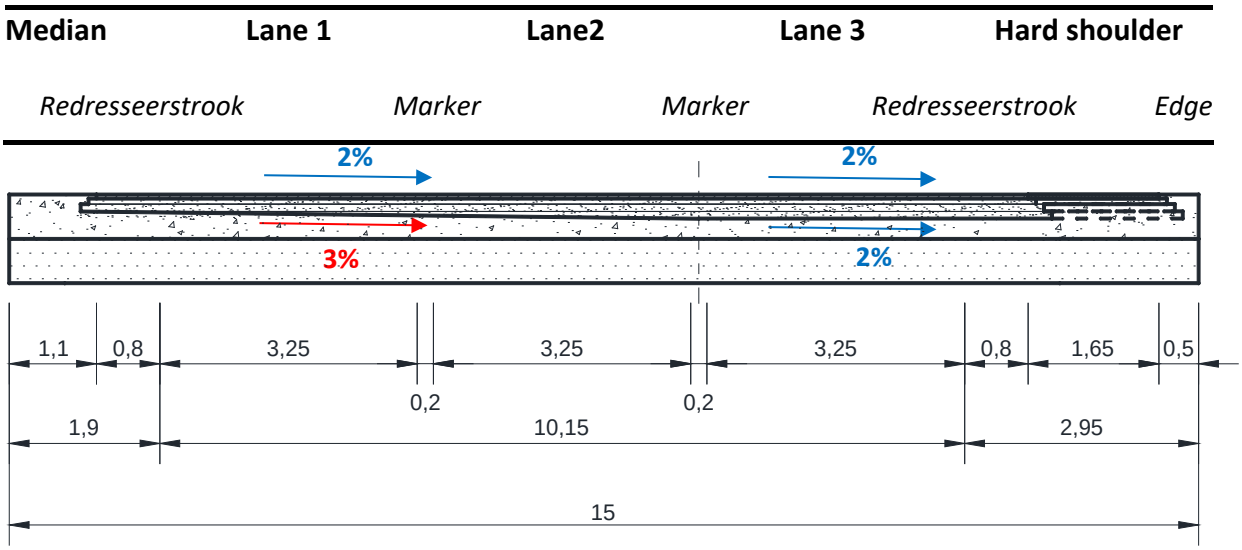

Figure 5.5 Cross section view of new pavement structural design (m)

According to the new design, the structural thickness of the third lane (heavy traffic lane) and the hard shoulder remains the same and therefore can be constructed following the normal procedure whilst the thickness of the rest part of the asphalt layers is reduced. To be specific only the light traffic parts of the third asphalt concrete (AC) layer is halved along the diagonal that creates a steeper slope. This steeper slope is also in favour of drainage. Accordingly the thickness of the unbound base under the reduced AC layer increases to maintain a "horizontal" pavement surface. Therefore the only construction challenge is the additional slope at the position between the AC bottom and the unbound base top.

For the unbound base, the slope can be easily obtained by the motor graders currently used in the construction. Notice that in the new design the light traffic lane structures are no longer parallel layers. Instead, in order to facilitate the construction, all the other layers' surface except the unbound base remain parallel to the pavement surface as before. Hence the preparation for the subgrade surface follows the same instruction.

For the AC layer, usually there are upper and lower limits for the allowable paving thickness by an asphalt layer. The minimum thickness per paving mat should be at least twice or preferable three times the maximum aggregate size in the asphalt mixture [9]. In this thesis, the maximum aggregate size used in the AC mixture is 22.4 mm, thus the minimum paving thickness is 67.2 mm. The maximum paving thickness is not only limited by the specification of the asphalt paver, but also by the ability of the rollers to obtain the adequate compaction [9]. As a result, the designed thickness of one mixture is often divided into multiple lifts for asphalt pavers to place. In this project for the original design the AC layer can be placed in three lifts, one of 75 mm and two of 80 mm, with static wheeled rollers or two lifts of 120 mm and 115 mm by pneumatic or vibratory rollers whose general thickness limit can be between 150 and 200 mm [9]. Nevertheless for the new design obviously the latter paving plan is preferable. The altered slope gradient in the new design can be easily calculated with the result of 1%. Including the standard 2% crossfall for water runoff, the final total slop gradient is still within the crown range of any normal asphalt paver [59]. By altering the angle of the screed, the first uneven AC lift can be placed. At the thinnest point the paving thickness can be set to 70 mm which is higher than the minimum limit while the thickest point is 150 mm. By doing so a "horizontal" surface of the bottom AC lift will be accomplished on which another 85 mm parallel AC lift is able to be easily placed following the routine procedure. This construction design will also help to obtain a more uniform AC layer with less longitudinal joints.

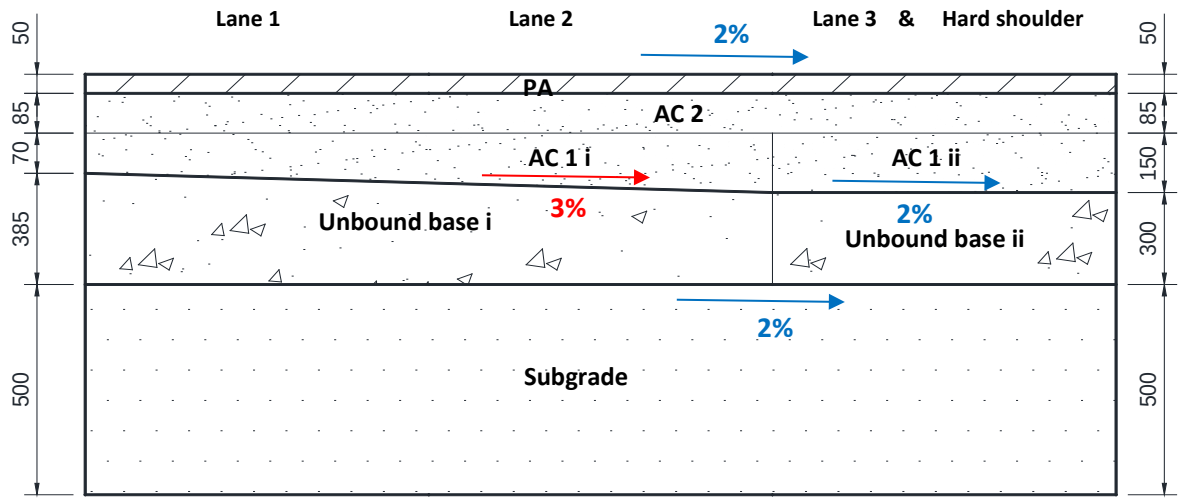

Figure 5.6 Proposed construction procedure for the new design pavement structure

5.2. Feasibility under different situations

During the long service life of a pavement, many varying traffic conditions may occur besides the normal average traffic flow and annual growth rate that has already been considered in the design phase. In many cases, such as routine maintenance or unexpected incident, the lightly trafficked lanes will have to bear denser and heavier traffic. The new designed pavement structure should also be able to cope with these situations. The ability of future replacement and expansion of the new design pavement structure is worth exploring as well.

5.2.1. Redundancy of the new design

In chapter 3 it has been illustrated that the new design enables the light traffic lanes to gain a similar performance prediction as the heavy traffic lane. Nevertheless there is still a certain gap between the predictions of the two parts, which will provide some considerable redundancy for the altered light traffic lane. Notice that in the Dutch design method the redundancy of the pavement is included by the introduction of several coefficients during the design procedure. In this section the discussion about the redundancy of the light traffic lane only focuses on its extra traffic bearing capacity.

The Miner's rule used in the Dutch design method is a linear damage accumulation model, which can be easily used to back-calculate the corresponding traffic flow. For example, the fatigue damage prediction (Miner value) for the elastic model in chapter 3.4.4 is 0.50, which is 0.04 below the maximum allowable value 0.54. Hence from the perspective of fatigue damage there is still

0.04/0.50=8% more traffic flow capacity for the new designed light traffic lane. By multiplying the current total traffic flow and dividing by the daily traffic flow, the new designed light traffic lane is able to bear the traffic flow of the heavy traffic lane for an extra period of almost 230 days. Therefore it is proven that the new design will still hold a certain capability of compensating the abnormal traffic flow distribution during routine maintenance or unexpected incidents.

5.2.2. Routine maintenance

Maintenance is an essential practice to guarantee the long-term performance and the aesthetic appearance of the pavement. The purpose of maintenance is to repair the deficiencies caused by distresses as well as to protect the pavement from further damage [9].

In the Netherlands, regular, annual inspections of the pavement surface are executed all the time. The data from these inspections then become the input for a damage prediction model developed by Rijkswaterstraat. Based on the prediction results the so-called preventive maintenance [61] is performed. The pavement surface will be replaced just before damage is expected. By doing so the unexpected occurrence of a service or vehicle accident will be prevented and in the long term this strategy is more cost-efficient than repairing. Since currently in the Netherlands, usually the wearing course or the upper 50 mm of the pavement is expected to be replaced, the new designed pavement structure will have no effect on this preventive maintenance.

Meanwhile, other preventative or corrective maintenance is still necessary from time to time to decrease the rate of deterioration or even correct specific pavement failures or area of distress. These maintenance activities may include sealcoats, crack or pothole filling, patching, etc. Almost all of these activities are performed at the surface or upper part of the asphalt layers. Therefore the new designed pavement structure will also have no effect on these maintenances.

5.2.3. Future expansion

In the Netherlands, road transportation overall has maintained a rising trend over the past decades, although the 2008 economic crisis slowed down this growth to some extent. The number of cars continuously increases whilst the year 2016 saw the first increase in the number of vans and heavy freight vehicles since 2011 [62]. The rising number of vehicles as well as the rate of usage demand a

larger capacity of the existing motorways. At some point the motorway will have to expand and add more lanes.

In some newly constructed projects, for instance the Amsterdam – Utrecht part of the A2 motorway, there is reserved area, usually at the median strip, for future expansion [63]. In this way the construction site for the future lane has already been prepared for asphalt layers to be placed. For other cases the expansion has to be situated outside the hard shoulder.

Figure 5.7 Reserved expansion area (median strip) of Rijksweg A2 (Amsterdam – Utrecht) [64]

For the new designed pavement, the latter expansion plan is preferable. Since the outermost (heavy traffic) lane and the hard shoulder share the same thickness design as the original pavement structure, the road can be easily expanded following the routine procedure. The expanded lane will have the same thickness design as the original heavy traffic lane which enables the new road to be more than adequate for bearing the extra traffic flow.

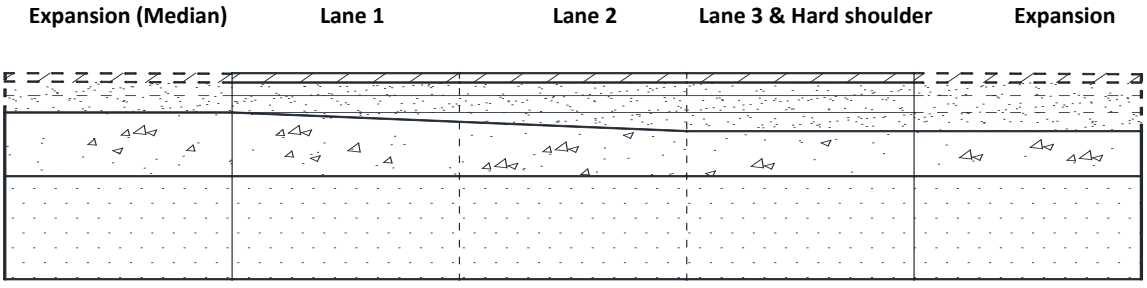

Figure 5.8 Proposed expansion plan for the new design pavement structure

However, for a new construction project, it is still more cost-efficient to reserve the construction site at the median strip for future expansion. In this case though the asphalt part thickness of the expanded

lane should be equal to the thinnest point of the existing passing lane (Lane 1) to maintain the integrity of the asphalt layer. The expanded lane will become the new passing lane. According to the traffic data the primary drive for the traffic growth is passenger cars, thus with the expended lane the new road should also be able to bear the extra traffic flow. Even so, further performance calculation for the expanded should be applied. In case the prediction result is negative, the overall pavement structure can still be strengthened by adding an extra asphalt layer on top of the entire road.

6. Conclusions and Recommendations

6.1. Conclusions

The literature review illustrates a brief history of the development of asphalt pavement structures and design methods. At present the asphalt pavement is constructed as a parallel multi-layer structure with a uniform thickness design solely based on the chosen design lane regardless the number of lanes the road contains. However, the traffic data analysis indicates that in practice neither the vehicles amount nor the axle load classes distribute evenly over different lanes. The structure thickness of the lighter traffic lanes is clearly overdesigned. Hence a potential of a new material-cost-efficient pavement structural design is noticed.

Further analysis of the traffic data on Amsterdam – Utrecht section of A2 motorway provided by NDW proves the uneven distribution of traffic flow over the entire road. The daily traffic amount as well as axle load classes of each lane are calculated and estimated. Using Dutch asphalt pavement structure design software OIA, the thickness design of each lane is based on their own traffic data separately. A considerable reduction of asphalt thickness is observed in the lighter traffic lanes. These thickness designs are set to be the base of a new structural design for asphalt pavement. To avoid stress concentration and construction difficulty, a slope design is proposed.

The finite element analysis software, CAPA-3D, is introduced to create a model for the pavement and execute the simulations. To restrain the model size and running time, a three-lane road with one hard shoulder is chosen for modelling. The 5-lane traffic data form NDW is transferred to fit in 3 lanes. Two asphalt materials, porous asphalt (PA) and asphalt concrete (AC), are converted into Prony series for the software based on their properties obtained from laboratory tests. The tire prints of all combinations of tire types and axle load classes are also calculated following the same procedure used in the OIA software. The model width along the longitudinal direction and time input (number of steps and interval) are determined by several preliminary tests. All the required input data for the modelling are obtained.

The stress and strain responses under 30 different loading combinations are calculated on both the original and the new pavement structural designs using the finite element model. The individual wheel

strain plots witness the same strain patterns obtained from the field tests. The pavement cross section strain plots indicate that in the new designed pavement structure the strain values of the thickness reduced part have indeed increased. However, it is encouraging to see that the strain responses of the thickness unchanged part, which is the heavy traffic lane, are not influenced by the reduced part. The horizontal strain values at the bottom of asphalt layer also shows that unlike the assumption used in the Dutch design method, in most cases, the longitudinal and transverse strains are not equal. Since both directions have a non-negligible chance to produce the maximum strain, the fatigue prediction should be executed based on both longitudinal and transverse strains.

Following the same procedure used in the OIA as well as the Dutch design method, the performance prediction for both the original and the new designed pavement structures are calculated. The results are positive. For the altered light traffic lane the Miner values of both fatigue and permanent deformation increase and turn to be closer to the values of the heavy traffic lane which indicates the material-cost-efficiency is indeed optimized in the new design.

By taking advantage of the finite element models, two real-life simulations of the traffic running on the road are performed. A rutting depth calculation following the American design method MEPDG is carried out with the resilient strain values obtained from the real-life simulations. The results to a certain extent do support the findings of previous performance prediction. The rutting depth of the light traffic lane in the new design indeed increases yet there is still a significant gap compared to the rutting depth of the heavy traffic lane. The vertical deformation plots backup the concept that the rutting depth of the pavement is an accumulation of the deformations in all layers, from top to bottom, of the entire pavement structure. However the limitation of the material model, especially for the PA, leads to a false vertical deformation prediction for the top asphalt layer.

A truck platooning simulation is also performed. The results from this rather preliminary test shows that truck platooning may cause more fatigue damage and permanent deformation problem than normal case. The shorter following distance in the platooning results in shorter rest time between trucks and can lead to larger horizontal strains at the bottom of the asphalt layer. However, further research on this topic is highly recommended to gain firmer conclusions.

The feasibility of construction and maintenance of the new designed pavement structure is discussed in the Chapter 5. It is proposed that the new design can be easily realized by the existing pavement construction equipment and machines. The current maintenance routines are also applicable without any alteration. As for the future expansion, although adding lanes outside the hard shoulder is preferred, construction at the median strip is also feasible but a further evaluation may be required.

In conclusion, the new designed pavement structure is evaluated from both design and construction's perspective. All results positively support the application of this new design. It manages to achieve a better material-cost-efficiency without compromising its serviceability or adding extra construction work or maintenance difficulty. The potential of reducing the thickness of the light traffic lanes has been proved. Further research investment is recommended.

6.2. Recommendations for further research

Temperature is a crucial influence factor for asphalt pavement. Although the current Dutch design method is set to a fixed temperature of 20℃, the response of the new designed asphalt pavement structure under other temperature conditions should be also investigated. Because the asphalt layer now is no longer uniform, the temperature influence distribution over the pavement cross section may also fluctuate.

As discussed in chapter 2, current calculation methods or software for pavement strain responses are almost all based on a parallel-layer system assumption. However in the new designed pavement structure, the light traffic lane contains "unparalleled" layers. To solve this incompatibility problem, in this thesis, the finite element analysis method is introduced. Nevertheless the performance prediction procedures used in this thesis, regardless of the Dutch or the American design method, are still deduced from field or laboratory tests applied on the parallel-layer structures. Hence future investigation and research on strain responses as well as pavement performance prediction of "unparalleled" structures are recommended.

In chapter 4 it has been discussed that the material model used in the current simulation cannot fully represent the real properties of the materials, especially the asphalt materials. As a result, the simulation cannot provide a proper prediction for vertical deformation of porous asphalt layer. Also the lack of plastic component cripple the credibility of predicting permanent deformation. For the future research it is preferable to introduce a new material model that contains elements representing the plastic properties of the materials and also be able to simulate the skeleton structure of the porous asphalt.

In the preliminary research of this thesis, several other designs for the pavement structure were proposed. The cross sections, especially the shapes of asphalt layer, were designed to match the stress distribution pattern along the transverse direction. In theory, this kind of design would have the maximum material-cost-efficiency which leads to an even more material saving capacity. A few models

were tested in the CAPA-3D and output several positive results. In some cases these “odd” shaped designs performed even better than the original design. Although this type of design will obviously introduce much more difficulties to both design and construction, it could still hold a great potential to be the next step for the pavement structure design and is worth further investigation.

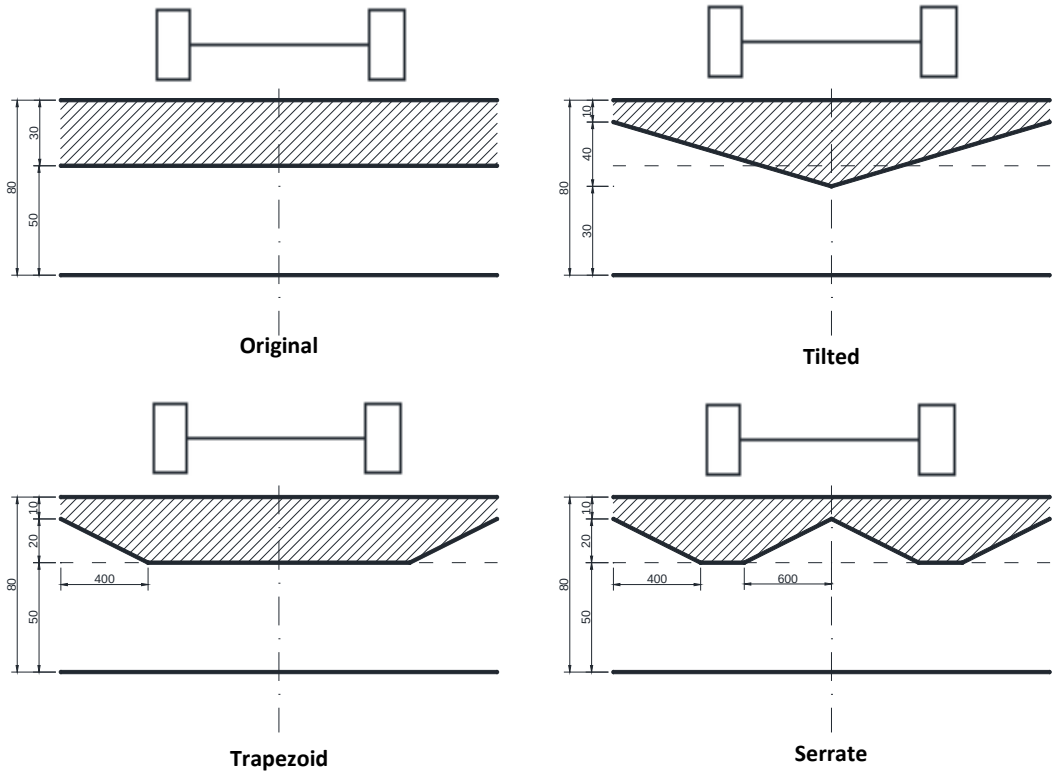

Figure 6.1 Other proposed designs for the asphalt pavement structure (single lane, mm)

Bibliography

[1] Nikolaides, A.F. (2016). Sustainable and long life flexible pavements. *Functional Pavement Design*, 693–704.

[2] Hein, D. K., Rao, S., & Lee, H. (2016). *Bases and Subbases for Concrete Pavements* (No. FHWA-HIF-16-005).

[3] Jenkins, K. (2006). Introduction to Road Pavements. *Hitchhiker's Guide to Pavement Engineering*, 1-11.

[4] Mathew, T. V. (2006). Transportation Engineering I. *Mumbai, India: Civil Engineering–Transportation Engineering. IIT Bombay, NPTEL ONLINE*.

[5] McNichol, D. (2005). *Paving the way: asphalt in America*.

[6] South African National Roads Agency Limited. (2013). South African Pavement Engineering Manual.

[7] Christopher, B. R., Schwartz, C., & Boudreau, R. (2006). *Geotechnical aspects of pavements: Reference manual*. US Department of Transportation, Federal Highway Administration.

[8] Weingroff, R. F. (2016). *Part 1: Essential to the National Interest*. The Greatest Decade 1956-1966: Celebrating the 50th Anniversary of the Eisenhower Interstate System. Federal Highway Administration, U.S. Department of Transportation.

[9] Lavin, P. (2003). *Asphalt pavements: a practical guide to design, production and maintenance for engineers and architects*. CRC Press.

[10] Pederson, N. J. (2007). Pavement Lessons Learned from the AASHO Road Test and Performance of the Interstate Highway System. *Transport Research Board*.

[11] American Association of State Highway, & Transportation Officials. (1993). *AASHTO Guide for Design of Pavement Structures, 1993* (Vol. 1). AASHTO.

[12] Croney, D., & Croney, P. (1991). *The design and performance of road pavements*.

[13] Robbins, M. M., Nam Tran, P. E., & Rodezno, C. (2014). Flexible Pavement Design–State of the Practice NCAT Report 14-04.

[14] Gemayel, C., & Maurovich, M. (2013). Mechanistic-Empirical Pavement Design.

[15] Witczak, M. W., Andrei, D., & Houston, W. N. (2004). Guide for mechanistic-empirical design of new and rehabilitated pavement structures. *Transportation Research Board of the National Research Council*, 1-91.

[16] Kim, M., Tutumluer, E., & Kwon, J. (2009). Nonlinear pavement foundation modeling for three-dimensional finite-element analysis of flexible pavements. *International Journal of Geomechanics*, *9*(5), 195-208.

[17] AHMED, M. A., OTUOZE, H. S., & MURANA, A. A. (2011). Development of Finite Element Response Model for Mechanistic-Empirical Design of Flexible Pavement. *Leonardo Electronic Journal of Practices and Technologies*, (19), 69-84.

[18] Molenaar, A., Erkens, S., Huurman, R., Medani, T., & Visser, T. (2002). Characterisation and Modelling of Airfield Pavement Structures for Tomorrow's Extra Large Aircraft. *Federal Aviation Administration Airport Technology Transfer Conference.* P-40.

[19] Siddharthan, R., Krishnamenon, N., & Sebaaly, P. (2000). Finite-layer approach to pavement response evaluation. *Transportation Research Record: Journal of the Transportation Research Board*, (1709), 43-49.

[20] Chabot, A., Chupin, O., Deloffre, L., & Duhamel, D. (2010). Viscoroute 2.0 a: tool for the simulation of moving load effects on asphalt pavement. *Road Materials and Pavement Design*, *11*(2), 227-250.

[21] Mallick, R. B., & El-Korchi, T. (2013). *Pavement engineering: principles and practice*. CRC Press.

[22] Tenison, J. H., & Hanson, D. I. (2009). *Pre-Overlay Treatment of Existing Pavements* (No. Project 20-5 (Topic 38-06)).

[23] Rijkswaterstaat. (2014). *Ontwerp Specificaties Asfaltverhardingen*. Nederland: Rijkswaterstaat.

[24] Sirgurdur, E. (2013). Failure Modes in Pavements. *KTH AF2903 Road Construction and Maintenance*, 1-12.

[25] Houben, L. J. M. (2003). Structural Design of Pavements–Part IV: Design of Concrete Pavements. *Lecture Notes CT4860.* Faculty of Civil Engineering and Geosciences, TU Delft.

[26] Pavement Design Guide. (2011). *Pavement Design Guide*. Austin, Texas.

[27] Wu, N. (2006). Equilibrium of lane flow distribution on motorways. *Transportation Research Record: Journal of the Transportation Research Board*, (1965), 48-59.

[28] Ryan, J. (2011). Dutch market relies on recycling. *Aggregates Business Europe*, *3.4*. Retrieved from http://www.aggbusiness.com/sections/market-reports/features/dutch-market-relies-on-recycling/

[29] Viti, F., Hoogendoorn, S., Immers, L., Tampère, C., & Lanser, S. (2008). National data warehouse: how the Netherlands is creating a reliable, widespread, accessible data bank for traffic information, monitoring, and road network control. *Transportation Research Record: Journal of the Transportation Research Board*, (2049), 176-185.

[30] A2: verbreding knooppunt Holendrecht – aansluiting Maarssen. (2008, April 20). *Rijkswaterstaat*. Retrieved from https://web.archive.org

[31] Russell, B. Z. (2010, July 27). Trucks vs. Cars on Pavement Damage. Retrieved from http://www.spokesman.com/blogs/boise/2010/jul/27/trucks-vs-cars-pavement-damage/

[32] CROW. (2012). *Achtergrondrapport Ontwerpinstrumentarium asfaltverhardingen (OIA)* (CROW-rapport D11-05). Ede, The Netherlands: CROW.

[33] Scarpas, A. (2000). CAPA-3D finite element system user's manual I, II, and III. *Delft University of Technology Publication*.

[34] *Handboek wegontwerp wegen buiten de bebouwde kom* (Vol. Dl. a, basiscriteria, Publicatie / cROW, 164a). (2002). Ede: CROW.

[35] Liao, Y. (2007). *Viscoelastic FE modeling of asphalt pavements and its application to US 30 perpetual pavement* (Doctoral dissertation, Ohio University).

[36] Vincent, J. F. (2012). Basic Elasticity and viscoelasticity. *Structural biomaterials*. Princeton University Press.

[37] Moldex3D Support – Viscoelasticity Model (Thermoplastic only). (n.d.). Retrieved from http://support.moldex3d.com/r13/moldex3d/module-introduction/standard-injection-molding/material/reference/viscoelasticity-model-thermoplastic-only/

[38] Fernanda, M., Costa, P., & Ribeiro, C. (2011, September). Parameter estimation of viscoelastic materials: a test case with different optimization strategies. In T. E. Simos, G. Psihoyios, C. Tsitouras, & Z. Anastassi (Eds.), *AIP Conference Proceedings* (Vol. 1389, No. 1, pp. 771-774). AIP.

[39] Tam, W. O., Solaimanian, M., & Kennedy, T. W. (2000). Development and use of static creep test to evaluate rut resistance of superpave mixes. *Work*, *1250*, 4.

[40] Perret, J., & Dumont, A. G. (2004). Strain and stress distributions in flexible pavements under moving loads. *International Journal of Road Materials and Pavement Design*, *5*(LAVOC-ARTICLE-2004-001), 203-225.

[41] Hernandez, J., Al-Qadi, I., Ozer, H., Greene, J., Choubane, B., Wu, R., … Weaver, E. (2014). Pavement responses as function of truck tire type. *Asphalt Pavements*, 1125-1134. doi:10.1201/b17219-138

[42] Sebaaly, B. E., & Mamlouk, M. S. (1987). *Prediction of pavement response to actual traffic loading*.

[43] Pezo, R. F., Marshek, K. M., & Hudson, W. R. (1989). *Truck tire pavement contact pressure distribution characteristics for the Bias Goodyear 18-22.5, the Radial Michelin 275/80R/24.5, the Radial Michelin 255/70R/22.5, and the Radial Goodyear 11R24. 5 tires* (No. FHWA/TX-90+ 1190-2F). Center for Transportation Research, Bureau of Engineering Research, University of Texas at Austin.

[44] Priest, A. L., & Timm, D. H. (2006). *Methodology and Calibration of Fatigue Transfer Functions for Mechanistic Empirical Flexible Pavement Design* (NCAT Report 06-03).

[45] Al-Qadi, I. L., Loulizi, A., Elseifi, M., & Lahouar, S. (2004). The Virginia Smart Road: The impact of pavement instrumentation on understanding pavement performance. *The Journal of Association of Asphalt Paving Technologists*, *83*, 427-66.

[46] Hjort, M., Haraldsson, M., & Jansen, J. M. (2008). *Road Wear from Heavy Vehicles: An Overview*. NVF Committee Vehicles and Transports, Nordiska vägtekniska förbundet.

[47] Laplace distribution - Wikipedia. (n.d.). Retrieved May 18, 2017, from https://en.wikipedia.org/wiki/Laplace_distribution

[48] Li, N. (2013). *Asphalt Mixture Fatigue Testing: Influence of Test Type and Specimen Size* (Doctoral dissertation, TU Delft, Delft University of Technology).

[49] Huang, W., Zhang, X., Rong, H., & Chen, B. (2015). Finite Element Method for predicting rutting depth of steel deck asphalt pavement based on Accelerated Pavement Test. *Proceedings of the 3rd International Conference on Mechanical Engineering and Intelligent Systems (ICMEIS 2015)*. doi:10.2991/icmeis-15.2015.177

[50] Hallenbeck, M., Rice, M., Smith, B., Cornell-Martinez, C., & Wilkinson, J. (1997). *Vehicle volume distributions by classification* (No. FHWA-PL-97-025,).

[51] TG Road Safety. (2010). *Safe distance between vehicles*. Paris, France: Conference of European Directors of Roads.

[52] Witczak, M. W., & El-Basyouny, M. M. (2004). Appendix GG-1: Calibration of Permanent Deformation Models for Flexible Pavements. *Guide for Mechanistic-Empirical Design of New and Rehabilitated Pavement Structures*.

[53] Tseng, K. H., & Lytton, R. L. (1989). Prediction of permanent deformation in flexible pavement materials. In *Implication of aggregates in the design, construction, and performance of flexible pavements*. ASTM International.

[54] Pellenbarg, N. B. (1997). Groundwater amangement in the Netherlands: background and legislation. In *ILRI workshop groundwater management* (pp. 137-149).

[55] Rijkswaterstaat. (2016). *European Truck Platooning Challenge 2016 - Lessons Learnt*. Dutch Ministry of Infrastructure and the Environment.

[56] What is Truck Platooning? - EU Truck Platoon Challenge. (n.d.). Retrieved from https://www.eutruckplatooning.com/About/default.aspx

[57] Engineering and Regional Operations. (2017). *Construction Manual* (M 41-01.28). Washington State Department of Transportation.

[58] Caterpillar. (n.d.). *New Equipment* [Photograph]. Retrieved from http://www.cat.com/en_GB/products/new/equipment/

[59] Caterpillar. (2014). *CAT® F-SERIES PAVERS AND SCREEDS* (QEHQ1822 (10/14)).

[60] *Equipment Operator, Basic* (NAVEDTRA 14081A). (2014). Naval Education and Trainingprofessional Developmentand Technology Center.

[61] Chartered Institution of Highways & Transportation (CIHT). (2012). *Road Maintenance Review International Comparison*. World Road Association (WRA) UK.

[62] Tjin-A-Tsoi, T. (Ed.). (2016). *Transport and mobility*. The Hague, The Netherlands: Statistics Netherlands.

[63] A2 motorway (Netherlands) - Wikipedia. (n.d.). Retrieved May 18, 2017, from https://en.wikipedia.org/wiki/A2_motorway_(Netherlands)

[64] Anp. (2016, February 4). [Photograph]. Retrieved from http://www.volkskrant.nl/binnenland/vanaf-mei-s-avonds-130-per-uur-op-a2-tussen-utrecht-en-amsterdam~a4238231/

[65] Volvo. (2015). *VOLVO FL* [photograph]. Retrieved from http://www.volvotrucks.com/en-en/trucks/volvo-fl.html

[66] Rijkswaterstaat adviesdienst verkeer en vervoer. (2012). *Atlas hoofdwegennet*. Den Haag: Rijkswaterstaat.

[67] Alvarez, A. E., Mahmoud, E., Martin, A. E., Masad, E., & Estakhri, C. (2010). Stone-on-Stone Contact of Permeable Friction Course Mixtures. *Journal of Materials in Civil Engineering, 22(11)*, 1129-1138. doi:10.1061/(asce)mt.1943-5533.0000117

[68] Van Haaster, B., Worrell, E., F. Fortuin, J. P., & Van Vliet, W. (2015). Potential Energy Savings by Reducing Rolling Resistance of Dutch Road Pavements. *Journal of Materials in Civil Engineering, 27(1)*, 04014101. doi:10.1061/(asce)mt.1943-5533.0000999

Appendix

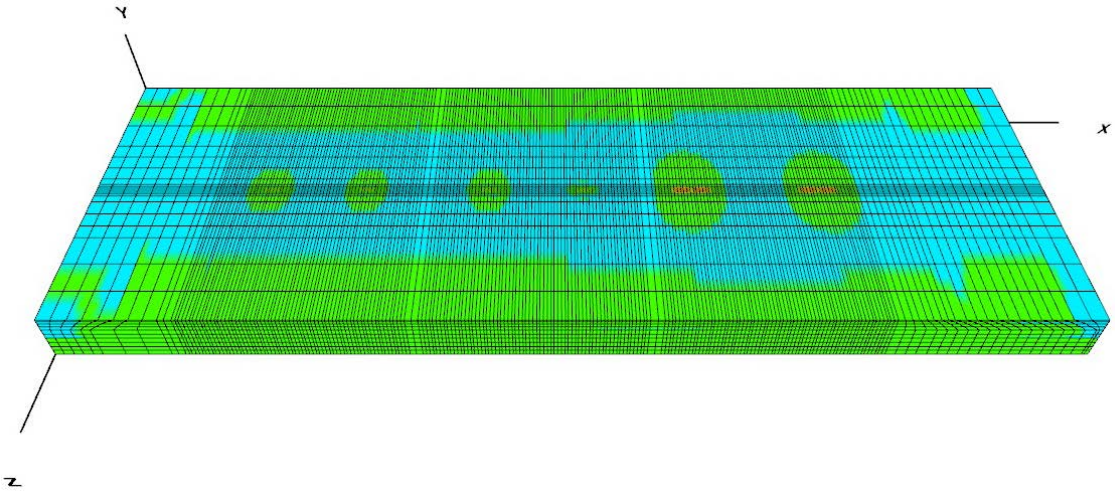

Figure A.1 Typical vertical strain contour (2 passenger cars and 1 truck with dual tires)

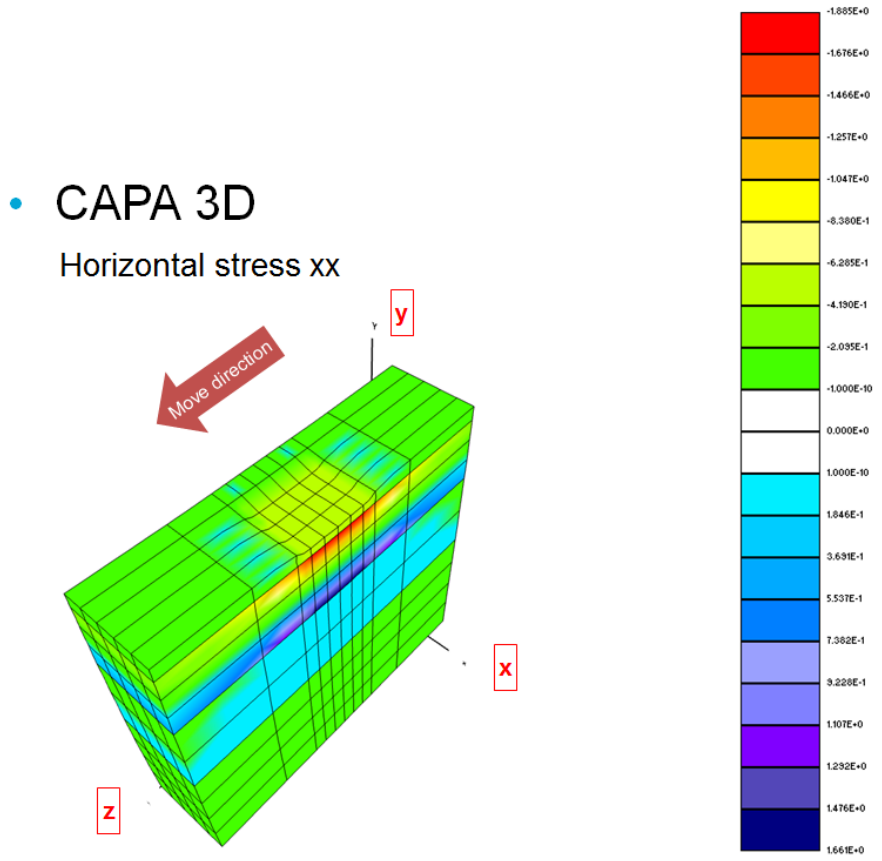

Figure A.2 Typical transverse strain contour (broadband)

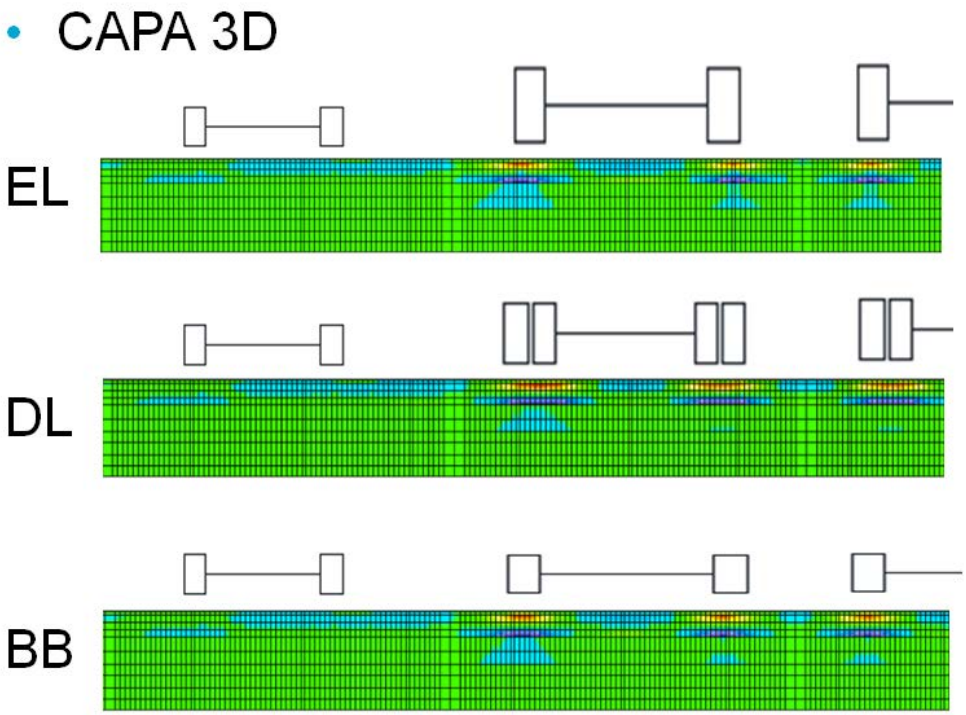

Figure A.3 Typical horizontal strain contours for different tire types (transverse cross section)

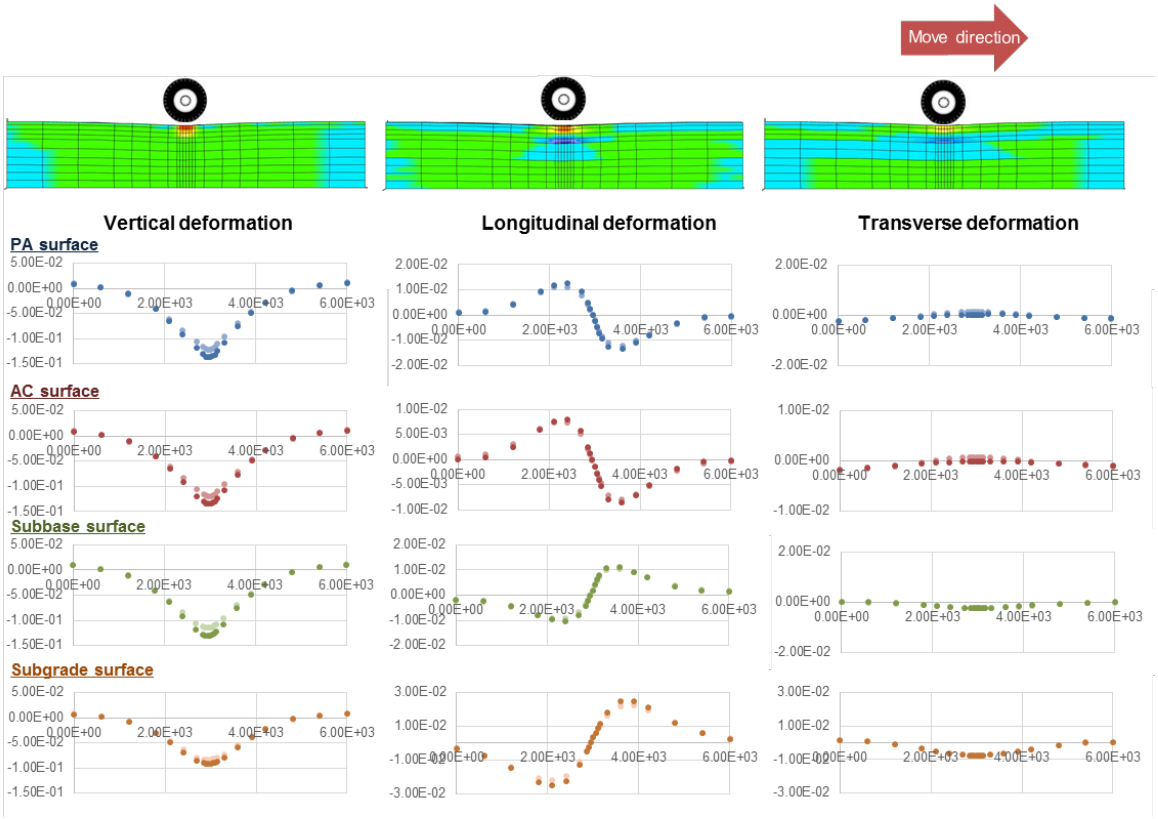

Figure A.4 Deformation plots of different pavement layers (longitudinal cross section)

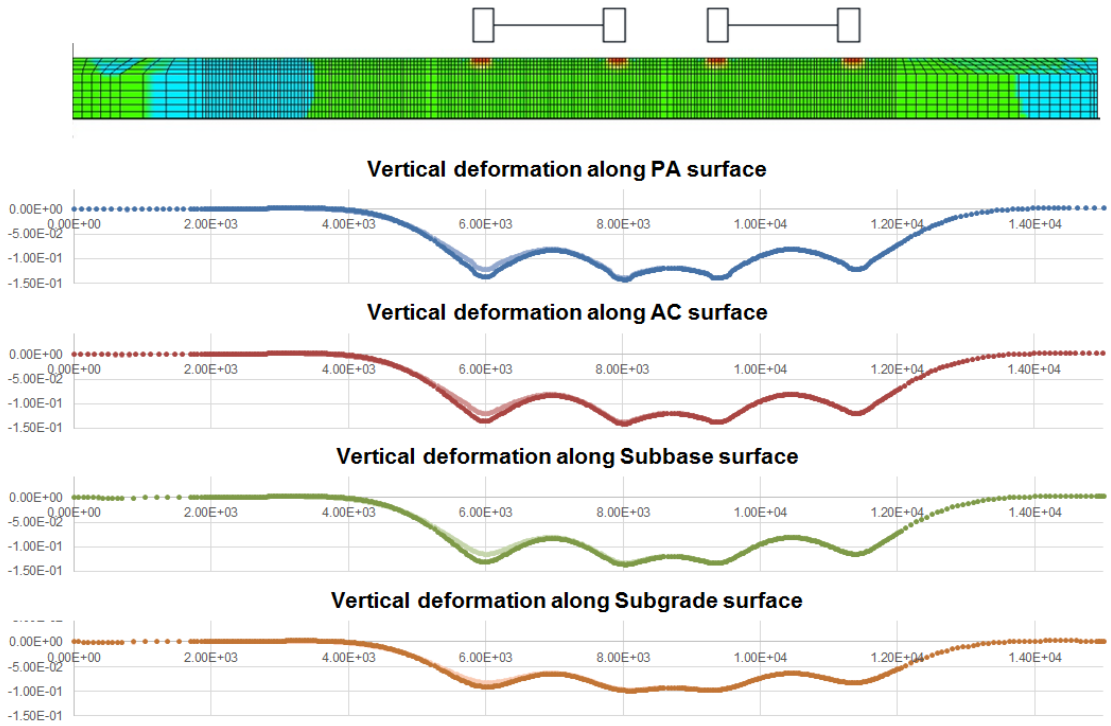

Figure A.5 Vertical deformation plots of different pavement layers (transverse cross section)

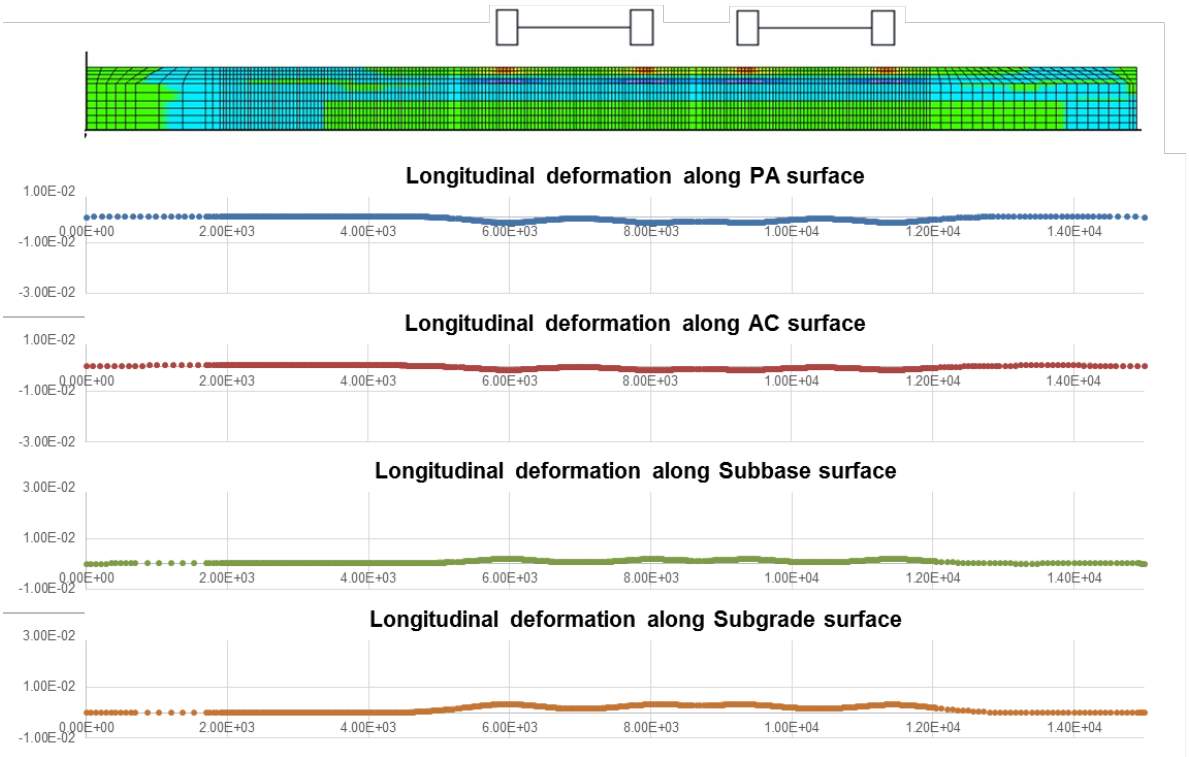

Figure A.6 Longitudinal deformation plots of different pavement layers (transverse cross section)

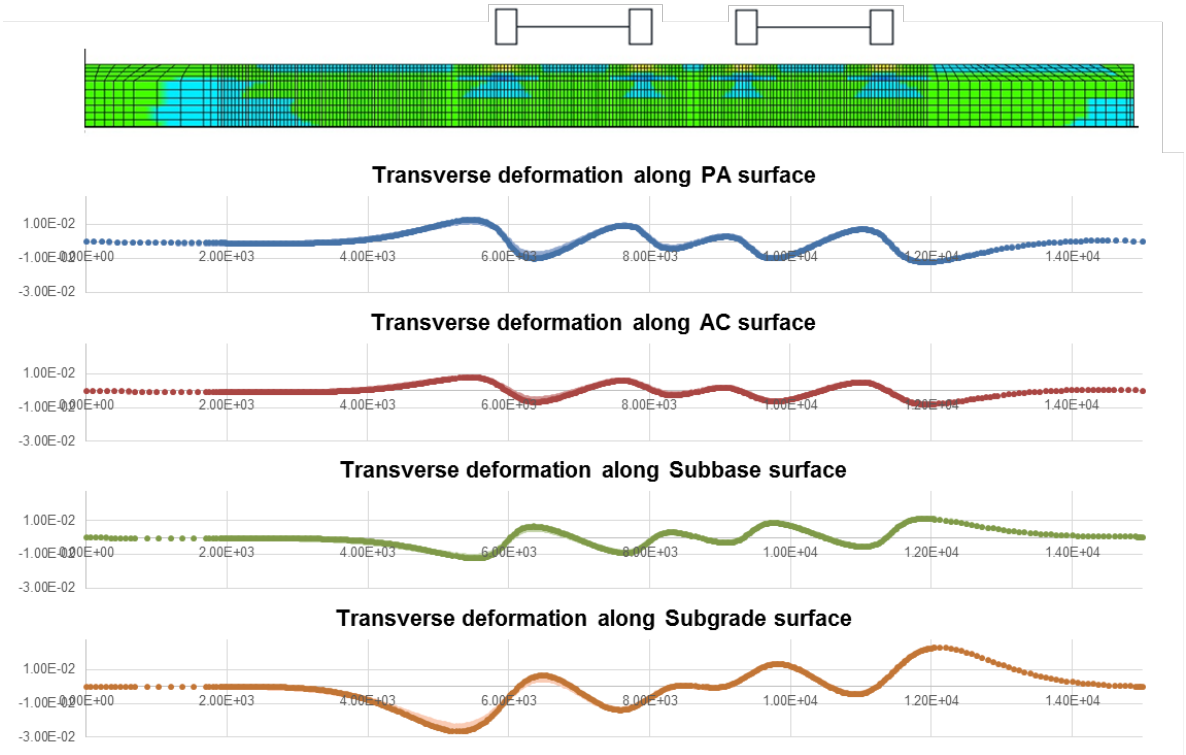

Figure A.7 Transverse deformation plots of different pavement layers (transverse cross section)

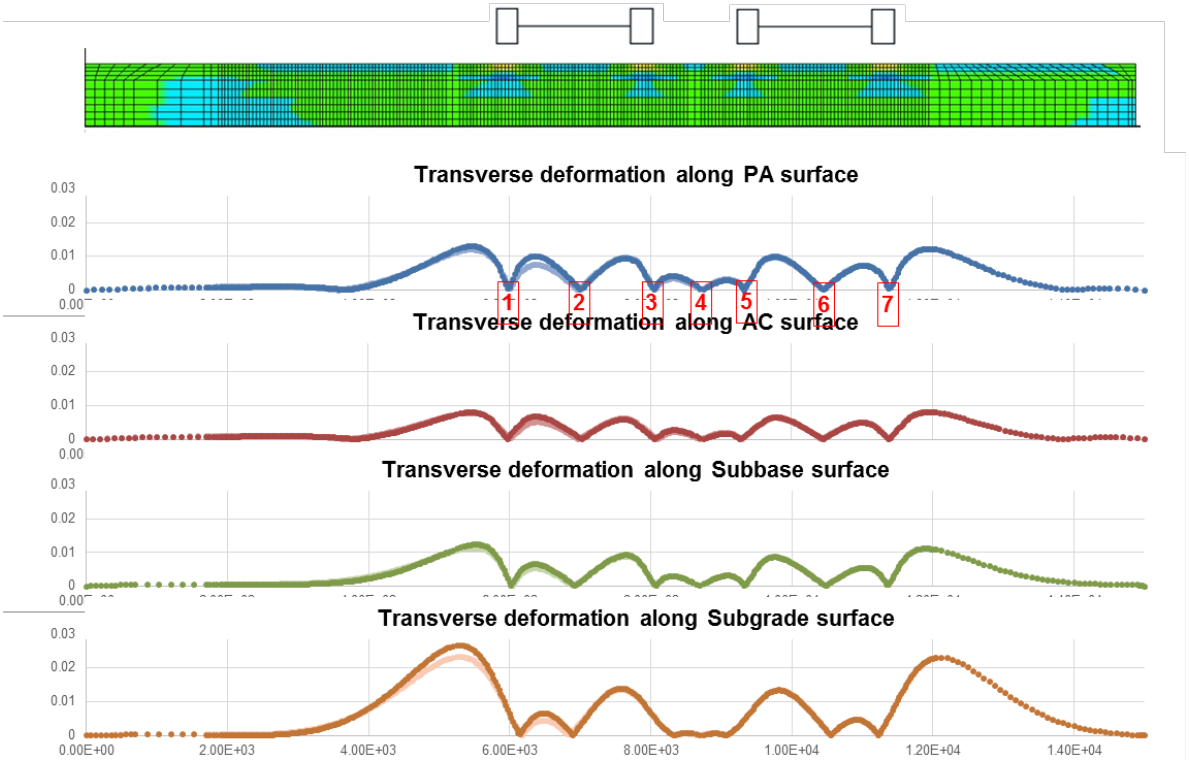

Figure A.8 Transverse deformation (absolute values) plots of different pavement layers (transverse cross section)

Author

Name:	Quanxin Xu
Student Number:	4308360
Mobile:	(+31)(0)631556025
E-mail:	Q.Xu@student.tudelft.nl
University:	Delft University of Technology
Faculty:	Civil Engineering and Geosciences
Master Programme:	Structural Engineering
Specialisation:	Pavement Engineering